Fall 2023

Quantifying Channel Change Following Post-Fire Debris Flows in a Steep, Coastal Stream, Big Sur, California

Telemak Olsen
Western Washington University, telemakolsen@gmail.com

Quantifying Channel Change Following Post-Fire Debris Flows in a Steep, Coastal Stream, Big Sur, California

By

Telemak Olsen

Accepted in Partial Completion
of the Requirements for the Degree
Master of Science

ADVISORY COMMITTEE

Dr. Allison Pfeiffer, Chair

Dr. Colin Amos

Dr. Noah Finnegan

GRADUATE SCHOOL

Dr. David L. Patrick, Dean

Master's Thesis

In presenting this thesis in partial fulfillment of the requirements for a master's degree at Western Washington University, I grant to Western Washington University the non-exclusive royalty-free right to archive, reproduce, distribute, and display the thesis in any and all forms, including electronic format, via any digital library mechanisms maintained by WWU.

I represent and warrant this is my original work, and does not infringe or violate any rights of others. I warrant that I have obtained written permissions from the owner of any third party copyrighted material included in these files.

I acknowledge that I retain ownership rights to the copyright of this work, including but not limited to the right to use all or part of this work in future works, such as articles or books.

Library users are granted permission for individual, research and non-commercial reproduction of this work for educational purposes only. Any further digital posting of this document requires specific permission from the author.

Any copying or publication of this thesis for commercial purposes, or for financial gain, is not allowed without my written permission.

Telemak Olsen

December 1st, 2023

Quantifying Channel Change Following Post-Fire Debris Flows in a Steep, Coastal Stream, Big Sur, California

A Thesis
Presented to
The Faculty of
Western Washington University

In Partial Fulfillment
Of the Requirements for the Degree
Master of Science

by
Telemak Olsen
December 2023

Abstract

Debris flows commonly occur following wildfire in steep landscapes, introducing large volumes of sediment to downstream fluvial systems. Fire-related sediment supply perturbations impact channel morphology, and importantly, fragile aquatic and riparian ecosystems downstream of disturbance. The Big Creek watershed drains 57 km^2 of steep chaparral and coast redwood forest along California's Central Coast. Streams in the Big Creek watershed typically exhibit step-pool/cascade morphology and serve as vital spawning habitat for anadromous Steelhead Trout (*Oncorhynchus mykiss*). In 2020, 97% of the Big Creek watershed burned in the Dolan Wildfire. In January 2021, an atmospheric river event triggered a series of post-fire debris flows and floods in Big Creek which drastically altered channel morphology.

Here, I characterize morphologic change following post-fire disturbance in Big Creek using pre- and post-fire structure from motion (SfM) and airborne light detection and ranging (lidar) datasets. I use topographic differencing to quantify post-fire topographic change within channels in the Big Creek watershed. I quantify grain size change using pre- and post-fire SfM datasets and couple these data with hydraulic and hydrologic modeling to estimate changes in sediment transport capacity and channel stability following post-fire disturbance in Big Creek. I also perform these analyses for Devil's Creek: a tributary of Big Creek which burned but did not experience post-fire debris flows within the main channel.

Post-fire debris flows initiated in Cathedral Creek and Brunette Creek, two steep tributaries of Big Creek, which delivered roughly 30,000 m^3 of material to Upper Big Creek. By October 2022, approximately 72% of debris flow material exported from Cathedral and Brunette Creek had been evacuated from the channel. Over 90% of the material remaining in Big Creek by 2022 was stored upstream of a valley-spanning log jam emplaced near the confluence of Upper Big Creek and Brunette Creek during post-fire debris flows. Upper Big Creek's initial

response to post-fire disturbance is characterized by substantial fining of the D_{16} and D_{50}, followed by re-coarsening 2-years post-fire. Conversely, Devil's Creek exhibits marginal fining 1-year post-fire, followed by little change 2-years post-fire. Changes in grain size distribution are responsible for considerable change in sediment transport capacity and channel stability. In Big Creek, sediment transport capacity increased 1-year post-fire, while channel stability decreased; 2-years post-fire, both sediment transport capacity and channel stability exhibit signs of recovery towards pre-fire conditions. In Devil's Creek, sediment transport capacity exhibited a substantial increase 1-year post-fire, followed by little change 2-years post-fire; changes in channel stability mirror trends in sediment transport capacity.

My findings indicate that post-fire geomorphic recovery occurs remarkably quickly in Upper Big Creek. Topographic differencing, sediment transport capacity, and channel stability analyses suggest that debris flows play an integral role in reconfiguring the vertical structure of steep, step-pool channels. Post-fire morphologic change has several potential implications for aquatic habitat; the quantitative data presented in this thesis may be valuable for biologists monitoring fish population dynamics in the Big Creek watershed.

Acknowledgements

Thank you to the Geological Society of America, the National Center for Airborne Laser Mapping, the Washington Section of the American Water Resources Association, the Western Washington University Research and Sponsored Programs Office, and the Western Washington University Geology Department for funding this research. I conducted my field work on the ancestral territory of the Salinian and Esselen Tribes, who have inhabited and stewarded the Santa Lucia Mountains and Big Sur coast since time immemorial.

I thank the many educators who have fostered my love for geoscience over the last seven years. I am especially thankful to my advisor, Dr. Allison Pfeiffer, for her steadfast support throughout every step of this process. I have learned so much from Allison's interdisciplinary approach to geomorphology and wealth of knowledge. Her kindness, patience, and dedication have helped me to overcome many challenges in completing this thesis. I am also especially grateful for my committee members, Dr. Noah Finnegan and Dr. Colin Amos for their guidance, encouragement, and thoughtful feedback.

I am grateful to the community of staff and researchers at Big Creek Reserve, who contributed so much to this thesis. I thank Dr. Mark Readdie and Big Creek Reserve staff members for their stewardship of Big Creek and support during field work. I thank Chuxuan Li, Dr. Daniel Horton, and Dr. Al Handwerger, for their collaboration; their knowledge and data contributions were essential in completing this thesis. I thank Dr. Tommy Williams and Dr. Dave Rundio for providing valuable insight into the ecological implications of post-fire geomorphic change in Big Creek. I thank Scott Walls for installing a network of GPS control points in Big Creek, which greatly improved the accuracy and efficiency of 2022 field surveys.

I thank Ben Paulson, Kate Blizzard, and Hye-In Park for their tireless work supporting Western's Geology department. I thank Ed Fordham, Charlie Vryhof, Colin Dechenne, and Isaac Apaez-Guttierez for providing integral field and laboratory assistance. I also thank Fluvial Geomorphology lab members Emily Loucks, Ashanie Long-Reid, and Brian Pinke for offering insightful feedback and fostering a collaborative, welcoming work environment. Lastly, I thank my family and friends both at home and in Bellingham; I am forever grateful for their enduring care and support.

Contents

Abstract iv

Acknowledgements vi

List of Tables ix

List of Figures x

List of Supplementary Figures xii

1.0 Introduction and Background 1

1.1 Overview 1

1.2 Geologic and Geomorphic Setting 2

1.3 Dolan Fire and Subsequent Debris Flows 4

1.4 Hydrologic Effects of Wildfire 5

1.5 Geomorphic Effects of Wildfire 6

1.5.1 Post-fire Debris Flows and Floods 6

1.5.2 Effects of Debris Flows on Channel Morphology 8

1.6 Effects of Debris Flows on Salmonid Populations 9

1.7 Climate Change 10

1.8 Hypotheses 11

2.0 Methodology 12

2.1 Structure from Motion (SfM) Photogrammetry 12

2.2 Vegetation Filtering 13

2.3 Grain Size Analysis 14

2.4 Hydrologic Analyses and Hydraulic Modeling 15

2.5 Sediment Transport Capacity 17

2.6 A_{stab} 20

2.7 Lidar and Topographic Differencing 21

3.0 Results 23
3.1. Field Observations 23
3.2. Topographic Differencing 25
3.3 Results of Structure from Motion Surveys 27
3.4. Grain Size 28
3.5. Hydraulic Modeling 29
3.6. Sediment Transport Capacity 30
3.7. Channel Stability 32
4.0 Discussion 33
4.1 Dilution from Post-fire Debris Flows to Debris Floods 33
4.2 Differences between Devil's Creek and Big Creek 34
4.3 Controls on Sediment Transport Capacity 35
4.4 Sources of Error 36
4.5 Partial Post-fire Sediment Budget 38
4.6 Timescales of Post-fire Fluvial Recovery 39
4.7 Debris Flows and Channel Reconfiguration 44
4.8 Potential Ecological Implications 45
4.9 Climate Implications 47
5.0 Conclusion 49
6.0 References 50
7.0 Tables 64
8.0 Figures 67
9.0 Supplemental Figures 87

List of Tables

Table 1. Data sources and model parameters for sediment transport capacity and A_{stab} model scenarios in Big Creek and Devil's Creek. 64
Table 2. Grain size quantiles for Upper Big Creek. 65
Table 3. Grain size quantiles for Devil's Creek. 66

List of Figures

Figure 1. (A) Footprint of the Dolan Fire and Big Creek watershed, and locations of study streams within the basin. (B) Study streams, structure from motion study area, debris flows paths, and elevation within the Big Creek watershed. 67
Figure 2. Yearly peak flow data from USGS stream gauges surrounding Big Creek. All yearly peak flows for surrounding stream gauges in 2021 took place during the atmospheric river event that triggered post-fire debris flows in the Big Creek watershed. Peak flow recurrence intervals for this date range from 1.5 to 5 years. 68
Figure 3. Timeline of structure from motion (SfM) and lidar surveys, and debris flow-related events superimposed on total daily precipitation measured at the Whale Point weather station within the Big Creek watershed. 68
Figure 4. Examples of initial, classified, and masked orthoimages for one reach in Big Creek. . 69
Figure 5. Modeled hydrograph, with and without the hydrologic influence of the Dolan Fire burn scar, for Upper Big Creek and Devil's Creek during the 2021 atmospheric river event which triggered post-fire debris flows. 70
Figure 6. Field photos taken after post-fire debris flows in the Big Creek watershed. (A) 3 m incision scar in Brunette Creek, one of the channels in which post-fire debris flows initiated. (B) Bouldery deposit behind the newly emplaced log jam just downstream of the confluence between Brunette Creek and Upper Big Creek. (C) Newly emplaced log jam just downstream of the confluence between Brunette Creek and Upper Big Creek. (D) High-water mark approximately 4 m above low-flow water level just downstream of the confluence between Devil's Creek and Big Creek. (E) Potential debris flood terraces in Lower Big Creek. 71
Figure 7. 2016, 2021, and 2022 orthoimages for one example reach in Upper Big Creek; stars represent landmarks visible in each timestep..... 72
Figure 8. DEMs of difference and volumetric change from 2011 to 2022 for selected sections of Cathedral Creek and Brunette Creek which experienced substantial geomorphic change..... 73
Figure 9. DEMs of difference and volumetric change from 2011 to 2022 for selected sections of Upper Big Creek which experienced substantial geomorphic change..... 74
Figure 10. DEMs of difference and volumetric change from 2011 to 2022 for selected sections of Devil's Creek which experienced moderate geomorphic change. 75

Figure 11. PebbleCounts-generated bed surface grain size distributions for each study reach in Upper Big Creek and Devil's Creek. 76
Figure 12. Grain locations, symbolized by PebbleCounts-measured b-axis diameter for one example reach in Upper Big Creek. 77
Figure 13. Reach-averaged shear stress and flow width through time in Big Creek and Devil's Creek. 78
Figure 14. Sediment transport capacity and A_{stab} through time in Big Creek and Devil's Creek. 79
Figure 15. Area-normalized sediment transport capacity for grain size bins across all reaches in Upper Big Creek and Devil's Creek. D_{max} represents the b-axis diameter of the largest mobile grain by area (across all study reaches) during each model timestep. 80
Figure 16. Valley cross sections for Upper Big Creek and Devil's Creek, with schematic illustrations of hypothetical post-fire hillslope sediment contributions. 81
Figure 17. Sediment transport capacity through time for study reaches in Upper Big Creek with constant bed surface grain size, channel geometry, and roughness. 82
Figure 18. Schematic of post-fire sediment contributions and storage for streams in the Big Creek watershed. 83
Figure 19. DEMs of difference and field photos at the confluence of Upper Big Creek and Brunette Creek and reaches downstream, which include SfM study reaches and the geomorphic features in Figures 9B, and 9C. Vertical structure in this section of the channel was reconfigured during post-fire debris flows. 84
Figure 20. Longitudinal profiles from 2011 and 2022 lidar datasets for sections of Upper Big Creek in which vertical structure was reconfigured during post-fire debris flows. 85
Figure 21. Schematic diagram of potential salmonid spawning habitat impacts of post-fire debris flows in Big Creek. 86

List of Supplementary Figures

Supplementary Figure 1. Full DEM of difference from 2011 to 2022 for (A) Cathedral Creek and (B, C) Brunette Creek. 87
Supplementary Figure 2. Full DEM of difference from 2011 to 2022 for (A, B) Upper Big Creek and (C) Lower Big Creek. 88
Supplementary Figure 3. Full DEM of difference from 2011 to 2022 for Devil's Creek. 89
Supplementary Figure 4. Full DEM of difference from 2011 to 2015 for (A) Big Creek and (B, C) Devil's Creek. 90
Supplementary Figure 5. Differenced normalized burn severity index in the Upper Big Creek and Devil's Creek watersheds. 91

1.0 Introduction and Background

1.1 Overview

Debris flows are a common geomorphic response to post-wildfire conditions in steep landscapes (Cannon and Reneau, 2000). Debris flows redistribute large volumes of sediment derived from hillslopes, steep channel beds, and channel margins and increase sediment supply to the downstream fluvial systems (Cannon and Reneau, 2000; Tang et al., 2019; Morell et al., 2021; Rengers et al., 2021). In August 2020, the Dolan Fire burned approximately 125,000 acres of steep, coastal terrain in Big Sur, CA (Figure 1A). In January 2021, intense rainfall triggered a series of post-fire debris flows in the Big Creek watershed, a 57 km^2 coastal basin within the footprint of the Dolan Fire (Figure 1A). Big Creek underwent considerable morphologic change resulting from the Dolan Fire and subsequent debris flows.

Few studies specifically examine the impact of post-fire debris flows on channel morphology, as high-resolution pre-fire baseline data are rare. I examine the impact of post-fire debris flows on reach- and bedform-scale channel morphology by comparing pre-fire structure from motion photogrammetry (SfM) data collected in Summer 2016 to post-fire SfM data collected in Summer 2021 and 2022. Additionally, I conduct geomorphic change analyses using pre-fire lidar datasets collected in 2011 and 2015 and a post-fire lidar dataset collected in 2022. Post-disturbance morphologic change in Big Creek and Devil's creek necessitate changes in sediment transport capacity and channel stability. In addition to quantifying morphologic changes, I quantify the impact of geomorphic and hydrologic change following the Dolan Fire and post-fire debris flows on sediment transport capacity and channel stability in Big Creek and Devil's Creek.

Big Creek supports a well-studied population of threatened anadromous steelhead trout (*Oncorhynchus mykiss*), and post-fire changes in reach-scale morphology likely have substantial impacts on spawning and resting habitat. Understanding the diverse geomorphic and ecological recovery patterns of stream channels in response to post-wildfire disturbance will become increasingly important as wildfire becomes more prevalent in the Western U.S. due to anthropogenic climate change (Westerling, 2016; Williams et al., 2019).

1.2 Geologic and Geomorphic Setting

The Big Creek watershed is a 57 km^2 coastal basin nestled in the Santa Lucia Mountains along California's Big Sur coast. The Big Sur coast is one of the steepest coastlines in the contiguous United States; total relief in the Big Creek watershed is 1543 m. Tectonically, Big Creek lies approximately 10 km east of the offshore San Gregorio-Hosgri Fault system. Big Creek is adjacent to the Big Sur bend, a transpressional region of the San Gregorio-Hosgri Fault system which accommodates approximately 3.35 mm of right-lateral displacement and 0.8 - 1.2 mm of vertical displacement per year (Johnson et al., 2018). Bedrock geology in the Santa Lucia Mountains is highly complex and somewhat poorly constrained. The Big Creek watershed consists largely of Cretaceous magmatic and metamorphic rocks within the Salinian Block in the upper watershed. The middle and lower watershed is characterized by Mesozoic granite, Franciscan group rocks, Cretaceous conglomerates, and a Salinian Block enclave (Dibblee Jr., 1974; Johnston et al., 2018).

Big Sur represents the point at which California's hot, dry southern coastal climates meet cooler, wetter northern coastal climates (Potter, 2010). Regional climate is characterized by extremely dry summers and wet winters (Henson and Usner, 1996). Average yearly precipitation ranges from 100 cm along the coast to 200 cm at higher elevations within the Santa Lucia

Mountains (Henson and Usner, 1996). Topography is a major control on regional climate; the Santa Lucia range lies perpendicular to prevailing westerly winds, creating an orographic effect and a steep temperature/elevation gradient (Henson and Usner, 1996; Daly et al., 2008). The Big Sur coastline experiences extreme precipitation in winter via atmospheric river events, which deliver between 20-50% of total precipitation in California (Dettinger et al., 2011). Multi-year droughts are also prevalent in coastal California; an estimated 37 droughts lasted three or more years over the last 1200 years in California, the most severe of which lasted from 2012 to 2016 (Griffin and Anchukaitis, 2014).

Ecology in California's Central Coast Bioregion is highly elevation-dependent (Henson and Usner, 1996). In the Big Creek watershed, ridgelines and upper valley walls are chaparral-dominated. Chaparral ecosystems in Big Sur are composed of evergreen shrubs including California Scrub Oak and Chamise, which thrive in Big Sur's dry summers and wet winters (Tietje et al., 2019). Chaparral ridgelines and upper valley walls transition to mixed hardwood-conifer forests along lower valley walls and valley floors. Mixed hardwood-conifer forests in the Big Creek watershed house Bigleaf Maples and a variety of Oak species in addition to Pines, Firs, Cedars, and Coast Redwoods (Tietje et al., 2019). Notably, streams in the Big Creek watershed contain O. Mykiss, for which spawning success is highly dependent on fluvial morphology (Everest and Meehan, 1981; Kondolf and Wolman, 1993; Harrison et al., 2018).

Streams in the Big Creek watershed are steep and bouldery. Study reaches in Upper Big Creek and Devil's Creek are dominated by step-pool and cascade morphology (Montgomery and Buffington, 1997). Channel gradients within my SfM study area range from 0.029 to 0.083. The steepest reaches are in Upper Big Creek, while reaches with the lowest slopes are in Devil's Creek (Figure 1B).

1.3 Dolan Fire and Subsequent Debris Flows

The Dolan Fire burned approximately 97% of the Big Creek watershed between August 18th, 2020, and October 13th, 2020 (Figure 1A); state investigations concluded that the wildfire was triggered by arson (Smith, 2022). In general, burn severity surrounding Big Creek and its tributaries was higher than burn severity surrounding Devil's Creek and its tributaries (USFS, 2020). The upper watershed experienced the most severe burns (USFS, 2020).

The atmospheric river event that triggered the 2021 Big Creek debris flows lasted from 7:00 pm on January 26th, 2021, until 12 am on January 29th, 2021. The storm produced 20.5 cm of total rainfall at the Whale Point weather station at an elevation of approximately 200 m within Big Creek watershed, with a maximum hourly rainfall magnitude of 1.5 cm. Rainfall from this storm alone accounts for 27% of total rainfall at the Whale Point weather station in 2021.

2021 debris flows destroyed the stream gauge in Lower Big Creek. USGS stream gauge data for the Big Sur River, San Antonio River, and Nacimiento River (all within 100 km of Big Creek) suggest that rainfall events responsible for post-fire debris flows in Big Creek were not particularly extreme compared to previous events (Figure 2). Weather stations surrounding these stream gauges were inactive during the 2021 atmospheric river; as such, I cannot rule out the possibility that Big Creek experienced significantly higher local rain intensity than the surrounding area and produced a notable 2021 peak flow.

Post-wildfire debris flows initiated in the headwaters of Brunette and Cathedral Creeks: small, steep tributaries of Big Creek with average gradients of 0.172 and 0.252, respectively (Figure 1B). Cathedral and Brunette Creek's confluences with Big Creek are 0.27 and 1.58 km upstream of my SfM study area, respectively. Evidence of debris flows in the form of newly deposited boulders, terraces, and swaths of fine sediment is readily apparent in Big Creek from

my SfM study area to its outlet into the Pacific Ocean. Terraces downstream of Big Creek's confluence with Devil's Creek contain sand and gravel-dominated deposits with no grading, which suggests debris flows in Big Creek may have diluted to debris floods at some point in Big Creek (Church and Jakob, 2020).

Unlike Big Creek, Devil's Creek shows little evidence of major debris flows. Contrasting post-fire conditions in Big Creek and Devil's Creek provide an opportunity for comparison between two similar streams in a burned watershed: one of which did experience major debris flows and one of which likely did not.

1.4 Hydrologic Effects of Wildfire

Wildfire serves to increase total runoff, streamflow volume, and peak flow magnitude via a variety of mechanisms. Wildfire removes vegetation from the burned landscape, reducing total evapotranspiration and increasing runoff (Loaiciga et al., 2001). Wildfire can also induce soil-water repellency, reducing permeability and infiltration capacity which promotes erosive overland flow on burned hillslopes (MacDonald and Huffman, 2004; Gabet and Sternberg, 2008). The severity and recovery timescales of these hydrologic responses to wildfire depend on basin characteristics, including burn severity, vegetation type, and soil characteristics (de Jonge et al., 1999; DeBano, 2000; MacDonald and Huffman, 2004). Each of these post-fire changes to basin hydrology exacerbate geomorphic responses to wildfire.

In Big Creek, rainfall intensity and peak flow in surrounding unburned watersheds were unremarkable during 2021 debris flows, but recent hydrologic modeling work suggests that the burn scar increased both peak flow discharge and total discharge by 234% and 891%, respectively, following the Dolan Fire (Li et al., 2022). As such, post-fire hydrologic changes are

likely partially responsible for post-fire debris flows (and the ensuing geomorphic response) in Big Creek.

1.5 Geomorphic Effects of Wildfire

Wildfire drives considerable geomorphic change, both directly and indirectly. Wildfire can directly weather and erode rock surfaces, creating weathering rinds and spalling rock fragments (Dragovich, 1993). Additionally, wildfire increases hillslope sediment yield via hillslope litter and sediment dam removal. Hillslope litter and sediment dams directly attenuate overland flow and store hillslope sediment, and their removal promotes hillslope erosion (Shakesby and Doerr, 2006; Lamb et al., 2013). Wildfire also contributes sediment to fluvial systems via mass movement (Shakesby and Doerr, 2006). Fire can trigger dry ravel, shallow landslides, and debris flows, as exemplified in Big Creek following the Dolan fire (Florsheim et al., 1991; Cannon et al., 1998; Meyer et al., 2001; Shakesby and Doerr, 2006).

1.5.1 Post-fire Debris Flows and Floods

Debris flows are viscous mixtures of water and sediment which typically initiate in very steep, convergent topography and run out into the fluvial network (Iverson, 2005; Hungr et al., 2014). Debris flows typically consist of approximately equal proportions of sediment and intergranular water, and often occur in a series of discrete surges (Iverson, 2005). Whereas clearwater floods transport sediment via bedload saltation and suspension in water, sediment transport in debris flows is driven by complex interactions between sediment and fluid, which are capable of producing sediment discharges over an order of magnitude greater than extreme clearwater floods (Iverson, 2005; Hungr et al., 2014). As such, debris flows have immense sediment transport capabilities, and can transport large clasts that would be immobile under typical fluvial conditions. Under experimental conditions, debris flows run out and sediment

begins to deposit abruptly as they reach channel slopes under 3˚ (Major, 1997). Debris flows leave behind deposits with wide grain size distributions, ranging from clay to large boulders, that sometimes exhibit inverse grading (Naylor, 1980; Coussot and Meunier, 1996).

A variety of processes may trigger debris flows in burned catchments (Cannon, 2001). Runoff during high-magnitude rainfall events can trigger debris flows via rill coalescence on hillslopes and progressive sediment accumulation (bulking) from the channel bed (Meyer and Wells, 1997). Additionally, fire can incinerate vegetation dams on hillslopes which store hillslope sediment, allowing hillslopes to deliver large volumes of sediment to stream channels, which is then incorporated into debris flows during subsequent rain events (Lamb et al., 2013; Dibiase and Lamb, 2020). Failure of in-channel sediment accumulations in burned watersheds can also trigger post-fire debris flows by mobilizing hillslope-derived sediment that has been re-deposited within channel networks (McGuire et al., 2017).

As they transport downstream, debris flows may dilute to debris floods within the debris flow channel or via oblique convergence with a steep tributary (Hungr et al., 2014; Church and Jakob, 2020). Debris floods mobilize most or all of the bed surface, destabilizing the channel bed (Hungr et al., 2014; Church and Jakob, 2020). While sediment transport in debris floods can far exceed sediment transport in clearwater floods, transport is still driven by the shear force of flowing water, with peak discharges resembling that of a clearwater flood (Hungr et al., 2014; Church and Jakob, 2020). Debris flood deposits tend to have more in common with typical fluvial deposits than with debris flow deposits. Debris flood deposits typically contain more sand than fluvial deposits but are commonly stratified and may contain imbricated clasts (Church and Jakob, 2020).

1.5.2 Effects of Debris Flows on Channel Morphology

Debris flows have profound effects on channel morphology. Debris flow-affected channels are typically characterized by erosion in headwaters and extensive deposition at and below debris flow termini (Cenderelli and Kite, 1998). Debris flows influence reach- and bedform-scale morphologic variables such as grain size, pool, and wood distribution in streams (Benda et al, 2003). Additionally, debris flows can influence reach-scale morphologic variables including channel width and slope (Foster et al., 2020). Recent work suggests significant variability in the mechanisms by which post-fire debris flows recruit sediment and the extent of channel scour (Tang et al., 2019; Morell et al., 2021; Rengers et al., 2021). While the majority of post-fire sediment yield is hillslope derived (Rengers et al., 2021), post-wildfire debris flows following the 2016 Fish fire and the 2018 Montecito fire recruited and re-distributed large volumes of coarse sediment stored within channel networks (Tang et al., 2019; Morell et al., 2021).

In the lower reaches of steep basins, post-fire debris flows represent an episodic increase in sediment supply. Increases in upstream sediment supply are associated with a variety of morphologic changes (Dietrich et al, 1989; Lisle and Hilton, 1992; Lane et al., 1996; Wang et al., 2021). In step-pool channels, episodic sediment supply increases are associated with bed surface grain size fining, elevated bedload transport rates, and aggradation (Dietrich et al, 1989; Wang et al., 2021). Steps and pools themselves are highly dynamic in response to sediment pulses (Wang et al., 2021). Increases in sediment supply are also associated with deposition of fine sediment derived from winnowing at low flows in pools (Lisle and Hilton, 1992). As sediment supply wanes following major sediment input, the channel bed surface coarsens and re-armors, which stabilizes channels and regulates sediment transport (Gran and Montgomery, 2005).

While previous studies explore the mechanics of post-fire debris flows (Meyer and Wells, 1997; Cannon, 2001; McGuire et al., 2017), sediment recruitment (Florsheim 1991; Lamb et al., 2013; Nyman et al., 2015; DiBiase and Lamb, 2020; Morell et al., 2021) and spatial patterns in debris flow erosion and deposition (Cenderelli and Kite, 1998; Morell et al., Rengers et al., 2021), opportunities to examine the impact of post-fire debris flows on reach- and bedform-scale channel morphology are rare due to a lack of high-resolution pre-fire baseline data. Examples of previous work that uses extensive pre- and post-disturbance field data to quantify channel change in response to debris flows include Foster et al. (2020), which examines channel change through a primarily ecological lens. The 2020 Dolan fire and subsequent debris flows in the Big Creek watershed present a rare opportunity to quantify reach-scale channel response in several reaches for which high resolution pre-fire geomorphic data exists.

1.6 Effects of Debris Flows on Salmonid Populations

Salmonid spawning habitat is largely dependent on channel morphology, and changes in grain size, pool, and gravel patch distribution can significantly impact salmonid populations (Kondolf and Wolman, 1993; Harrison et al., 2018). Salmonid species require spawning gravels that are fine enough to easily move, yet coarse and well-sorted such that water can circulate within and deliver oxygen to pore spaces (Everest and Meehan, 1981; Harrison et al., 2018). Salmonid species can successfully spawn in a wide variety of grain sizes, but the majority of the spawning substrate must be finer than the maximum grain size movable by the fish, which is a function of fish length (Kondolf and Wolman, 1993; Riebe et al., 2014).

Debris flows have direct and potentially catastrophic immediate effects on fish living in channels through which debris flows travel, but post-debris flow increases in sediment supply have the potential to both negatively and positively impact salmonid populations. Debris flows

introduce large volumes of fine sediment, which can inhibit oxygen circulation in salmonid redds, reducing spawning success (Everest and Meehan, 1981). Debris flows are also associated with pool burial; pools serve resting habitat for adult fish preparing to spawn (Everest and Meehan, 1981). As such, reductions in the number and depth of pools can negatively impact fish (Everest and Meehan, 1981; Wheaton et al., 2010). Increases in sediment supply are also associated with bed surface grain size fining, which leaves redds on the channel bed more susceptible to scour (Buffington and Montgomery, 1999; May et al., 2009). Conversely, debris flows have the potential to create new salmonid spawning habitat. Debris flow deposits can bridge previously insurmountable steps and allow fish to migrate further upstream (Foster et al., 2020). Additionally, sudden increases in sediment supply can generate new spawning habitat in sediment-poor channel networks (Harrison et al., 2018). In general, salmonid response to geomorphic disturbance is unpredictable and highly site-specific (Foster et al., 2020).

Big Creek supports a well-studied population of threatened O. Mykiss. O. Mykiss population response to post-fire disturbance is beyond the scope of this thesis, but ongoing, biannual National Marine Fisheries Service-led O. mykiss surveys in Big Creek and Devil's Creek dating back to 2008 present a unique opportunity to pair quantitative datasets on post-fire changes in channel morphology and fish population in the future.

1.7 Climate Change

Climate and geomorphic processes are inextricably linked. Anthropogenic climate change has already and will continue to influence the timing and magnitude of geomorphic processes along California's Big Sur coast. Although total annual precipitation is not projected to change significantly in California, recent work finds that precipitation patterns will continue to become increasingly volatile, and temporally concentrated in the wet winter (Cayan et al., 2008; Persad

et al., 2020). Atmospheric river events, one of which triggered 2021 debris flows in Big Creek, are also projected to become longer and stronger, albeit less frequent (Espinoza et al., 2018). Temperatures are also projected to increase across California by 1.5° - 4.5° C by 2100, with more warming projected in the summer (Cayan et al., 2008). Recent work also projects an increase in the frequency of extreme wet and dry periods, and a marked increase in rapid dry- to wet-period transitions in coastal California, which is linked to fire activity (Swain et al., 2018; Homann et al., 2022).

In California, warmer summers and longer, more frequent, intense droughts will promote wildfire conditions, while more frequent, intense wet periods and precipitation events in winter will exacerbate geomorphic response to wildfire (Cayan et al., 2008; Florsheim et al., 2017; Swain et al., 2018; Williams et al., 2019; Persad et al., 2020). As fire continues to exert a progressively greater impact on landscapes in the Western U.S., research examining the extensive geomorphic and ecological impacts of wildfire will become increasingly important.

1.8 Hypotheses

This work tests the following hypotheses related to post-fire geomorphic change in the Big Creek watershed:

- I expect Big Creek to exhibit major morphologic change in response to post-fire debris flows, characterized by bed surface fining and systematic aggradation. I expect Devil's Creek to exhibit similar, but lower-magnitude morphologic changes to Big Creek.
- Fining of the bed surface grain size distribution in Big Creek will trigger cascading effects on channel dynamics, as evidenced by elevated sediment transport capacities and channel instability.

- Eventually, I expect Big Creek to experience a slow return to pre-fire conditions. Following initial bed surface fining, I expect to observe marginal bed surface coarsening 2-years post-fire as routine high-flow events begin to evacuate debris flow-related sediment from the channel.

2.0 Methodology

2.1 Structure from Motion (SfM) Photogrammetry

Structure from Motion (SfM) photogrammetry is an inexpensive method of constructing high-resolution, three-dimensional models of terrain. To construct three dimensional models using SfM photogrammetry, the user collects a suite of photos of the terrain of interest from multiple angles (Micheletti et al., 2015). A scale invariant feature transform algorithm then identifies common points present in multiple photos and constructs a three-dimensional network of like-points that approximates the form and color of the terrain (Micheletti et al., 2015).

Prior to the 2020 Dolan Fire, Dr. Allison Pfeiffer collected a suite of SfM data for approximately 200 m of channel in Upper Big Creek and 200 m of channel in Devil's Creek. In September 2021, 1 year after the Dolan Fire and 6 months after post-fire debris flows in Big Creek, I collected another suite of SfM data covering the same regions of Upper Big Creek and Devil's Creek (Figure 1B). In August 2022, I collected an additional suite of SfM data encompassing the same study reaches as 2016 and 2021 SfM surveys. I systematically captured photos of the channel bed and banks using a DSLR camera with a wide-angle lens mounted on a 3 m pole. Each photo included substantial overlap with other photos included in the SfM model.

During the September 2021 survey, I used an Emlid Reach real-time-kinematics GPS system and a laser rangefinder to collect ground control data for each reach. Channels in the Big Creek watershed are often confined and surrounded by steep canyon walls, which impede line-

of-sight for GNSS satellites and reduce positional accuracy. As such, I had little success in obtaining accurate positional coordinates during the 2021 SfM survey. During the August 2022 survey, I used a Total Station and GPS control points in Big Creek created by Scott Walls in 2022 to collect spatially explicit SfM data. I generated high-resolution point clouds, DEMs, and orthoimages from these photos using Agisoft Metashape Professional. I co-registered 2016, 2021, and 2022 orthoimages to one another to ensure consistency between measurements across orthoimages. After co-registering orthoimages to one another, I measured the radii of 20 12-bit targets used for photo alignment throughout each orthoimage to assess and correct any minor differences in scale between orthoimages.

2.2 Vegetation Filtering

To prepare pre- and post-fire SfM-derived orthoimages for grain size data collection, I manually outlined and masked out the water surface and performed an object-based, supervised classification in ArcGIS Pro to mask vegetation out of each image. I segmented each orthoimage, created a training dataset composed of segments from each segmented orthoimage, and created a reference point dataset for accuracy assessment. I used two information classes for this classification: vegetation and non-vegetation. Training and reference datasets contained between 100 – 500 features in each orthoimage for each information class and included samples from throughout each orthoimage and a variety of spectral signatures within each information class. I used a support vector machine classifier in ArcGIS Pro, which renders training data in multi-dimensional space (here, segments as red, blue, and green values in 3-dimensional space) and generates hyperplanes between object clusters to divide objects into desired information classes (Cortes and Vapnik, 1995; Chapelle et al., 1999). This classification produced user and producer accuracies greater than 90% for both information classes in every orthoimage (Figure 4).

2.3 Grain Size Analysis

The bed surface grain size distribution in stream channels has important implications for sediment transport and channel stability (Wilcock and Crowe, 2003; Dietrich et al., 2005; Mackenzie and Eaton, 2017; Eaton et al., 2020). Additionally, salmonid species require specific grain size conditions for successful spawning (Kondolf and Wolman, 1993; Riebe et al., 2014; Harrison et al., 2018). I use PebbleCounts, a python-based remote sensing tool, to characterize grain size distribution in pre- and post-fire orthoimagery. PebbleCounts uses a K-means segmentation algorithm, which clusters pixels that are similar in color and spatial location to identify and automatically measure grains in orthoimagery (Purinton and Bookhagen, 2019). PebbleCounts generates best-fit ellipses from manually selected segments, and measures ellipse diameter along and perpendicular to the longest axis (assumed to be a- and b-axis grain diameter, respectively), segment area, and ellipse area (Purinton and Bookhagen, 2019).

I modified pre-processing scripts from Purinton and Bookhagen (2021) to divide SfM-derived orthoimages into 4000- by 4000-pixel tiles and perform manual PebbleCounts. PebbleCounts includes automatic image filtering functionality, which does not require extensive user input. However, in preliminary analyses, automatic image filtering produced inaccurate results compared to manual K-means segmentation-based PebbleCounts. I use b-axis grain diameter and ellipse area outputs from PebbleCounts to generate area-weighted grain size distributions. In principle, this method is similar to traditional field-based pebble count and grid count methods of quantifying surface grain size distribution, where the number of measured particles is determined by the number of grains that are successfully delineated by k-means segmentation (Bunte and Abt, 2001).

The PebbleCounts method provides a robust characterization of surface grain size distributions, with several limitations. I note that grain size measurements only capture exposed portions of channel bars, but 2016, 2021, and 2022 SfM surveys took place during the lowest flows of the year with the highest possible bar exposure. I also note that this method does not capture grains with segments that include fewer than 20 pixels. As such, there exists a lower threshold for measured grains that is dependent on pixel resolution. My grain size analyses do not capture grains with b-axis diameters smaller than approximately 0.025 m; this value remains relatively constant across all study reaches and timesteps.

Quantifying the grain size distribution in Upper Big Creek and Devil's Creek before and after post-fire disturbance provides insight into channel dynamics. I use PebbleCounts-generated grain size distributions to estimate sediment transport capacity and channel stability before and after post-fire disturbance in Upper Big Creek and Devil's Creek. I describe these calculations in sections 2.5 Sediment Transport Capacity, and 2.6 Astab, below.

2.4 Hydrologic Analyses and Hydraulic Modeling

To ensure that comparisons between SfM data products capture geomorphic change rather than hydrologic change, discharge during 2016, 2021, and 2022 SfM survey periods must be comparable. In one geomorphically unchanged reach in Devil's Creek, I observe little change in water surface extent between 2016, 2021, and 2022 orthoimages. Thus, I assume that flow differences during 2016, 2021, and 2022 SfM surveys are negligible and measured grain size differences between 2016, 2021, and 2022 SfM datasets are not related to changes in exposed bar area due to lower or higher flows on days photos were collected.

Calculations of sediment transport capacity and channel stability metrics require an estimate of bed shear stress. HEC-RAS is a hydraulic modeling tool developed by the U.S. Army

Corps of Engineers that models open channel flow in 1- and 2-dimensions. I use HEC-RAS to model steady flow in 1-dimension and approximate reach-averaged bed shear stress under pre- and post-fire hydrologic and morphologic conditions for SfM study reaches in Upper Big Creek and Devil's Creek. I input two simulated peak flow discharges from Li et al. (2022) for both Upper Big Creek and Devil's Creek into HEC-RAS (Figure 5). Li et al. (2022) modifies WRF-Hydro, a physics-based weather and hydrologic forecasting model, to simulate streamflow in four burned watersheds in coastal California, including the Big Creek watershed. Li et al. (2022) presents two streamflow simulations for the rainfall event that took place between January 26th and 29th, 2021, which triggered post-fire debris flows in Big Creek. They present a burn-scar simulation, which accounts for post-fire hydrologic changes, and a baseline simulation, which does not account for post-fire hydrologic changes. I use modeled discharges from model cells in Upper Big Creek and Devil's Creek just upstream of their confluence. USGS stream gauges surrounding Big Creek record between a 1 and 5-yr recurrence interval peak flow on January 27th - 28th (Figure 2), and thus I assume that the baseline peak flow for Upper Big Creek presented in Li et al. (2022) represents peak flow in the 1-5 yr range of recurrence intervals.

I run HEC-RAS using infrared lidar from 2015 to simulate pre-fire channel geometry, and infrared lidar from 2022 to simulate post-fire conditions. Infrared lidar does not penetrate the water surface; as such, our HEC-RAS flow model is superimposed upon the low flow water surface in Upper Big Creek and Devil's Creek. Precipitation data from within the Big Creek watershed suggests that both 2015 and 2022 lidar datasets were collected during low flow periods (Figure 3).

Study reaches in Upper Big Creek and Devil's Creek have step pool/cascade morphology, and median grain sizes greater than 256 mm. I assign a uniform Manning's

roughness coefficient of 0.045 $m^{1/6}$ for channel beds prior to the Dolan Fire in Upper Big Creek and Devil's Creek based on these characteristics (Arcement and Schneider, 1989). Hydraulic roughness decreased throughout Big Creek following post-fire debris flows via the influx of fine material and increased by 2022 as bed surface grain size coarsened. I apply a Manning's roughness coefficient of 0.037 $m^{1/6}$ for 2021 model runs and a Manning's roughness coefficient of 0.041 $m^{1/6}$ for 2022 model runs in Upper Big Creek to account for systematic variability in roughness through time (Arcement and Schneider, 1989). I maintain a constant Manning's roughness coefficient in Devil's Creek for all timesteps, as post-fire changes in the surface grain size distribution were minimal. Study reaches in Upper Big Creek and Devil's Creek are generally confined and do not have established floodplains, but valley walls in Big Creek and Devil's Creek are moderately vegetated and often contain *Acer macrophyllum* (Bigleaf Maple) and *Sequoia sempervirens* (Coast Redwood) that provide considerable flow resistance. I assign a uniform Manning's roughness coefficient of 0.105 for valley walls based on these characteristics (Arcement and Schneider, 1989). Flow parameters for channels in the Big Creek watershed are difficult to constrain and are likely a source of error in sediment transport capacity and channel stability calculations. See 4.4 Sources of Error for further discussion of potential error in hydraulic, sediment transport capacity, and channel stability models.

2.5 Sediment Transport Capacity

Sediment transport capacity is a function of grain size and shear stress, both of which changed following post-fire debris flows in Big Creek. Wilcock and Crowe (2003) provides an empirically based system of equations to estimate sediment transport capacity as a function of grain size distribution, bed shear stress, and critical Shields stress for the mean grain size (referred to as reference Shields stress in Wilcock and Crowe (2003)). I use PebbleCounts-

generated grain size distributions and reach-averaged bed shear stresses from pre- and post-fire HEC-RAS flow models to calculate volumetric sediment transport capacity for each reach in Big Creek and Devil's Creek (Table 1). I note that for post-fire sediment transport capacity models, surface grain size distribution and hydraulic roughness evolve from 1 year to 2 years post-fire, while channel geometry remains constant. This method provides the best possible approximation of actual channel conditions, given that 2021 lidar coverage of the Big Creek watershed does not exist. Modest flows in Big Creek between 2021 and 2022 data collection periods certainly reworked channel bedforms and sediment patches but did not mobilize boulders. Big Creek is boulder-rich and heavily confined by bedrock valley walls; these immobile hard-points are the primary controls on reach-scale channel geometry. As such, I assume any differences in channel geometry between 2021 and 2022 are inconsequential.

Wilcock and Crowe (2003) provides a function for critical Shields stress which requires knowledge of the bed surface sand fraction, which I do not quantify in PebbleCounts-generated grain size distributions. Instead, I use a slope-dependent function for critical Shields stress (τ^*_c) in steep mountain channels, modified from Prancevic and Lamb (2015):

$$\tau_c^* = 0.39S^{0.44} \quad (1)$$

where S is the reach-averaged channel slope. Prancevic and Lamb (2015) use the tangent of the slope angle (θ), but channel slopes throughout my study area are low enough such that the small-angle approximation is appropriate, and S is equivalent to tan(θ).

In a submerged channel bed with a non-uniform grain size distribution, larger grains protrude further from the bed surface, and thus a larger portion of a grain's surface area is

exposed to flow (Einstein, 1950; Diplas, 1987). In effect, larger grains hide smaller grains from shear stress exerted by flowing water. As such, grains at the coarse end of the grain size distribution are more easily transported than their smaller counterparts when size is accounted for. Wilcock and Crowe (2003) provides a hiding function to account for this phenomenon when calculating reference shear stress for a given grain size fraction (τ_{ri}) (Eq. 2, 3, 4).

$$\frac{\tau_{ri}}{\tau_{rm}} = \left(\frac{D_i}{D_{sm}}\right)^b \tag{2}$$

Where D_i is b-axis length for size class i (m), D_{sm} is mean bed surface b-axis length (m), and τ_{rm} is reference shear stress (Pa):

$$\tau_{rm} = (S-1)\tau_c^* \rho g D_{sm} \tag{3}$$

Where S is channel slope (dimensionless), ρ is density of water (kg/m^3), g is acceleration due to gravity (m/s^2), and:

$$b = \frac{0.67}{1 + \exp\left(1.5 - \frac{D_i}{D_{sm}}\right)} \tag{4}$$

Wilcock and Crowe (2003) describes dimensionless transport rate (W_i^*) for each size class as a function of the ratio between bed shear stress and the reference shear stress for each size class (Eq. 5, 6).

$$W_i^* = \begin{cases} 0.002\phi^{7.5} \\ 14\left(1 - \frac{0.894}{\phi^{0.5}}\right)^{4.5} \end{cases} \quad (5)$$

Where:

$$\phi = \frac{\tau}{\tau_{ri}} \quad (6)$$

Where τ is reach-averaged bed shear stress (Pa). I use this dimensionless transport rate to calculate volumetric sediment transport rate (q) in Big Creek and Devil's Creek (Eq. 7).

$$q = \frac{W_i^* F_i u_*^3 w}{(S-1)g} \quad (7)$$

Where F_i is the proportion of size i on the bed surface, w is flow width, and u_* is shear velocity ($u_* = [\tau/\rho]^{0.5}$).

2.6 A_{stab}

Channel stability for a given discharge is dependent on the mobility of bed surface sediment. If the surface grain size distribution in channels throughout the Big Creek watershed changed following the Dolan Fire, channel stability likely evolved in tandem with grain size. A_{stab} is a metric for channel stability that refers to the proportion of a channel bed that is immobile at a given shear stress (Eaton et al., 2020). A_{stab} is predicated on the idea that a subset of immobile grains can maintain channel stability even when the dimensionless shear stress

associated with D_{50} exceeds the threshold for motion (Eaton et al., 2020). I use grain size distributions from 2016, 2021, and 2022, reference shear stress for each grain size class (Eq. 2), and channel bed shear stress from HEC-RAS flow modeling to calculate A_{stab} in Big Creek and Devil's Creek in 2016, 2021, and 2022. A_{stab} is equal to the sum of the fraction of each size class that is immobile under a given shear stress (Eq. 7, 8).

$$A_{stab} = \Sigma I_i F_i \tag{7}$$

Where F_i is the areal proportion of size i on the bed surface, and the fraction of grains that are immobile for a given flow (I_i) is:

$$I_i = 1 - \left(\frac{1}{1 + exp\left(-4.3\left(\frac{\tau}{\tau_{ri}} - 1.5\right)\right)} \right) \tag{8}$$

2.7 Lidar and Topographic Differencing

Pre-fire near infrared lidar datasets for Big Creek and Devil's creek were collected for two National Center for Airborne Laser Mapping (NCALM) sponsored projects in 2011 and 2015 (OpenTopography, 2013, 2017). In 2022, NCALM collected a post-fire near infrared lidar dataset, encompassing Big Creek, Devil's Creek, Cathedral Creek, and Brunette Creek (OpenTopography, 2023). 2011, 2015, and 2022 lidar surveys yielded vertical accuracies of 0.20, 0.15, and 0.1 m, respectively, and point densities of 10 pts/m^2. NCALM classified ground point

returns for each survey and generated 1 m-resolution digital terrain model raster datasets (DTMs) using a Kriging algorithm (OpenTopography, 2013, 2017, 2022).

I use DTM differencing to identify zones of significant geomorphic change in Big Creek, Devil's Creek, Cathedral Creek, and Brunette Creek. Before conducting differencing, I generated high-resolution 3-dimensional meshes from 1-meter DTMs and co-registered meshes to one another using an iterative closest point algorithm. I use Geomorphic Change Detection (GCD) Software (Bailey et al., 2020) to generate a DEM of difference (DoD) between 2011 and 2022 lidar-generated, co-registered digital terrain models. I interpret positive values in my DoD as deposition, and negative values in my DoD as incision.

To minimize noise captured in my DoD, I created homogenous maximum vertical error surfaces for each lidar dataset and used GCD's probabilistic thresholding functionality to capture topographic change that exceeds a 99% probability threshold (Bailey et al., 2020). I restrict DTM differencing analyses to channels and channel margins in Big Creek, Devil's Creek, Cathedral Creek, and Brunette Creek; steep valley walls in the Big Creek watershed exacerbate any co-registration error between lidar datasets and are thus more likely to produce inaccurate DoD values. As such, DTM differencing analyses presented here do not capture hillslope contributions. Notably, my differencing analyses do not capture topographic change from dry ravel outside of channels, which is a well-documented post-fire sediment loading mechanism and likely played a substantial role in priming channels in the Big Creek watershed for post-fire debris flows.

I also conduct differencing between 2011 and 2015 lidar datasets to better understand regular channel dynamics and identify geomorphic change specifically associated with 2021 post-fire debris flows in Big Creek. I note systematic distortion between 2015 and 2011 lidar

datasets towards the edge of the 2015 DTM; as such, areas in which I observe major distortion are not included in differencing analyses. I validated the results of DTM differencing using field photos and observations from 2016 and 2021 field campaigns. Identifying hotspots of geomorphic change in Big Creek, Devil's Creek, Cathedral Creek, and Brunette Creek provides insight into how river networks accommodate anomalous post-fire sediment loads, from colluvial hollow to river outlet.

3.0 Results

3.1. Field Observations

Field observations throughout Big Creek, Brunette Creek, and Cathedral Creek provide insight into the physical characteristics of post-fire debris flows in the Big Creek watershed. Scour marks on sturdy trees along channel margins in Big Creek suggest flow heights up to 4 m above the current channel bed during 2021 post-fire debris flows (Figure 6D). In Brunette Creek, up to 3 m of incision occurred just upstream of its confluence with Upper Big Creek (Figure 6A). Throughout Upper Big Creek, I observed extensive deposition of poorly sorted terraces up to 1 meter in height, composed of sand to large boulders (Figure 6B). Immediately downstream of Big Creek's confluence with Brunette Creek, post-fire debris flows have emplaced a valley-wide log jam, approximately 6 m tall and 35 m wide (Figure 6C). I also observed a valley-spanning, boulder-rich wedge of sediment built up behind the log jam (Figure 6B). Downstream of Big Creek's confluence with Devil's Creek, freshly deposited terraces up to 1.5 m tall flank the channel in many places (Figure 6E). Terraces in Lower Big Creek tend to be composed of sand to cobbles, with some small boulders interspersed throughout. In general, the grain size distribution of debris flow-related deposits in Big Creek becomes finer with distance downstream.

Post-fire debris flows in Big Creek had substantial impacts on channel morphology and low-flow hydraulics. Immediately following post fire debris flows, debris flow terraces and swaths of sand, gravel, and cobbles replaced bouldery, vegetated banks throughout Upper Big Creek. Large wood and dense riparian vegetation were largely absent in Big Creek immediately following 2021 post-fire debris flows. Several large, deep pools in Upper Big Creek surveyed in 2016 no longer existed in 2021. Sediment patches in Big Creek became more abundant, finer, and less uniform in Big Creek following post-fire debris flows. These changes amounted to substantial decreases in low-flow hydraulic complexity and average wetted width immediately following the Dolan Fire (Figure 7). Additionally, several large boulders that were present in 2016 were no longer present in 2021, and multiple new boulders have been deposited and/or exhumed throughout Big Creek.

In 2022, many of the drastic post-fire geomorphic features in Big Creek appeared to have begun a gradual return towards pre-fire conditions. Pioneer riparian species have re-colonized channel margins and mid-channel bars throughout Big Creek. Gravel patches, while still more abundant than in 2016, became coarser and more uniform in grain size (Figure 7). In Upper Big Creek, much of the sand that was deposited during 2021 debris flows was evacuated between 2021 and 2022 surveys. Average wetted width also increased from 2021 to 2022 (Figure 7). These changes amount to increased hydraulic complexity and morphologic diversity throughout Big Creek. In Lower Big Creek, widespread debris flow terraces receded substantially, and in some areas, completely by 2022. In general, 2022 field observations indicate partial, but widespread reversals of sweeping post-fire geomorphic change in Big Creek.

Comparatively, Devil's Creek appeared to have experienced considerably less geomorphic change following the Dolan Fire. Pools, boulders, large wood, and dense riparian

vegetation were still widespread throughout the channel bed and banks in Devil's Creek during both 2021 and 2022 surveys. Following the Dolan Fire, several isolated swaths of fine sediment were deposited at the base of valley walls surrounding Devil's Creek but had not been incorporated into the channel as of 2022. In 2022, some sediment patches in Devil's Creek became finer, but reach-scale channel structure remained unchanged.

3.2. Topographic Differencing

Topographic differencing between 2011 and 2022 datasets records substantial systematic topographic change throughout the Big Creek watershed. Both Cathedral and Brunette Creek are dominated by systematic scour, with large failures visible in multiple locations down the length of both channels (Figure 8A, B, D, E). Cumulatively, Cathedral and Brunette Creek lost approximately 32,000 m^3 of material between 2011 and 2022; I infer that the majority of this material was lost via scour during 2021 post-fire debris flows. Cathedral Creek exported approximately 22,690 m^3 of material, while Brunette Creek exported approximately 8,950 m^3 of material. The final 200 m of Cathedral Creek lost approximately 6,550 m^3 of material, with a maximum of 5 m of incision from 2011 to 2022; this area exhibits the greatest magnitude of incision per unit area within my lidar study area (Figure 8B).

Upstream of its confluence with Brunette Creek, Upper Big Creek is largely characterized by net deposition (Figure 9). One prominent depositional hotspot lies approximately 250 m downstream of Big Creek's confluence with Cathedral Creek (Figure 9A). This large stretch of channel accumulated approximately 5,270 m^3, and exhibits a maximum elevation increase of 3.5 m and an average increase of 0.21 m per unit area within the channel between 2011 and 2022. The most notable depositional feature in Big Creek is located behind the valley-spanning log jam at Big Creek's confluence with Brunette Creek (Figure 6, Figure 9B).

Cumulatively, 3300 m^3 of material was deposited behind the log jam between 2011 and 2022, with a maximum observed increase of 5 m. Accumulation behind this log jam accounts for 10% of total material exported from Cathedral and Brunette Creek, and 37% of total material deposited upstream of Big Creek's confluence with Brunette Creek. Deposition behind this valley-spanning log jam accounts for the greatest magnitude of deposition per unit area within my lidar study area.

Downstream of its confluence with Brunette Creek, Upper Big Creek is largely dominated by incision (Figure 10C). The most notable erosional feature lies 200 m downstream of the confluence with Brunette Creek, where debris flows removed a large log jam and incised into alluvium built up behind this log jam. Approximately 980 m^3 of material was removed from the area between 2011 and 2022, with maximum local incision of approximately 4.5 m and an average of 0.19 m of incision per unit area within the channel.

Lower Big Creek exhibits comparatively little change from 2011 to 2022 (Supplementary Figure 2C). Debris flood terraces, which are prevalent throughout Lower Big Creek, account for approximately 800 m^3 of accumulated material from Big Creek's outlet to approximately 300 m upstream, and exhibit a maximum elevation increase of 3 m. I note that terraces visible in my DoD don't convey the maximum terrace extent observed during 2021 field surveys, as they degraded considerably between 2021 field surveys and 2022 lidar surveys.

In Devil's Creek, topographic differencing reveals sporadic topographic change from 2011 to 2022. The most prominent depositional features in Devil's Creek exist along channel margins near the outlets of small drainages (Figure 10B). The largest of these features lies along a stretch of channel approximately 1,100 m upstream of the confluence of Devil's Creek and Big Creek; this reach gained approximately 1,300 m^3 of material between 2011 and 2022 (Figure

10B). Some sections of Devil's Creek exhibit localized incision, including one reach approximately 650 m upstream of the confluence of Devil's Creek and Big Creek which lost approximately 640 m^3 of material between 2011 and 2022 (Figure 10C). Other sections of Devil's Creek appear to have been reworked, with localized aggradation and incision but little net export or import of material (Figure 10A). Cumulatively, the lower 5 km of Devil's Creek gained approximately 444 m^3 of material between 2011 and 2022, or 0.03 m per unit area within the channel. In general, Devil's Creek does not appear to have experienced widespread systematic aggradation or incision in response to the Dolan Fire.

Topographic differencing between 2011 and 2015 lidar datasets indicates some topographic change from 2011 to 2015, but changes are minor and appear to be far less systematic in comparison to differencing between 2011 and 2022 DTMs (Supplementary Figure 4). I note that 2015 lidar coverage of Big Creek does not include Cathedral Creek, Brunette Creek, or the upper- and lower-most sections of Big Creek, and thus I do not include those portions of the basin in this analysis.

3.3 Results of Structure from Motion Surveys

2016, 2021, and 2022 SfM surveys yielded high-resolution orthoimagery of Big Creek and Devil's Creek. SfM surveys produced orthoimages with pixel resolutions ranging from 1.0 to 1.9 mm across all study reaches and survey periods (Figure 7). Georeferencing successfully corrected minor scale differences between 2016, 2021, and 2022 orthoimagery. 2016, 2021, and 2022 SfM surveys made use of 12-bit coded targets with consistent diameters to aid in SfM photo alignment. I use these targets to detect lingering scale distortion in the resulting orthoimagery after georeferencing. Target diameters across 2016, 2021, and 2022 orthoimages are consistent in all but two 2022 orthoimages in Devil's Creek. For these improperly scaled

images, I apply a correction factor based on the ratio of mean target radius in incorrectly scaled orthoimages to mean target radius in correctly scaled orthoimages for all grain size measurements. Mean target diameters fall within 1% of one another across all orthoimages, aside from 2 images for which I applied a correction factor (with mean scale differences of 3.5% and 4.1%). I note minor positional distortion between 2016, 2021, and 2022 orthoimages. I use SfM-generated orthoimages to evaluate changes in grain size alone, for which measurements are entirely scale-dependent and do not take absolute position into account. Thus, any minor positional distortion between orthoimages has negligible effects on the results that follow.

3.4. Grain Size

Both Big Creek and Devil's Creek contain grains ranging from sand to large boulders across all timesteps. I note that our orthoimage-based grain size distributions neglect sand, only encompassing grains from 0.02 m to 2.24 m. Both Big Creek and Devil's Creek generally exhibit downstream fining of the D_{16} and D_{50} across all timesteps, with few exceptions. In both Big Creek and Devil's Creek, pre-fire grain size distributions typically contain the coarsest D_{16} and D_{50} grain sizes (Table 2).

Post-fire debris flows triggered substantial change in bed surface grain size distribution across all three study reaches in Upper Big Creek. Grain size changes from 2016 to 2021 in Upper Big Creek are characterized by fining in the lower half of the grain size distribution (Table 2, Figure 11A, C, E). D_{16} fined substantially from 2016 to 2021 across all study reaches by an average of 0.22 m. D_{50} also fined across all study reaches from 2016 to 2021 by an average of 0.24 m (Table 2, Figure 11A, C, E, Figure 12). While both D_{16} and D_{50} exhibit similar trends across all reaches, study reaches in Upper Big Creek exhibit no pervasive patterns of change in D_{84}.

Grain size changes from 2021 to 2022 in Upper Big Creek are generally characterized by coarsening in the finer half of the grain size distribution (Table 2, Figure 11A, C, E, Figure 12). D_{16} and D_{50} coarsened across all study reaches by an average of 0.07 m and 0.20 m, respectively. Average D_{84} increased marginally but did not change systematically across all reaches from 2021 to 2022. In general, Upper Big Creek exhibits no pervasive longitudinal trends in bed surface grain size change. Notably, the middle reach in Upper Big Creek exhibited the highest magnitude of D_{16} and D_{50} fining immediately following disturbance and the highest magnitude of D_{16} coarsening from 2021 to 2022 (Figure 11C).

Devil's Creek exhibited far less pronounced changes in surface grain size distribution following the Dolan Fire (Table 3, Figure 11B, D, F). Like Upper Big Creek, changes in Devil's Creek's grain size distribution are most apparent in the finer half of the grain size distribution. D_{16} became marginally finer in all Devil's Creek study reaches from 2016 to 2021. The magnitude of D_{16} fining decreased with distance downstream. D_{50} and D_{84} exhibited no systematic change across study reaches in Devil's Creek from 2016 to 2021 (Table 3, Figure 11B, D, F). From 2021 to 2022, D_{16} remained constant across all study reaches. D_{50} became marginally finer in two study reaches and remained constant in one reach; fining of the D_{50} decreased downstream from 2021 to 2022. Average D_{84} also became marginally finer, but did not exhibit systematic change across all three study reaches in Devil's Creek (Table 3, Figure 11B, D, F).

3.5. Hydraulic Modeling

1-D hydraulic modeling in HEC-RAS produced reach-averaged bed shear stresses and flow widths for modeled high flow events under baseline and burn-scar conditions in Big Creek and Devil's Creek. Pre-fire, modeled, reach-averaged shear stresses in Big Creek range from 343

to 562 Pa, while reach-averaged wetted widths range from 8.30 to 12.6 m. Hydraulic modeling which assumes no post-fire changes in peak flow discharge yields decreases in reach-averaged shear stress and increases in flow width 1-year post-fire, which result from both morphologic changes recorded between lidar surveys and decreased hydraulic roughness from grain size fining. 2-years post-fire, Upper Big Creek exhibits marginal increases in shear stress and flow width, which stem from hydraulic roughness increases via re-coarsening of the bed surface (Figure 13A, C). Hydraulic modeling which accounts for elevated post-fire peak flow discharge yields substantial increases in reach-averaged shear stresses and flow widths 1-year post-fire, followed by marginal increases in shear stresses and negligible change in flow width 2-years post-fire (Figure 13A, C).

In Devil's Creek, hydraulic modeling which does not account for post-fire hydrologic change yields minimal change in shear stress and flow width from pre-fire to 1- and 2-years post-fire conditions. Hydraulic modeling which does account for post-fire hydrologic change yields substantial increases in both reach-averaged flow width and shear stress 1- and 2-years post fire (Figure 13B, D).

3.6. Sediment Transport Capacity

Sediment transport is a function of surface grain size distribution and bed shear stress. Thus, post-fire changes in sediment transport capacity reflect post-fire changes in surface grain size distribution, as well as the influences of evolving post-fire channel geometry, hydraulic roughness, and basin hydrology. In the following section, I present results from sediment transport capacity models which account for burn-scar-related changes in basin hydrology in both Big Creek and Devil's Creek. I also present results from sediment transport capacity models which do not account for burn-scar-related changes in basin hydrology. These baseline

simulations serve as a reference to highlight changes in sediment transport capacity that stem from post-fire geomorphic change, rather than hydrologic change. Results from sediment transport capacity models which do account for burn-scar-related changes in basin hydrology provide more realistic approximations of post-fire conditions in Big Creek.

Big Creek's sediment transport capacity response to post-fire debris flows is characterized by dramatic increases immediately following disturbance, followed by a partial recovery towards pre-fire conditions (Figure 14A*)*. Assuming no changes in post-fire peak flow discharge, cumulative modeled baseline sediment transport capacity in Upper Big Creek increases nearly 4-fold immediately following post-fire disturbance, with two of three reaches exhibiting considerable increases in sediment transport capacities. Accounting for post-fire elevated peak flow values, cumulative sediment transport capacity in Upper Big Creek increases 14-fold following the Dolan Fire; both the volume and maximum grain size of the modeled sediment transport load in Big Creek increase (Figure 14A, Figure 15A, C, E). Assuming no changes in post-fire peak flow discharge, modeled sediment transport capacity decreases across two of three reaches in Big Creek from 1-year post-fire to 2-years post-fire. Accounting for post-fire increases in peak flow discharge, sediment transport capacity decreases across all study reaches, while the grain size distribution of the modeled sediment load becomes coarser (Figure 14A, Figure 15A, C, E).

In Devil's Creek, channel geometry and hydraulic roughness remained relatively constant, and post-fire changes to the surface grain size distribution were generally less dramatic than in Big Creek. Initial post-fire increases in sediment transport capacity, however, are prominent across all reaches as pre-fire sediment transport capacities are close to zero (Figure 14B). Assuming no post-fire changes to basin hydrology, average sediment transport capacity in

Devil's Creek increases from near-zero to 0.6 m^3/s 1-year post-fire. Accounting for post-fire hydrologic change, average modeled sediment transport capacity increases from near-zero to 3.0 m^3/s 1-year post-fire; both the volume and grain size of the modeled sediment load increase 1-year post-fire (Figure 14B, Figure 15B, D, F). Sediment transport capacity models which do not account for post-fire hydrologic change yield marginal decreases in cumulative sediment transport capacity from 1-year to 2-years post-fire across all study reaches. Models which account for post-fire changes in hydrology yield a marginal increase in cumulative sediment transport capacity in Devil's Creek from 1-year to 2-years post-fire, with no pervasive trends across study reaches. The grain size distribution of the modeled sediment load in Devil's Creek remains largely unchanged from 1-year to 2-years post-fire (Figure 14B, Figure 15B, D, F).

3.7. Channel Stability

I estimate post-fire changes in channel stability using A_{stab}, which describes the areal fraction of the bed that is immobile during a given flow (Eaton et al., 2020). Post-fire bed surface grain size and hydrologic evolution in Big Creek precipitated substantial changes in channel stability, which mirror changes in sediment transport capacity (Figure 14C). Prior to the Dolan Fire and subsequent debris flows, study reaches in Upper Big Creek were highly stable, with A_{stab} values ranging from 0.93 to 0.97. Several decades of biannual field observations by NMFS fisheries biologists support this model result (T. Williams, personal communication, 2023). Accounting for changes in post-fire hydrology, A_{stab} decreases in all study reaches in Upper Big Creek by an average of 36%. 2-years post-fire, A_{stab} increases across all study reaches by an average of 18%. Approximations of A_{stab} in Upper Big Creek which do not account for post-fire hydrologic change yield similar, but less pronounced patterns, characterized by a substantial

increase in A_{stab} 1-year post-fire, followed by a lower-magnitude decrease 2-years post-fire (Figure 14C).

Like Upper Big Creek, all study reaches in Devil's Creek were exceptionally stable prior to the Dolan Fire, with A_{stab} values ranging from 0.96 to 0.98. A_{stab} decreases across all study reaches in Devil's Creek 1-year post-fire, regardless of hydrological conditions (Figure 14D). From 1-year to 2-years post fire, calculations which account for changes in post-fire hydrology yield no pervasive change in A_{stab} across all study reaches in Devil's Creek, while approximations of A_{stab} in Devil's Creek which do not account for post-fire hydrologic change yield increases in A_{stab} from 1-year to 2-years post-fire across all study reaches (Figure 14D).

Notably, for both burn scar and baseline peak flow simulations in Upper Big Creek and Devil's Creek, A_{stab} never reaches below 0.5. Even after substantial grain size fining, with peak flow magnitudes exacerbated by post-fire hydrologic conditions, this metric suggests relative channel stability during clearwater flows in both Upper Big Creek and Devil's Creek across all timesteps.

4.0 Discussion

4.1 Dilution from Post-fire Debris Flows to Debris Floods

Major debris flows in the Big Creek watershed initiated in Cathedral Creek and Brunette Creek during an atmospheric river event, which took place from January 26th to January 29th, 2021. A valley-spanning log jam was emplaced just downstream of the confluence of Big Creek and Brunette Creek during post-fire debris flows. Behind the log jam, a valley-wide, boulder-rich deposit potentially indicates where some debris flows in Upper Big Creek diluted to debris floods (Figure 6B). The log jam likely trapped large volumes of debris flow material, reducing the sediment/water ratio of the mixture and triggering dilution to debris flood. The log jam

continues to trap sediment from upstream, limiting sediment supply in Upper Big Creek below the Brunette Creek confluence. Terraces near the outlet of Lower Big Creek are composed of sand to cobbles; boulders are largely absent from these downstream terraces (Figure 6E). Deposits that make up these downstream terraces resemble characteristic debris flood deposits, rather than debris flow deposits (Church and Jakob, 2020). As such, any debris flows that traveled through Upper Big Creek before log jam emplacement likely diluted to debris floods at, or downstream of Big Creek's confluence with Devil's Creek.

4.2 Differences between Devil's Creek and Big Creek

Differences in connectivity and burn severity likely explain the disparate fluvial responses to wildfire in Devil's Creek and Upper Big Creek, two otherwise similar environments. Connectivity describes the efficiency of material flux between components of a geomorphic system (Wohl et al., 2019). With respect to the post-fire geomorphic evolution of Upper Big Creek and Devil's Creek, I discuss connectivity between stream channels and post-fire sediment sources like hillslopes, gullies, and colluvial hollows. Upper Big Creek is incised into a narrow, tightly confined canyon, in which steep valley walls often serve as channel margins. Devil's Creek sits in a much broader valley, with similarly steep valley walls that are often up to 30 m away from the channel itself. As such, a typical reach in Upper Big Creek exhibits greater connectivity to hillslope sediment sources than a typical reach in Devil's Creek. (Figure 16). In Devil's Creek, deposits at the base of gullies adjacent to the channel indicate substantial post-fire sediment delivery to the valley, but a lack of sweeping geomorphic change and structural reorganization in the channel itself suggests no debris flows passed through the channel itself in the two years following the Dolan Fire.

Compounding upon differences in connectivity between Upper Big Creek and Devil's Creek, burn severity also varied between sub-basins. Burn severity is a significant control on post-fire sediment yield (Benavides-Solorio and MacDonald, 2001; Shakesby and Doerr, 2006). Fire intensity partially dictates the degree to which vegetation and litter are removed from hillslopes, which governs sediment delivery to the fluvial system (Shakesby and Doerr, 2006). Differenced normalized burn ratio (dNBR) is a spectral index for burn severity that is dependent on reflectance in near infrared (NIR) and shortwave infrared (SWIR) wavelengths (Keeley, 2009). Living, healthy vegetation typically exhibits high reflectance in NIR wavelengths, and low reflectance in SWIR wavelengths; burned areas typically exhibit low reflectance in NIR wavelengths and high reflectance in SWIR wavelengths (Keeley, 2009). Following the Dolan Fire, mean dNBR in the Upper Big Creek watershed was 35% greater than in the Devil's Creek watershed (Supplementary Figure 5). Thus, burned hillslopes surrounding Devil's Creek likely contributed less sediment than burned hillslopes surrounding Upper Big Creek.

4.3 Controls on Sediment Transport Capacity

Post-fire changes in sediment transport capacity and channel stability stem from changes to basin hydrology and channel morphology (surface grain size, channel geometry and hydraulic roughness). To evaluate each variable's respective influence on post-fire sediment transport capacity, I conduct a simple sensitivity analysis, comparing my best approximation of sediment transport capacity through time in Upper Big Creek to scenarios in which each variable remains constant at pre-fire conditions, while the others evolve over time.

In Big Creek, post-fire changes in bed surface grain size distribution are responsible for considerable increases in sediment transport capacity 1-year post-fire (Figure 17A). Additionally, bed surface coarsening is entirely responsible for decreases in sediment transport capacity 2-

years post-fire. This result supports my initial hypothesis; post-fire changes in grain size do indeed have cascading effects on channel dynamics in Upper Big Creek. Post-fire changes in channel geometry recorded in repeat lidar surveys have highly variable effects on post-fire sediment transport capacities in Big Creek (Figure 17C), but do not appear to exert any systematic influence on sediment transport capacity. Changes in hydraulic roughness serve as a negative feedback on post-fire sediment transport capacity evolution in Upper Big Creek, dampening both the initial response signal and the recovery signal (Figure 17E). As bed surface grain size becomes finer, hydraulic roughness decreases, which in turn reduces bed shear stress and sediment transport capacity. As the bed surface grain size coarsens, hydraulic roughness increases, which increases bed shear stress and sediment transport capacity.

In Devil's Creek, grain size change does not account for the majority of post-fire sediment transport increases 1-year post-fire. Rather, post-fire increases in discharge account for most of the modeled sediment transport capacity increase 1-year post fire, while marginal grain size change accounts for minor variance in sediment transport capacity 2-years post-fire (Figure 17D). Unlike Big Creek, post-fire changes to channel geometry in Devil's Creek do appear to subtly amplify post-fire increases in sediment transport capacity increases across all study reaches (Figure 17D).

4.4 Sources of Error

Possible sources of error in sediment transport capacity calculations stem from necessary geomorphic assumptions in my analysis. Remotely-sensed bed surface grain size distributions are representative of boulders that protrude out of the water surface and bars exposed at low flow. Surface grain size distributions exclude any submerged particles, and any particles smaller than approximately 2.5 cm. Thus, my sediment transport capacity calculations rely on bed

surface grain size distributions which do not include fully submerged particles or particles smaller than 2.5 cm. Post-fire disturbance introduced large volumes of sand and fine gravel, much of which had diameters smaller than 2.5 cm. I assume that most grains smaller than 2.5 cm are transported in suspension during flows for which I model sediment transport capacity, but the exclusion of particles smaller than 2.5 cm may be responsible for a considerable underestimation of 1-year post-fire sediment transport capacity. Wetted width decreased following post-fire disturbance in Upper Big Creek, and thus the percentage of bed surface grains that were submerged decreased marginally. I assume any error stemming from differences in the percentages of submerged particles on the bed surface are inconsequential, as 2016 total wetted area across study reaches in Upper Big Creek is only 13% greater than 2021 total wetted area.

Hydraulic modeling, while ultimately necessary for sediment transport capacity and channel stability models, may also introduce considerable uncertainty. See section 2.4 Hydrologic Analyses for a detailed discussion of limitations associated with hydraulic modeling methods used in this study. Importantly, studies from other sites suggest that the hydrologic impact of wildfire subsides over time, with some watersheds exhibiting 95% recovery within 7 years (Wagenbrenner et al., 2021). Timescales of post-fire hydrologic recovery are dependent on several variables, including post-fire precipitation patterns, aspect, and burn severity (Kinoshita and Hogue, 2011). Following the 2009 Station Fire in Southern California, hillslopes in the Arroyo Seco watershed (approximately 350 km southeast of Big Creek, and of similar size to the Big Creek watershed) exhibited substantial decreases in modeled saturated hydraulic conductivity within one year after the fire, followed by persistent increases towards pre-fire conditions for 5 years post-fire, at which point modeled saturated hydraulic conductivity had returned to pre-fire conditions (Liu et al., 2021). Burn scar modeled discharges for Upper Big

Creek and Devil's Creek reflect hydrologic conditions immediately after the Dolan Fire. Thus, model hydrographs for Upper Big Creek and Devil's Creek likely represent reasonable peak flows for 1 year after the Dolan Fire. By 2 years after the Dolan Fire, however, hydrologic conditions had potentially recovered considerably. Realistically, 2-year post-fire hydrologic conditions likely exist between baseline and burn scar discharge values used here.

4.5 Partial Post-fire Sediment Budget

Volumetric change analyses from topographic differencing provide the foundation for a partial post-fire sediment budget for channels in the Big Creek watershed. Total material export from Cathedral and Brunette Creek serves as a lower bound for post-fire debris flow volumes. Cathedral and Brunette Creek exhibit approximately 32,000 m^3 of scour between 2011 and 2022 (Figure 18); this value falls within the range of previously documented for post-fire debris flow volumes (Gatwood et al., 2000; Pak and Lee, 2008; Gartner et al., 2014; Oakley et al., 2023). I note that this analysis does not account for material that was deposited in Cathedral and Brunette Creek between the onset of the Dolan Fire and post-fire debris flows. This invisible, through-flowing sediment load likely accounts for a considerable portion of total post-fire sediment yield; following the Dolan Fire, dry ravel likely loaded Cathedral and Brunette Creek, priming channels for post-fire debris flows (Dibiase and Lamb, 2020). Furthermore, my analysis also fails to quantify post-fire sediment contributions from Upper Big Creek upstream of its confluence with Cathedral Creek.

Approximately 8,800 m^3 of deposited material remained in the reaches downstream from these two tributaries by 2022 (Figure 18). An overwhelming majority of debris flow material remaining resides in Upper Big Creek, upstream of the large jam just below the confluence with Brunette Creek. Under the assumption that scour volumes in Cathedral and Brunette Creek

reasonably approximate post-fire debris flow volume, 72% (or approximately 23,000 m^3) of post-fire debris flow material sourced from Cathedral and Brunette had exited the fluvial system by 2022 (Figure 18). This suggests that, while post-fire debris flows triggered sweeping change to channel dynamics and morphology throughout Big Creek, residence time for most debris flow-related sediment in Big Creek was quite brief.

4.6 Timescales of Post-fire Fluvial Recovery

Upper Big Creek experienced rapid geomorphic recovery following post-fire debris flows. Within 2-years after the Dolan Fire, D_{16} and D_{50} had re-coarsened substantially across all study reaches in Upper Big Creek; by 2022, average D_{50} coarsened to 95% of pre-fire D_{50}. Furthermore, I estimate that, by volume, 72% of post-fire sediment contributed by colluvial hollows in which debris flows initiated had exited the watershed by 2022. This largely contradicts my initial hypothesis, in which I suggest that fire-related morphologic change in Upper Big Creek would be reversed slowly, over multiple wet seasons. An overwhelming majority of debris flow material remaining in the watershed is stored upstream of the Brunette Creek log jam.

6 months after 2022 SfM data collection, a bomb cyclone event triggered widespread flooding across California. The USGS stream gauge near the outlet of the Carmel River, approximately 50 km north of Big Creek, recorded a 10-year recurrence interval flood. Qualitative field observations following the 2023 flood event indicate further coarsening of the bed surface grain size distribution downstream of the Brunette Creek log jam and erosion of debris flood terraces in Lower Big Creek (M. Readdie, personal communication, 2023). Whereas reaches in Upper Big Creek downstream of the Brunette Creek log jam exhibit strong recovery

signals toward pre-fire channel morphology following these floods, the area just upstream of the log jam has experienced continued aggradation.

While there has been little published work surrounding the magnitude and timescales of fluvial recovery from post-fire debris flows, recent studies surrounding dam removals (scheduled events with ample opportunity to collect pre-event baseline datasets) may serve as a comparison point for my findings in Big Creek. In general, rivers are quite resilient to sediment pulses from dam removals, typically regaining stability within several years (Major et al., 2017). In the following section, I summarize work surrounding fluvial responses to two major dam removals that may serve as relevant analogs for post-fire debris flows in Big Creek.

The Carmel River watershed encompasses 650 km^2 of the Santa Lucia Mountains along California's central coast, roughly 50 km north of Big Creek (East et al., 2023). Thus, the 2015 San Clemente dam removal on the Carmel River serves as an excellent climatic analog for post-fire disturbance in Big Creek. The San Clemente dam removal released approximately 65,000 m^3 of sediment into the Carmel River over 4 years. Following dam removal, bed surface sand fraction increased downstream of the dam; notably, fining was less prevalent in confined reaches. Approximately 6 years after the dam removal, sand fractions in reaches downstream of the former dam began to resemble pre-removal values (East et al., 2023). East et al. (2023) estimate less than 2 years of transit time for dam-derived sediment to reach the mouth of the Carmel River, approximately 30 km downstream of the Dam. While the dam removal delivered a similar volume of sediment to the Carmel River as Cathedral and Brunette Creek did to Big Creek, the Carmel River drains a far larger watershed than Big Creek. Whereas the San Clemente dam removal delivered approximately 150 tons of sediment per km^2 of watershed area,

post-fire debris flows in Big Creek delivered approximately 1400 tons of sediment per km^2 of watershed area, and thus associated sediment supply perturbations may not be analogous.

The Elwha River drains 833 km^2 on the north coast of Washington's Olympic Peninsula (East et al., 2018). The progressive removal of two dams on the Elwha River began in 2011; by 2014, both dams had been removed entirely. Dam removals re-introduced approximately 5 million m^3, or multiple decades worth of sediment yield, into the Elwha River, and thus potentially serves as an appropriate analog for post-fire sediment delivery in Big Creek (East et al., 2018). Dam removals on the Elwha River drastically altered channel morphology, triggering widespread aggradation and deposition of fine sediment downstream of dams. In two of their three study reaches, bed surface grain size had coarsened to pre-removal levels by 1-2 years after dam removal; but in one study reach, bed surface grain size remained finer than pre-disturbance conditions 5 years after dams were removed (East et al., 2018). Normalized by drainage area, dam removals on the Elwha River delivered approximately 6-times as much sediment as post-fire debris flows in Cathedral and Brunette Creek.

Dam removals along both the Elwha and Carmel rivers were engineered to mitigate catastrophic downstream response. As such, sediment pulses that followed the San Clemente and Elwha River dam removals were dispersed over the course of several years. Conversely, volcanic eruptions can introduce large volumes of sediment to steep drainage basins over a very short period. There exists an impressive body of work surrounding the fluvial response to the 1991 eruption of Mt. Pinatubo (e.g. Gran and Montgomery, 2005; Gran et al., 2011); these studies lack pre-disturbance baseline data, but still serve as another valuable comparison point for post-fire geomorphic evolution in Big Creek.

Gran and Montgomery (2005) present a conceptual model for post-eruption fluvial evolution which is largely applicable for fluvial recovery following post-fire debris flows in Big Creek. The first post-eruption phase is characterized by widespread lahars, and structural instability in disturbed channels (Gran and Montgomery, 2005). In Big Creek, this phase is analogous to the period between the end of the Dolan Fire and the first wet season after post-fire debris flows, during which debris flows overhauled bedforms and vertically restructured the channel. The post-eruption fluvial recovery phase begins once lahars stop occurring. In this phase, the fluvial system evacuates excess sediment delivered in the prior phase, progressively re-coarsening the bed surface grain size distribution in upper, then lower portions of the basin. As this phase continues, the bed surface re-armors, reducing sediment transport capacity (Gran and Montgomery, 2005). In Big Creek, this phase began during the first wet season after post-fire debris flows, during which routine high flows evacuated fines from the channel, re-coarsening the bed surface. In turn, this reduced sediment transport capacity and increased channel stability. This framework adequately captures the dominant processes and sequence of events governing post-fire geomorphic evolution in Big Creek; however, the timescales of post-fire evolution differ significantly between Big Creek and streams surrounding Mt. Pinatubo. Whereas the recovery phase began several years after Mt. Pinatubo's eruption, fluvial recovery in Big Creek began just 1 year after the Dolan Fire. Volumetric differences in post-disturbance sediment delivery to Big Creek and drainages surrounding Mt. Pinatubo account for much of this discrepancy, but the presence of the Brunette Creek log jam likely plays an integral role.

The rate at which channels recover from catastrophic sediment supply perturbations depends on the rate at which excess sediment is evacuated from the fluvial system (Gran and Montgomery, 2005). In Big Creek, an overwhelming majority of debris flow-derived sediment

remaining in the channel is stored upstream of the Brunette Creek confluence (Figure 9, Figure 18). Reaches in Upper Big Creek downstream of the Brunette Creek confluence, including reaches within my SfM study area, exhibit net incision relative to pre-fire conditions by 2022. The Brunette Creek log jam serves to trap large volumes of sediment from Cathedral Creek, effectively cutting off upstream sediment supply to Upper Big Creek. This, in conjunction with elevated sediment transport capacities from grain size change and post-fire basin hydrology, spurs rapid evacuation of fire-related sediment and post-fire morphologic recovery in Upper Big Creek, downstream of Brunette Creek. Importantly, although this study provides some insight into the rate of post-fire recovery in Big Creek, it does not capture the timescales of full post-fire geomorphic recovery.

Devil's Creek and Upper Big Creek exhibit vastly different timescales of post-fire geomorphic change. Upper Big Creek experienced extreme fining immediately following post-fire debris flows, followed by substantial coarsening 2-years post-fire. Conversely, Devil's Creek exhibits only minor fining 1-year post-fire, followed by very little change 2-years post-fire. The Dolan Fire is still responsible for additional sediment delivery to Devil's Creek, as evidenced by minor net aggradation and grain size fining. However, whereas the majority of post-fire sediment delivery in Big Creek happened during one event, post-fire sediment delivery to Devil's Creek is likely occurring more gradually as the channel slowly incorporates sediment deposited on channel margins. Devil's Creek's initial geomorphic response to the Dolan Fire resembles post-fire geomorphic change in Big Creek, only far less extreme; this result supports my initial hypothesis. However, unlike Big Creek, Devil's Creek did not exhibit a strong geomorphic recovery signal 2-years post-fire, which indicates a substantial difference in the timescales of post-fire sediment delivery between the two streams.

4.7 Debris Flows and Channel Reconfiguration

Large wood and boulders control channel structure in step pool streams (Keller et al., 2015; Hassan et al., 2023). Post-fire debris flows in Upper Big Creek mobilized large boulders and both introduced and removed wood into and from the channel, and thus were capable of reconfiguring the vertical structure of the channel. Large, immobile grains, often with diameters upwards of 1 m, govern step pool dynamics and vertical channel structure in Big Creek. My analysis suggests that clearwater floods alone are not capable of restructuring the channel. In Upper Big Creek, even under burn scar hydrologic conditions and after considerable bed surface fining, clearwater floods are not capable of mobilizing the coarse half of the grain size distribution, let alone these large keystones which support wood jams and make up steps (Figure 15). Furthermore, over 50% of the bed surface across all study reaches in Upper Big Creek remains stable at every timestep, regardless of hydrologic conditions. Eaton et al., (2020) found that experimental gravel- to cobble-bedded channels become unstable below a threshold A_{stab} value of approximately 15%. Long term field observations further corroborate that channels in the Big Creek watershed tend towards long-term vertical stability. Prior to the Dolan Fire, fish biologists conducting repeat O. Mykiss population surveys note the long-term persistence of steps and pools in Big Creek for over a decade (T.Williams, personal communication, 2023).

Topographic differencing analyses further support the long-term pre-fire stability in Big Creek, and the channel restructuring capabilities of post-fire debris flows. Topographic differencing between 2011 and 2015 lidar datasets indicates scattered, minor topographic change in Big Creek between 2011 and 2015 (Supplementary Figure 4). During this period, channel structure remained unchanged. Topographic differencing between 2011 and 2022 lidar datasets showcases sweeping geomorphic change and major adjustments to vertical structure in Big

Creek, wherein several existing steps were destroyed, and one new valley-wide bench was created (Figure 19, Figure 20). Considering the period of relative channel stability between 2011 and 2015, it is clear that the 2021 post-fire debris flows in Big Creek removed existing steps and emplaced new valley wide benches, reconfiguring the vertical structure of Big Creek (Figure 19, Figure 20). Low-frequency, high-magnitude events are required to enact large-scale changes to channel structure in step pool streams (Chin and Wohl, 2005; Lenzi et al., 2006; Hassan et al., 2023). I suggest that debris flow events are critical, and in some cases may be required, to overhaul vertical channel structure in steep, bouldery, step pool streams like Big Creek. In Big Creek, clearwater floods cannot generate the requisite force to restructure the channel, and thus high sediment transport rates and instability caused by grain size fining may be inconsequential for large-scale channel dynamics. However, regardless of implications for vertical channel structure, post-fire bed surface instability and elevated sediment transport rates likely have substantial implications for salmonid habitat in Big Creek.

4.8 Potential Ecological Implications

Post-fire geomorphic change in Big Creek has a myriad of potential implications for aquatic ecosystems and salmonid spawning habitat. Documenting the ecological impacts of post-fire debris flows is beyond the scope of this thesis, but the quantitative geomorphic data presented herein may be of use to fish biologists monitoring spawning habitat and O. Mykiss populations in the Big Creek watershed.

Post-fire debris flows had immediate adverse effects on salmonids in Big Creek, as debris flows took place during winter, when O. Mykiss typically return to freshwater habitats, and thus removed any fish in the channel. Following post-fire debris flows, Big Creek was largely inundated with fine sediment; excess fine sedimentation has adverse effects on spawning habitat.

Increased fine sediment loads in riverine ecosystems can smother salmonid spawning substrate and limit primary production, which reduces available food sources for salmonids (Kemp et al., 2011). The months following post-fire debris flows in Big Creek coincide with O. Mykiss spawning season, and thus the salmonid population in Big Creek likely suffered from a year of little to no production due to post-fire geomorphic disturbance. Furthermore, fining of the bed surface grain size distribution in Big Creek and post-fire changes in basin hydrology are responsible for channel instability and elevated sediment transport capacities, both of which increase the risk of redd scour, further reducing the areal percentage of the bed that is suitable for spawning. Additionally, several step-pools throughout Big Creek were buried during post-fire debris flows, eliminating integral resting habitat for salmonids and reducing habitat diversity as a whole (Everest and Meehan, 1981). Over longer timescales, however, salmonids may benefit from the introduction of new, suitably sized spawning gravels into a formerly marginal spawning habitat in Big Creek (Figure 21).

Notably, the presence of nearby Devil's Creek significantly improves recovery prospects for salmonids in the Big Creek watershed. Devil's Creek experienced far less geomorphic change than Upper Big Creek, and thus serves as a stable refuge habitat for salmonids in the Big Creek watershed. Fish can spend Upper Big Creek's dynamic geomorphic recovery period in Devil's Creek, and eventually return to what was once a marginal spawning habitat in Upper Big Creek, now refreshed with suitable spawning substrate. Ongoing O. Mykiss surveys in Big Creek and Devil's Creek will provide further insight into the fish population response to post-fire disturbance in the Big Creek watershed.

Previous work suggests that salmonids are uniquely resilient to catastrophic disturbance, but post-fire debris flows in Big Creek are responsible for a cascade of ecological impacts

beyond salmonid habitat. Post-fire debris flows in Big Creek removed large wood from long stretches of the channel. Wood serves to increase habitat diversity and modulate stream temperature; wood supply recovers on decadal timescales in headwater streams (Cover et al., 2010). Debris flows also simplified channel morphology, further decreasing habitat diversity and thus, biodiversity. Furthermore, debris flows are responsible for a period of geomorphic dynamism and unstable substrate in Big Creek, which may be detrimental to fluvial ecosystems (Foster et al., 2020). Thus, understanding the timescales of post-fire geomorphic recovery is critical in understanding the re-establishment of riparian and aquatic ecosystems in Big Creek.

4.9 Climate Implications

Geomorphic disturbance of the magnitude observed in Big Creek requires a combination of processes—wildfire followed by extreme precipitation. This combination of events will likely become more frequent in the future, via a variety of mechanisms (Cayan et al., 2008; Swain et al., 2018; Persad et al., 2020; Lukovic et al., 2021; Homann et al., 2022). Southern and Central California's already intensely seasonal climate has and will continue to become more seasonal (Lukovic et al., 2021; Swain, 2021). While total rainfall volume may not be predicted to change, the predicted shift towards drier autumns leaves dead and dormant vegetation more susceptible to burning for an extended period (Lukovic et al., 2021; Swain, 2021). Notably, dormant vegetation includes seasonal grasses which dominate ridgelines throughout the Big Sur region. This, coupled with projected temperature increases across California leaves the region increasingly susceptible to wildfire in the future (Cayan et al., 2008). Furthermore, extreme dry to wet transition periods, or climate whiplash events, are projected to become more frequent (Swain et al., 2018). Recently published paleoclimate research by Homann et al. (2022) links these climate whiplash events to periods of elevated wildfire occurrence.

Winter flood hydrographs along California's Central Coast are dominated by atmospheric river events (Dettinger, 2011). Climate models project an increase in extremes related to atmospheric river events, including an increase in years during which many atmospheric rivers take place, and atmospheric river events with above-average vapor capacity and transport (Dettinger, 2011). Coupled with more frequent climate whiplash events, this suggests that periods most susceptible to drought will more frequently be followed by periods during which major floods occur more frequently.

Increasingly frequent extreme disturbance events like post-fire debris flows in Big Creek bring about considerable ecological and geomorphic uncertainty. While salmonids tend to be remarkably resilient to major disturbance events, primary producers may suffer from repeat disturbance events, triggering cascading long-term effects on salmonid populations (Cover et al., 2010). Geomorphically, more frequent extreme disturbance events may lead to more frequent reorganization of channel structure in a channel that is accustomed to prolonged structural stability.

Since 1911, 17 fires have burned some portion of the Big Creek watershed. Including the Dolan Fire, 7 wildfires have burned over 20% of the basin, while 3 have burned over 95% of the basin over the past 110 years. Prior to the Dolan Fire, the 1999 Kirk Fire most recently burned 97% of the Big Creek watershed (Cal Fire, updated 2023). However, chapparal ecosystems, which dominate ridgelines in the Big Creek watershed, are susceptible to repeat fires over short (<5 years) return intervals (Lippitt et al., 2013). The Big Creek watershed itself demonstrates this short-term fire recurrence, as both the Gamboa Fire (which burned 25% of the basin) and Gorda-Rat Fire (which burned 100% of the basin) occurred within 4 years of one another. This thesis does not capture timescales of full post-fire geomorphic recovery, but Upper Big Creek's

preliminary recovery signal suggests that, in most instances, geomorphic recovery may outpace the wildfire return interval in the Big Creek watershed.

5.0 Conclusion

This study characterizes geomorphic response to post-fire debris flows in the Big Creek watershed— a steep basin along California's Central Coast. I find that steep tributaries contributed approximately 30,000 m^3 of material to Big Creek, which triggered substantial downstream fining of the bed surface grain size distribution and sweeping changes to channel dynamics. Increases in post-fire discharge and bed surface fining following the Dolan Fire increased sediment transport capacity in Upper Big Creek. However, the largest grains in the channel, which govern channel structure, remained immobile 1-year post-fire, even under exacerbated clearwater flood conditions. 2-years post-fire, Upper Big Creek's bed surface grain size distribution has re-coarsened substantially. Post-fire debris flows removed existing steps that had persisted in Upper Big Creek for at least a decade prior to the Dolan Fire, and emplaced one newly formed, valley-spanning log jam upstream of study reaches in Upper Big Creek which serves to trap upstream sediment supply, and thus may partially account for rapid grain size recovery downstream.

Work that couples the results presented here with existing pre- and post-fire fish population and genetics data in the Big Creek watershed will improve understanding of how salmonids respond to catastrophic disturbance and extreme sediment supply perturbations. As anthropogenic climate change continues to increase the frequency of post-fire disturbance events, and high-resolution data geomorphic datasets become more widely available, so too will opportunities to characterize and quantify post-fire geomorphic change.

6.0 References

Arcement, G., and Schneider, V., 1989, Guide for selecting Manning's roughness coefficients for natural channels and flood plains:

Bailey, P., Wheaton, J., Reimer, M., and Brasington, J., 2020, Geomorphic Change Detection Software.

Benavides-Solorio, J., and MacDonald, L.H., 2001, Post-fire runoff and erosion from simulated rainfall on small plots, Colorado Front Range: Hydrological Processes, v. 15, p. 2931–2952.

Benda, L., Veldhuisen, C., and Black, J., 2003, Debris flows as agents of morphological heterogeneity at low-order confluences, Olympic Mountains, Washington: GSA Bulletin, v. 115, p. 1110–1121.

Buffington, J.M., and Montgomery, D.R., 1999, Effects of sediment supply on surface textures of gravel-bed rivers: Water Resources Research, v. 35, p. 3523–3530.

Bunte, K., and Abt, S.R., 2001, Sampling surface and subsurface particle-size distributions in wadable gravel-and cobble-bed streams for analyses in sediment transport, hydraulics, and streambed monitoring: U.S. Department of Agriculture, Forest Service, Rocky Mountain Research Station.

Burner, C.J., 1951, Characteristics of Spawning Nests of Columbia River Salmon: Fishery Bulletin of the Fish and Wildlife Service, v. 52, p. 95–103.

Cal Fire California Fire Perimeters (all), Updated 2023.

Cannon, S.H., 2001, Debris-flow generation from recently burned watersheds: Environmental and Engineering Geoscience, v. 7, p. 321–341.

Cannon, S., and Degraff, J., 2009, Cascading consequences of climate change and expanding population on the threat of wildfire and post fire debris-flow hazards, Western U.S. (Invited): AGU Fall Meeting Abstracts.

Cannon, S.H., Powers, P.S., and Savage, W.Z., 1998, Fire-related hyperconcentrated and debris flows on Storm King Mountain, Glenwood Springs, Colorado, USA: Environmental Geology, v. 35, p. 210–218.

Cannon, S.H., and Reneau, S.L., 2000, Conditions for generation of fire-related debris flows, Capulin Canyon, New Mexico: Earth Surface Processes and Landforms: The Journal of the British Geomorphological Research Group, v. 25, p. 1103–1121.

Cayan, D.R., Maurer, E.P., Dettinger, M.D., Tyree, M., and Hayhoe, K., 2008, Climate change scenarios for the California region: Climatic Change, v. 87, p. 21–42.

Cenderelli, D.A., and Kite, J.S., 1998, Geomorphic effects of large debris flows on channel morphology at North Fork Mountain, eastern West Virginia, USA: Earth Surface Processes and Landforms: The Journal of the British Geomorphological Group, v. 23, p. 1–19.

Chapelle, O., Haffner, P., and Vapnik, V.N., 1999, Support vector machines for histogram-based image classification: IEEE Transactions on Neural Networks, v. 10, p. 1055–1064.

Chin, A., and Wohl, E., 2005, Toward a theory for step pools in stream channels: Progress in Physical Geography: Earth and Environment, v. 29, p. 275–296.

Church, M., and Jakob, M., 2020, What Is a Debris Flood? Water Resources Research, v. 56, p. e2020WR027144.

Church, M., and Zimmermann, A., 2007, Form and stability of step-pool channels: Research progress: Water Resources Research, v. 43.

Cortes, C., and Vapnik, V., 1995, Support-vector networks: Machine learning, v. 20, p. 273–297.

Coussot, P., and Meunier, M., 1996, Recognition, classification and mechanical description of debris flows: Earth-Science Reviews, v. 40, p. 209–227.

Cover, M.R., de la Fuente, J.A., and Resh, V.H., 2010, Catastrophic disturbances in headwater streams: the long-term ecological effects of debris flows and debris floods in the Klamath Mountains, northern California: Canadian Journal of Fisheries and Aquatic Sciences, v. 67, p. 1596–1610.

Curran, J.C., and Wilcock, P.R., 2005, Characteristic dimensions of the step-pool bed configuration: An experimental study: Water Resources Research, v. 41.

Daly, C., Halbleib, M., Smith, J.I., Gibson, W.P., Doggett, M.K., Taylor, G.H., Curtis, J., and Pasteris, P.P., 2008, Physiographically sensitive mapping of climatological temperature and precipitation across the conterminous United States: International Journal of Climatology, v. 28, p. 2031–2064.

DeBano, L.F., 2000, Water repellency in soils: a historical overview: Journal of Hydrology, v. 231–232, p. 4–32.

Dettinger, M., 2011, Climate Change, Atmospheric Rivers, and Floods in California – A Multimodel Analysis of Storm Frequency and Magnitude Changes1: JAWRA Journal of the American Water Resources Association, v. 47, p. 514–523.

Dettinger, M.D., Ralph, F.M., Das, T., Neiman, P.J., and Cayan, D.R., 2011, Atmospheric Rivers, Floods and the Water Resources of California: Water, v. 3, p. 445–478.

Dibblee Jr, T.W., 1974, Geologic maps of the Monterey, Salinas, Gonzales, Point Sur, Jamesburg, Soledad, and Junipero Serra 15’ quadrangles, Monterey County, California: USGS Open-File Report.

DiBiase, R.A., and Lamb, M.P., 2020, Dry sediment loading of headwater channels fuels post-wildfire debris flows in bedrock landscapes: Geology, v. 48, p. 189–193.

Dietrich, W.E., Kirchner, J.W., Ikeda, H., and Iseya, F., 1989, Sediment supply and the development of the coarse surface layer in gravel-bedded rivers: Nature, v. 340, p. 215–217.

Dietrich, W.E., Nelson, P.A., Yager, E., Venditti, J.G., Lamb, M.P., and Collins, L., 2005, Sediment patches, sediment supply, and channel morphology: River Coastal and Estuarine Morphodynamics, p. 79–90.

Diplas, P., 1987, Bedload Transport in Gravel-Bed Streams: Journal of Hydraulic Engineering, v. 113.

Dragovich, D., 1993, Fire-accelerated boulder weathering in the Pilbara, Western Australia: Zeitschrift für Geomorphologie, p. 295–307.

East, A.E., Harrison, L.R., Smith, D.P., Logan, J.B., and Bond, R.M., 2022, Six years of fluvial response to a large dam removal on the Carmel River, California, USA: Earth Surface Processes and Landforms, v. n/a.

East, A.E., Logan, J.B., Mastin, M.C., Ritchie, A.C., Bountry, J.A., Magirl, C.S., and Sankey, J.B., 2018, Geomorphic Evolution of a Gravel-Bed River Under Sediment-Starved Versus Sediment-Rich Conditions: River Response to the World's Largest Dam Removal: Journal of Geophysical Research: Earth Surface, v. 123, p. 3338–3369.

Eaton, B.C., MacKenzie, L.G., and Booker, W.H., 2020, Channel stability in steep gravel–cobble streams is controlled by the coarse tail of the bed material distribution: Earth Surface Processes and Landforms, v. 45, p. 3639–3652.

Ebel, B.A., 2020, Temporal evolution of measured and simulated infiltration following wildfire in the Colorado Front Range, USA: Shifting thresholds of runoff generation and hydrologic hazards: Journal of Hydrology, v. 585, p. 124765.

Einstein, H.A., 1950, The Bed-load Function for Sediment Transportation in Open Channel Flows: U.S. Department of Agriculture, 92 p.

Espinoza, V., Waliser, D.E., Guan, B., Lavers, D.A., and Ralph, F.M., 2018, Global Analysis of Climate Change Projection Effects on Atmospheric Rivers: Geophysical Research Letters, v. 45, p. 4299–4308.

Everest, F.H., and Meehan, W.R., 1981, Forest Management and Anadromous Fish Habitat Productivity: Transactions of the 46th North American Wildlife and Natural Resources Conference, p. 10.

Florsheim, J.L., Chin, A., Kinoshita, A.M., and Nourbakhshbeidokhti, S., 2017, Effect of storms during drought on post-wildfire recovery of channel sediment dynamics and habitat in the southern California chaparral, USA: Earth Surface Processes and Landforms, v. 42, p. 1482–1492.

Florsheim, J.L., Keller, E.A., and Best, D.W., 1991, Fluvial sediment transport in response to moderate storm flows following chaparral wildfire, Ventura County, southern California: Geological Society of America Bulletin, v. 103, p. 504–511.

Foster, A.D., Claeson, S.M., Bisson, P.A., and Heimburg, J., 2020, Aquatic and riparian ecosystem recovery from debris flows in two western Washington streams, USA: Ecology and Evolution, v. 10, p. 2749–2777.

Gabet, E.J., and Sternberg, P., 2008, The effects of vegetative ash on infiltration capacity, sediment transport, and the generation of progressively bulked debris flows: Geomorphology, v. 101, p. 666–673.

Gartner, J.E., Cannon, S.H., and Santi, P.M., 2014, Empirical models for predicting volumes of sediment deposited by debris flows and sediment-laden floods in the transverse ranges of southern California: Engineering Geology, v. 176, p. 45–56.

Gatwood, E., Pederson, J., Casey, K., 2000. Los Angeles district method for prediction of debris yields. U.S. Army Corps of Engineers, Los Angeles District.

Gran, K.B., and Montgomery, D.R., 2005, Spatial and temporal patterns in fluvial recovery following volcanic eruptions: Channel response to basin-wide sediment loading at Mount Pinatubo, Philippines: GSA Bulletin, v. 117, p. 195–211.

Gran, K.B., Montgomery, D.R., and Halbur, J.C., 2011, Long-term elevated post-eruption sedimentation at Mount Pinatubo, Philippines: Geology, v. 39, p. 367–370.

Griffin, D., and Anchukaitis, K.J., 2014, How unusual is the 2012–2014 California drought? Geophysical Research Letters, v. 41, p. 9017–9023.

Harrison, L.R., East, A.E., Smith, D.P., Logan, J.B., Bond, R.M., Nicol, C.L., Williams, T.H., Boughton, D.A., Chow, K., and Luna, L., 2018, River response to large-dam removal in a Mediterranean hydroclimatic setting: Carmel River, California, USA: River response to large-dam removal: Earth Surface Processes and Landforms, v. 43, p. 3009–3021.

Harvey, B.C., and Lisle, T.E., 1999, Scour of Chinook Salmon Redds on Suction Dredge Tailings: North American Journal of Fisheries Management, v. 19, p. 613–617.

Hassan, M.A., Saletti, M., Johnson, J.P.L., Ferrer-Boix, C., Venditti, J.G., and Church, M., 2020, Experimental Insights Into the Threshold of Motion in Alluvial Channels: Sediment Supply and Streambed State: Journal of Geophysical Research: Earth Surface, v. 125, p. e2020JF005736.

Hassan, M.A., Saletti, M., McDowell, C., and Li, W., 2023, Sediment Dynamics and Bed Stability in Step-Pool Streams: Insights From 18 Years of Field Observations: Water Resources Research, v. 59, p. e2022WR032864.

Henson, P., and Usner, D.J., 1996, The Natural History of Big Sur: University of California Press, 464 p.

Homann, J., Oster, J.L., de Wet, C.B., Breitenbach, S.F.M., and Hoffmann, T., 2022, Linked fire activity and climate whiplash in California during the early Holocene: Nature Communications, v. 13, p. 7175.

Hungr, O., Leroueil, S., and Picarelli, L., 2014, The Varnes classification of landslide types, an update: Landslides, v. 11, p. 167–194.

Iverson, R.M., 2005, Debris-flow mechanics, *in* Debris-flow Hazards and Related Phenomena, Berlin, Heidelberg, Springer Berlin Heidelberg, Springer Praxis Books, p. 105–134.

Iverson, R.M., 1997, The physics of debris flows: Reviews of Geophysics, v. 35, p. 245–296.

Johansen, M.P., Hakonson, T.E., and Breshears, D.D., 2001, Post-fire runoff and erosion from rainfall simulation: contrasting forests with shrublands and grasslands: Hydrological Processes, v. 15, p. 2953–2965.

Johnson, J.P.L., Aronovitz, A.C., and Kim, W., 2015, Coarser and rougher: Effects of fine gravel pulses on experimental step-pool channel morphodynamics: Geophysical Research Letters, v. 42, p. 8432–8440.

Johnson, S.Y., Watt, J.T., Hartwell, S.R., and Kluesner, J.W., 2018, Neotectonics of the Big Sur Bend, San Gregorio-Hosgri Fault System, Central California: Tectonics, v. 37, p. 1930–1954.

Johnston, S.M., Singleton, J.S., Chapman, A.D., and Murray, G., 2018, Geologic map and structural development of the northernmost Sur-Nacimiento fault zone, central California coast: Geosphere, v. 15, p. 171–187.

de Jonge, L., Jacobsen, O., and Moldrup, P., 1999, Soil Water Repellency: Effects of Water Content, Temperature, and Particle Size: Soil Science Society of America Journal - SSSAJ, v. 63.

Keeley, J.E., 2009, Fire intensity, fire severity and burn severity: a brief review and suggested usage: International Journal of Wildland Fire, v. 18, p. 116–126.

Keller, E.A., Bean, G., and Best, D., 2015, Fluvial geomorphology of a boulder-bed, debris-flow—Dominated channel in an active tectonic environment: Geomorphology, v. 243, p. 14–26.

Kemp, P., Sear, D., Collins, A., Naden, P., and Jones, I., 2011, The impacts of fine sediment on riverine fish: Hydrological Processes, v. 25, p. 1800–1821.

Kinoshita, A., and Hogue, T., 2011, Spatial and Temporal Controls on Post-fire Hydrologic Recovery in Southern California Watersheds: Fuel and Energy Abstracts, v. 87.

Kondolf, G.M., and Wolman, M., 1993, The Sizes of Salmonid Spawning Gravels: Water Resources Research - WATER RESOUR RES, v. 29, p. 2275–2286.

Lamb, M.P., Levina, M., DiBiase, R.A., and Fuller, B.M., 2013, Sediment storage by vegetation in steep bedrock landscapes: Theory, experiments, and implications for postfire sediment yield: Journal of Geophysical Research: Earth Surface, v. 118, p. 1147–1160.

Lane, S.N., Richards, K.S., and Chandler, J.H., 1996, Discharge and sediment supply controls on erosion and deposition in a dynamic alluvial channel: Geomorphology, v. 15, p. 1–15.

Lenzi, M.A., Mao, L., and Comiti, F., 2006, Effective discharge for sediment transport in a mountain river: Computational approaches and geomorphic effectiveness: Journal of Hydrology, v. 326, p. 257–276.

Li, C., Handwerger, A.L., Wang, J., Yu, W., Li, X., Finnegan, N.J., Xie, Y., Buscarnera, G., and Horton, D.E., 2022, Augmentation of WRF-Hydro to simulate overland-flow- and streamflow-generated debris flow susceptibility in burn scars: Natural Hazards and Earth System Sciences, v. 22, p. 2317–2345.

Lippitt, C.L., Stow, D.A., O'Leary, J.F., and Franklin, J., 2013, Influence of short-interval fire occurrence on post-fire recovery of fire-prone shrublands in California, USA: International Journal of Wildland Fire, v. 22, p. 184.

Lisle, T.E., 1989, Sediment transport and resulting deposition in spawning gravels, north coastal California: Water Resources Research, v. 25, p. 1303–1319.

Lisle, T.E., and Hilton, S., 1992, The Volume of Fine Sediment in Pools: An Index of Sediment Supply in Gravel-Bed Streams1: JAWRA Journal of the American Water Resources Association, v. 28, p. 371–383.

Liu, T., McGuire, L.A., Wei, H., Rengers, F.K., Gupta, H., Ji, L., and Goodrich, D.C., 2021, The timing and magnitude of changes to Hortonian overland flow at the watershed scale during the post-fire recovery process: Hydrological Processes, v. 35, p. e14208.

Loáiciga, H.A., Pedreros, D., and Roberts, D., 2001, Wildfire-streamflow interactions in a chaparral watershed: Advances in Environmental Research, v. 5, p. 295–305.

Luković, J., Chiang, J.C.H., Blagojević, D., and Sekulić, A., 2021, A Later Onset of the Rainy Season in California: Geophysical Research Letters, v. 48, p. e2020GL090350.

MacDonald, L.H., and Huffman, E.L., 2004, Post-fire Soil Water Repellency: Persistence and Soil Moisture Thresholds: Soil Science Society of America Journal, v. 68, p. 1729–1734.

MacKenzie, L.G., and Eaton, B.C., 2017, Large grains matter: contrasting bed stability and morphodynamics during two nearly identical experiments: Earth Surface Processes and Landforms, v. 42, p. 1287–1295.

Madej, M.A., Sutherland, D.G., Lisle, T.E., and Pryor, B., 2009, Channel responses to varying sediment input: A flume experiment modeled after Redwood Creek, California: Geomorphology, v. 103, p. 507–519.

Major, J.J., 1997, Depositional processes in large-scale debris-flow experiments: The Journal of Geology, v. 105, p. 345–366.

Major, J.J., East, A.E., O'Connor, J.E., Grant, G.E., Wilcox, A.C., Magirl, C.S., Collins, M.J., and Tullos, D.D., 2017, Geomorphic Responses to Dam Removal in the United States - a Two-Decade Perspective, *in* Tsutsumi, D. and Laronne, J.B. eds., Gravel-Bed Rivers, Chichester, UK, John Wiley & Sons, Ltd, p. 355–383.

May, C.L., Pryor, B., Lisle, T.E., and Lang, M., 2009, Coupling hydrodynamic modeling and empirical measures of bed mobility to predict the risk of scour and fill of salmon redds in a large regulated river: Water Resources Research, v. 45.

McGuire, L.A., Rengers, F.K., Kean, J.W., and Staley, D.M., 2017, Debris flow initiation by runoff in a recently burned basin: Is grain-by-grain sediment bulking or en masse failure to blame? Geophysical Research Letters, v. 44, p. 7310–7319.

Meyer, G. A., and Wells, S. G., 1997, Fire-Related Sedimentation Events on Alluvial Fans, Yellowstone National Park, U.S.A.: SEPM Journal of Sedimentary Research, v. Vol. 67.

Meyer-Peter, E., and Müller, R., 1948, Formulas for Bed-Load transport: IAHSR 2nd meeting, Stockholm, appendix 2.

Montgomery, D.R., and Buffington, J.M., 1997, Channel-reach morphology in mountain drainage basins: Geological Society of America Bulletin, v. 109, p. 596–611.

Naylor, M.A., 1980, The Origin of Inverse Grading in Muddy Debris Flow Deposits--A Review: SEPM Journal of Sedimentary Research, v. Vol. 50.

Micheletti, N., Chandler, J.H., and Lane, S.N., 2015, Structure from Motion (SfM) Photogrammetry: Geomorphological Techniques, p. 12.

Morell, K.D., Alessio, P., Dunne, T., and Keller, E., 2021, Sediment Recruitment and Redistribution in Mountain Channel Networks by Post-Wildfire Debris Flows: Geophysical Research Letters, v. 48, p. e2021GL095549.

Niemeyer, R.J., Bladon, K.D., and Woodsmith, R.D., 2020, Long-term hydrologic recovery after wildfire and post-fire forest management in the interior Pacific Northwest: Hydrological Processes, v. 34, p. 1182–1197.

Nourbakhshbeidokhti, S., Kinoshita, A.M., Chin, A., and Florsheim, J.L., 2019, A workflow to estimate topographic and volumetric changes and errors in channel sedimentation after disturbance: Remote Sensing, v. 11, p. 586.

Nyman, P., Smith, H.G., Sherwin, C.B., Langhans, C., Lane, P.N.J., and Sheridan, G.J., 2015, Predicting sediment delivery from debris flows after wildfire: Geomorphology, v. 250, p. 173–186.

Oakley, N.S., Liu, T., McGuire, L.A., Simpson, M., Hatchett, B.J., Tardy, A., Kean, J.W., Castellano, C., Laber, J.L., and Steinhoff, D., 2023, Toward probabilistic post-fire debris-flow hazard decision support: Bulletin of the American Meteorological Society,.

OpenTopography, 2013, California Coast: Big Creek, Vincente, Arroyo Seco, Scotts Creek, UCSC.

OpenTopography, 2016, Big Creek, California.

OpenTopography, 2023, Quantifying Channel Change in a Steep Coastal Stream, CA 2022.

Pak, J.H., and Lee, J.-J., 2008, A Statistical Sediment Yield Prediction Model Incorporating the Effect of Fires and Subsequent Storm Events1: JAWRA Journal of the American Water Resources Association, v. 44, p. 689–699.

Parker, G., and García, M. (Eds.), 2006, River, Coastal and Estuarine Morphodynamics: Proceedings of the 4th IAHR Symposium on River, Coastal and Estuarine Morphodynamics (RCEM 2005, Urbana, Illinois, USA, 4-7 October 2005): Taylor & Francis.

Persad, G.G., Swain, D.L., Kouba, C., and Ortiz-Partida, J.P., 2020, Inter-model agreement on projected shifts in California hydroclimate characteristics critical to water management: Climatic Change, v. 162, p. 1493–1513.

Potter, C., Shupe, J., Gross, P., Genovese, V., and Klooster, S., 2010, Modeling river discharge rates in California watersheds: Journal of Water and Climate Change, v. 1, p. 36–54.

Prancevic, J.P., and Lamb, M.P., 2015, Particle friction angles in steep mountain channels: Journal of Geophysical Research: Earth Surface, v. 120, p. 242–259.

Prosser, I.P., and Williams, L., 1998, The effect of wildfire on runoff and erosion in native Eucalyptus forest: Hydrological Processes, v. 12, p. 251–265.

Purinton, B., and Bookhagen, B., 2019, Introducing PebbleCounts: a grain-sizing tool for photo surveys of dynamic gravel-bed rivers: Earth Surface Dynamics, v. 7, p. 859–877.

Purinton, B., and Bookhagen, B., 2021, Tracking Downstream Variability in Large Grain-Size Distributions in the South-Central Andes: Journal of Geophysical Research: Earth Surface, v. 126, p. e2021JF006260.

Recking, A., Leduc, P., Liebault, F., and Church, M., 2012, A field investigation of the influence of sediment supply on step-pool morphology and stability: Geomorphology, v. 139–140, p. 53–66.

Rengers, F.K., McGuire, L.A., Kean, J.W., Staley, D.M., Dobre, M., Robichaud, P.R., and Swetnam, T., 2021, Movement of Sediment Through a Burned Landscape: Sediment Volume Observations and Model Comparisons in the San Gabriel Mountains, California, USA: Journal of Geophysical Research: Earth Surface, v. 126, p. e2020JF006053.

Riebe, C.S., Sklar, L.S., Overstreet, B.T., and Wooster, J.K., 2014, Optimal reproduction in salmon spawning substrates linked to grain size and fish length: Water Resources Research, v. 50, p. 898–918.

Shakesby, R.A., and Doerr, S.H., 2006, Wildfire as a hydrological and geomorphological agent: Earth-Science Reviews, v. 74, p. 269–307.

Sklar, L., and Dietrich, W.E., 1998, River longitudinal profiles and bedrock incision models: Stream power and the influence of sediment supply, *in* Tinkler, J. and Wohl, E. eds., Geophysical Monograph Series, Washington, D. C., American Geophysical Union, v. 107, p. 237–260.

Smith, H., 2022, Man convicted of setting Big Sur wildfire that killed 12 endangered condors: Los Angeles Times.

Stoof, C.R., Vervoort, R.W., Iwema, J., van den Elsen, E., Ferreira, A.J.D., and Ritsema, C.J., 2012, Hydrological response of a small catchment burned by experimental fire: Hydrology and Earth System Sciences, v. 16, p. 267–285.

Swain, D.L., 2021, A Shorter, Sharper Rainy Season Amplifies California Wildfire Risk: Geophysical Research Letters, v. 48.

Swain, D.L., Langenbrunner, B., Neelin, J.D., and Hall, A., 2018, Increasing precipitation volatility in twenty-first-century California: Nature Climate Change, v. 8, p. 427–433.

Tang, H., McGuire, L.A., Rengers, F.K., Kean, J.W., Staley, D.M., and Smith, J.B., 2019, Evolution of debris-flow initiation mechanisms and sediment sources during a sequence of postwildfire rainstorms: Journal of Geophysical Research: Earth Surface, v. 124, p. 1572–1595.

Tietje, W.D., Preston, W.L., and Polyakov, A.Y., 2019, California Naturalist Series: Natural History of the Central Coast Bioregion: University of California, Agriculture and Natural Resources.

U.S. Forest Service, 2020, Dolan Fire Burned-Area Report.

Vapnik, V., 1999, The nature of statistical learning theory: Springer science & business media.

Wagenbrenner, J.W., Ebel, B.A., Bladon, K.D., and Kinoshita, A.M., 2021, Post-wildfire hydrologic recovery in Mediterranean climates: A systematic review and case study to identify current knowledge and opportunities: Journal of Hydrology, v. 602..

Wang, J., Hassan, M.A., Saletti, M., Chen, X., Fu, X., Zhou, H., and Yang, X., 2021, On How Episodic Sediment Supply Influences the Evolution of Channel Morphology, Bedload Transport and Channel Stability in an Experimental Step-Pool Channel: Water Resources Research, v. 57.

Westerling, A.L., 2016, Increasing western US forest wildfire activity: sensitivity to changes in the timing of spring: Philosophical Transactions of the Royal Society B: Biological Sciences, v. 371.

Wheaton, J.M., Brasington, J., Darby, S.E., Merz, J., Pasternack, G.B., Sear, D., and Vericat, D., 2010a, Linking geomorphic changes to salmonid habitat at a scale relevant to fish: River Research and Applications, v. 26, p. 469–486.

Wheaton, J.M., Brasington, J., Darby, S.E., and Sear, D.A., 2010b, Accounting for uncertainty in DEMs from repeat topographic surveys: improved sediment budgets: Earth Surface Processes and Landforms, v. 35, p. 136–156.

Wilcock, P.R., and Crowe, J.C., 2003, Surface-based transport model for mixed-size sediment: Journal of hydraulic engineering, v. 129, p. 120–128.

Williams, A.P., Abatzoglou, J.T., Gershunov, A., Guzman-Morales, J., Bishop, D.A., Balch, J.K., and Lettenmaier, D.P., 2019, Observed impacts of anthropogenic climate change on wildfire in California: Earth's Future, v. 7, p. 892–910.

Wohl, E. et al., 2019, Connectivity as an emergent property of geomorphic systems: Earth Surface Processes and Landforms, v. 44, p. 4–26.

7.0 Tables

Table 1. Data sources and model parameters for sediment transport capacity and A_{stab} model scenarios in Big Creek and Devil's Creek.

	Model Scenario	Modeled Discharge from Li et al., 2022 (m^3/s)	Channel Geometry Data Source	Grain Size Data Source	Manning's Roughness Coefficient ($m^{1/6}$)
Big Creek					
	pre-fire	23.25	2016 lidar	2016 SfM Orthoimagery	0.045
	1-year post-fire, baseline	23.25	2022 lidar	2021 SfM Orthoimagery	0.037
	1-year post-fire, burn-scar	86.73	2022 lidar	2021 SfM Orthoimagery	0.037
	2-year post-fire, baseline	23.25	2022 lidar	2022 SfM Orthoimagery	0.041
	2-year post-fire, burn-scar	86.73	2022 lidar	2022 SfM Orthoimagery	0.041
Devil's Creek					
	pre-fire	19.69	2016 lidar	2016 SfM Orthoimagery	0. 045
	1-year post-fire, baseline	19.69	2022 lidar	2021 SfM Orthoimagery	0. 045
	1-year post-fire, burn-scar	80.89	2022 lidar	2021 SfM Orthoimagery	0. 045
	2-year post-fire, baseline	19.69	2022 lidar	2022 SfM Orthoimagery	0. 045
	2-year post-fire, burn-scar	80.89	2022 lidar	2022 SfM Orthoimagery	0. 045

Table 2. Grain size quantiles for Upper Big Creek.

Upstream Reach					
Year	D_{min} (m)	D_{16} (m)	D_{50} (m)	D_{84} (m)	D_{max} (m)
2016	0.02	0.38	0.76	1.31	1.94
2021	0.03	0.16	0.67	1.30	1.77
2022	0.02	0.22	0.74	1.46	1.97
Middle Reach					
2016	0.02	0.35	0.76	1.23	1.80
2021	0.03	0.10	0.48	1.28	1.90
2022	0.03	0.22	0.85	1.50	2.24
Downstream Reach					
2016	0.02	0.31	0.71	1.07	1.25
2021	0.03	0.11	0.37	1.36	1.74
2022	0.02	0.14	0.53	1.26	1.73

Table 3. Grain size quantiles for Devil's Creek.

Upstream Reach					
Year	D_{min} (m)	D_{16} (m)	D_{50} (m)	D_{84} (m)	D_{max} (m)
2016	0.03	0.26	0.59	1.20	1.74
2021	0.03	0.15	0.57	1.25	1.45
2022	0.03	0.14	0.44	0.95	1.57
Middle Reach					
2016	0.03	0.26	0.67	1.20	1.58
2021	0.03	0.22	0.58	1.03	1.26
2022	0.03	0.23	0.53	0.93	1.59
Downstream Reach					
2016	0.03	0.21	0.50	0.99	1.21
2021	0.02	0.20	0.51	1.00	1.78
2022	0.03	0.20	0.52	1.09	1.50

8.0 Figures

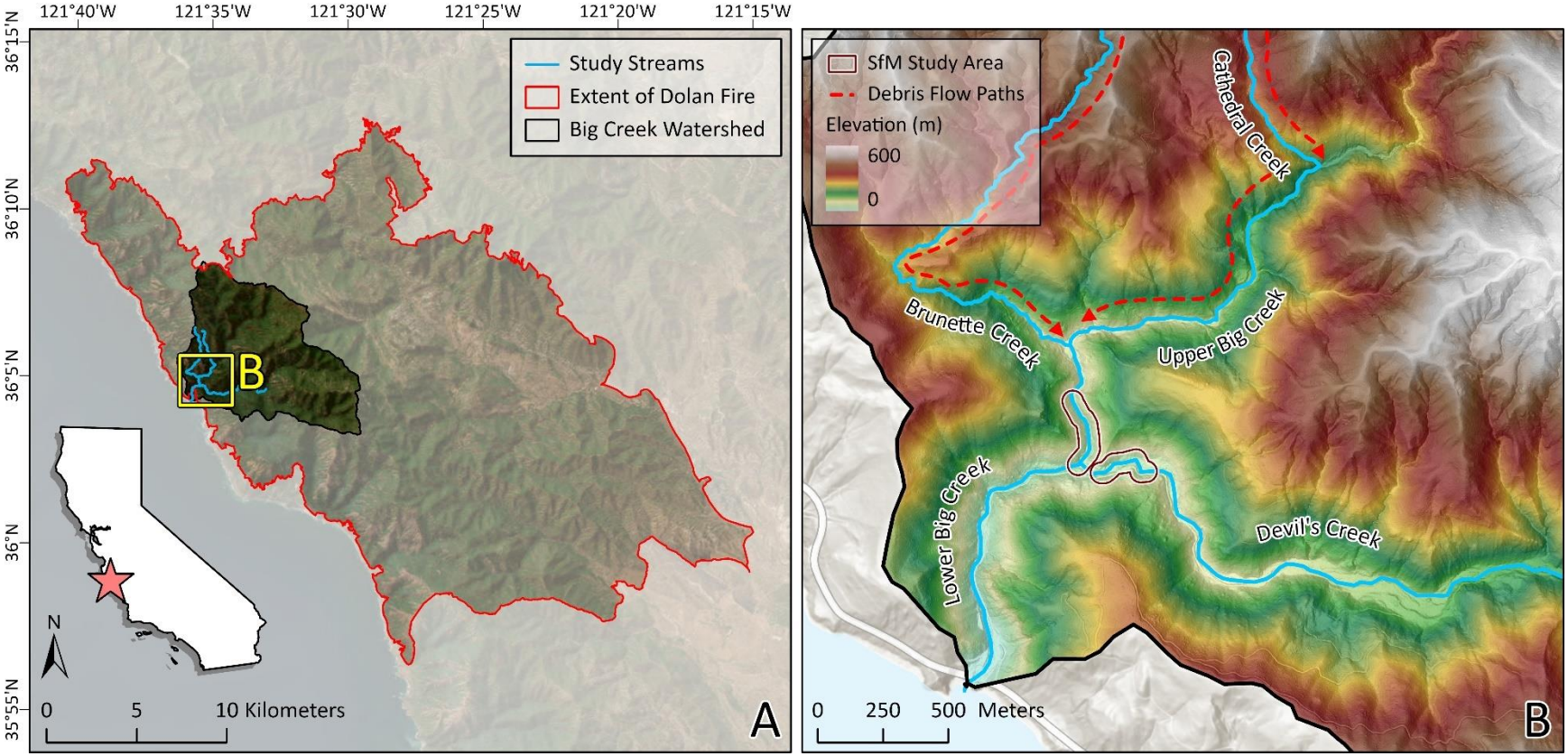

Figure 1. (A) Footprint of the Dolan Fire and Big Creek watershed, and locations of study streams within the basin. (B) Study streams, structure from motion (SfM) study area, debris flows paths, and elevation within the Big Creek watershed.

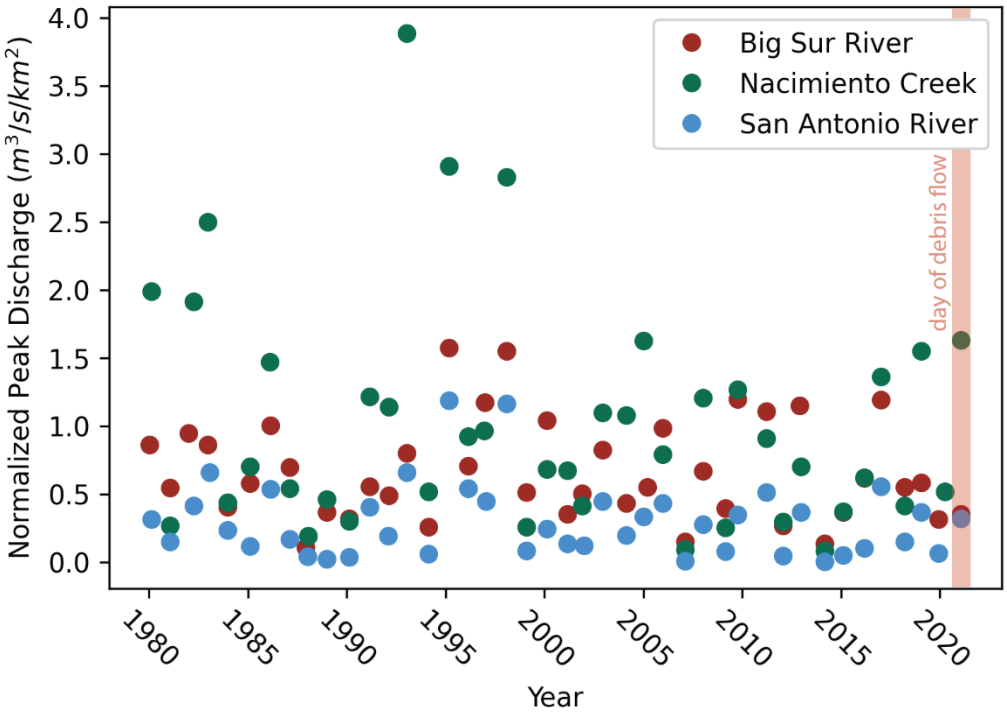

Figure 2. Yearly peak flow data from USGS stream gauges surrounding Big Creek. All yearly peak flows for surrounding stream gauges in 2021 took place during the atmospheric river event that triggered post-fire debris flows in the Big Creek watershed. Peak flow recurrence intervals for this date range from 1.5 to 5 years.

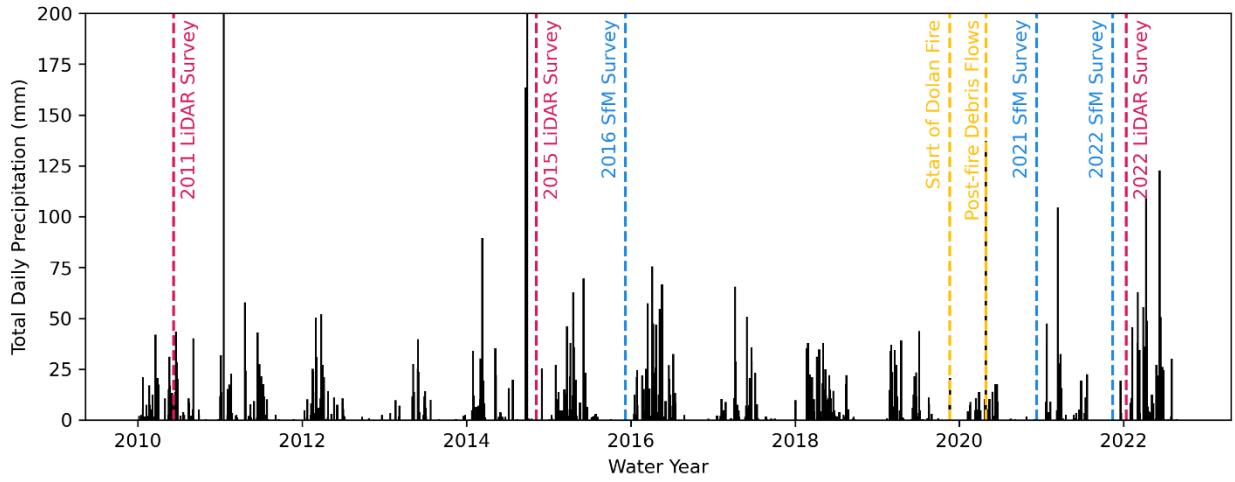

Figure 3. Timeline of SfM and lidar surveys, and debris flow-related events superimposed on total daily precipitation measured at the Whale Point weather station within the Big Creek watershed.

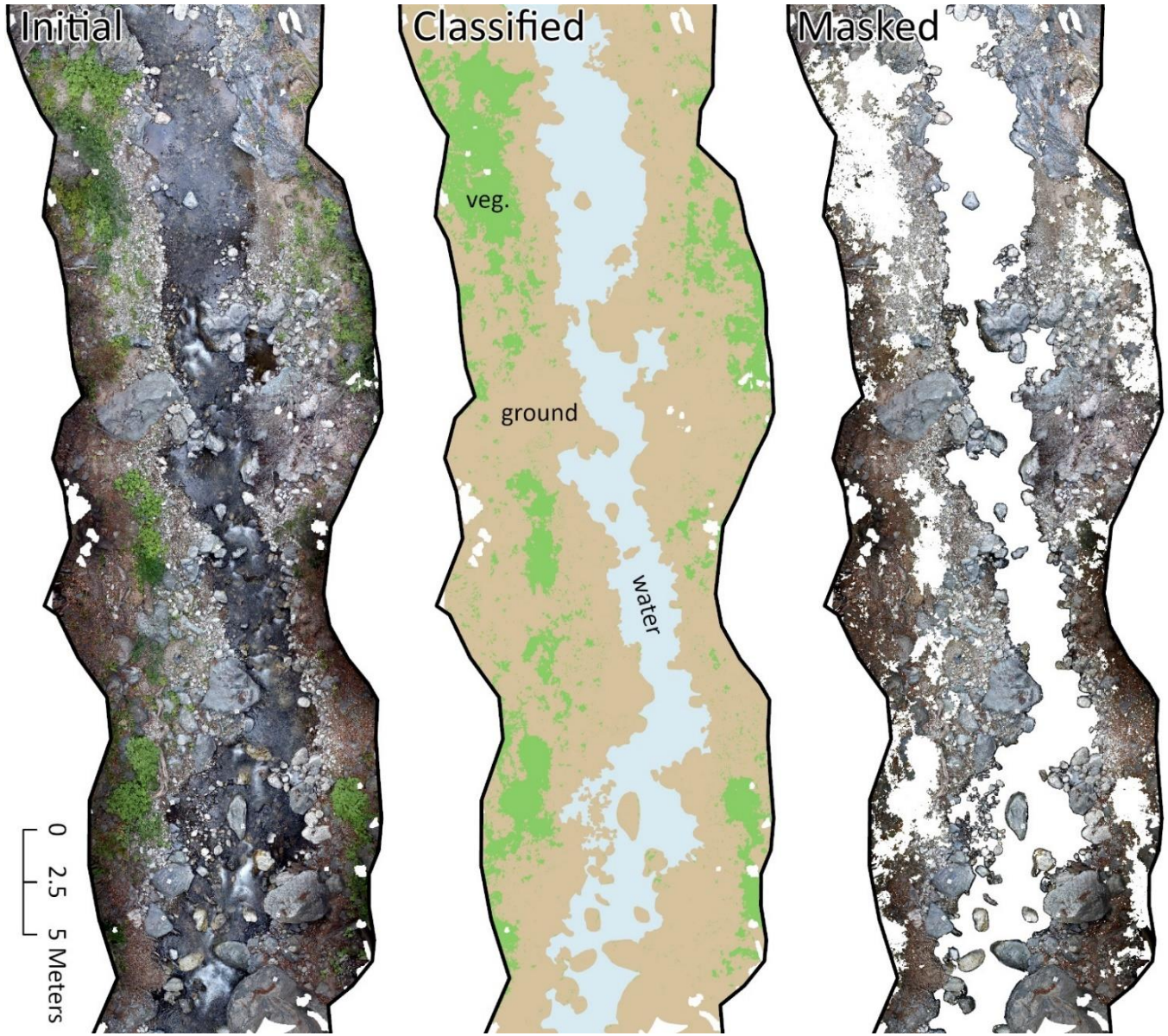

Figure 4. Examples of initial, classified, and masked orthoimages for one reach in Big Creek.

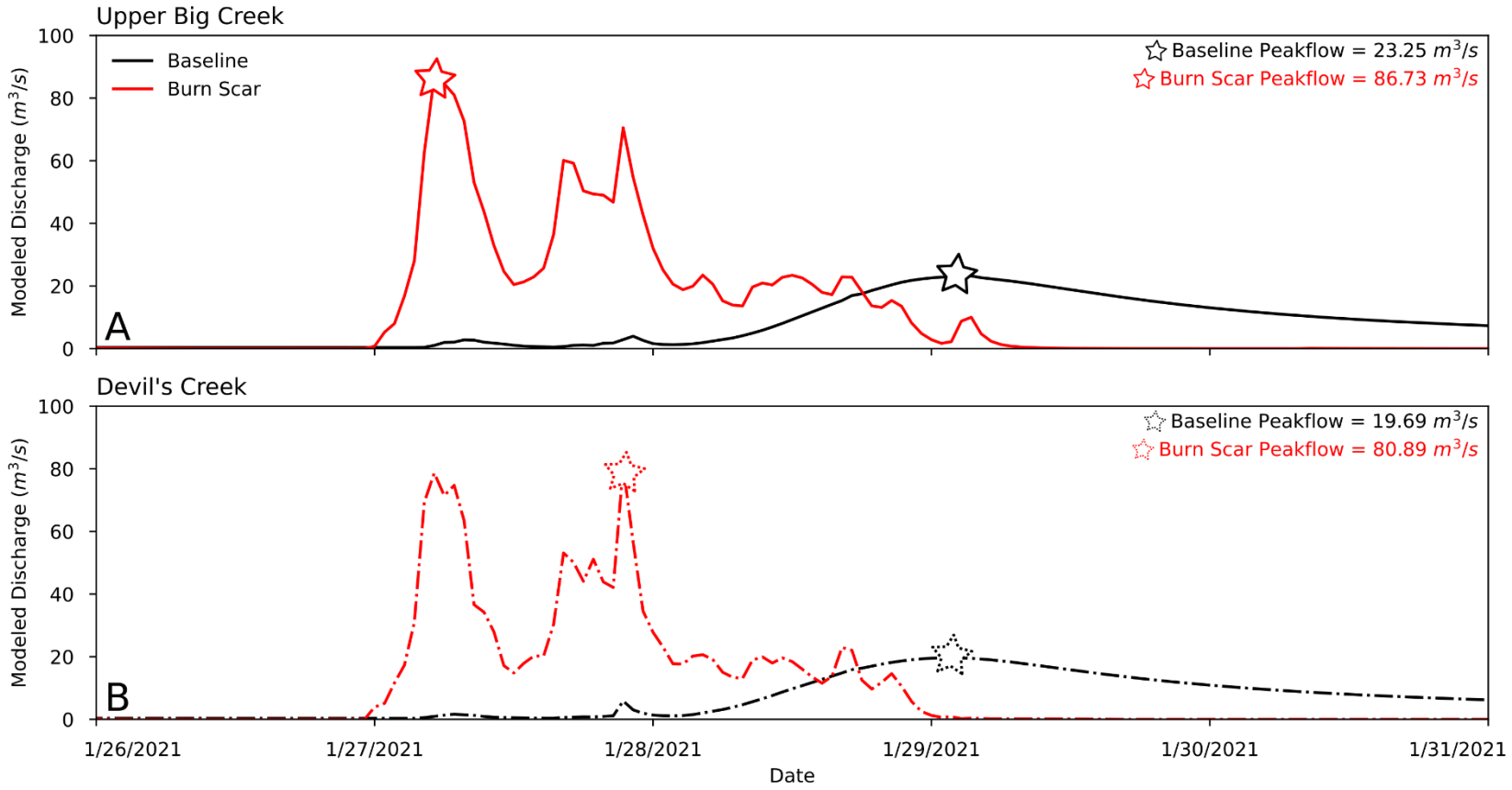

Figure 5. Modeled hydrograph data from Li et al., 2022, with and without the hydrologic influence of the Dolan Fire burn scar, for Upper Big Creek and Devil's Creek during the 2021 atmospheric river event which triggered post-fire debris flows.

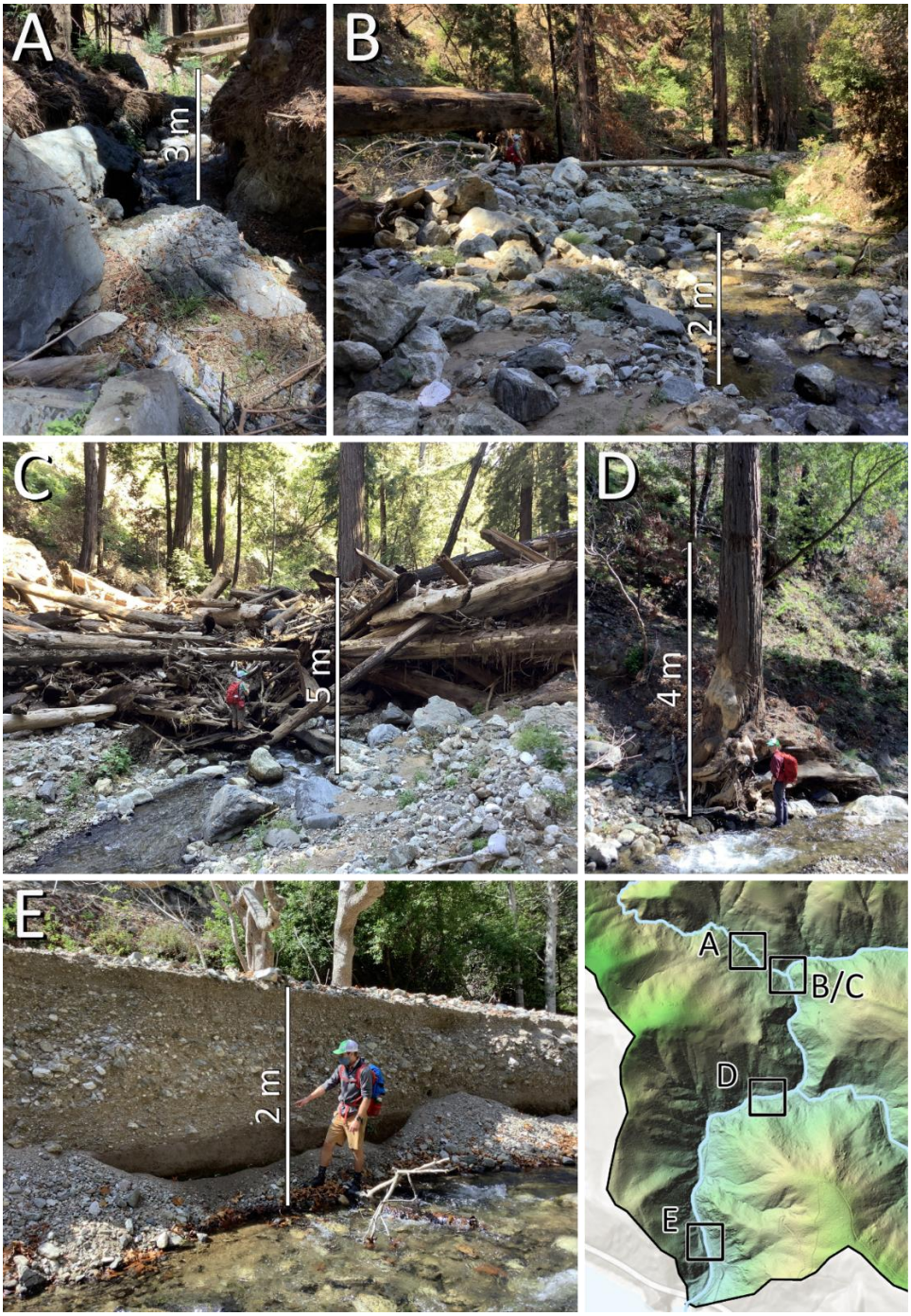

Figure 6. Field photos taken after post-fire debris flows in the Big Creek watershed. (A) 3 m incision scar in Brunette Creek, one of the channels in which post-fire debris flows initiated. (B) Bouldery deposit behind the newly emplaced log jam just downstream of the confluence between Brunette Creek and Upper Big Creek. (C) Newly emplaced log jam just downstream of the confluence between Brunette Creek and Upper Big Creek. (D) High-water mark approximately 4 m above low-flow water level just downstream of the confluence between Devil's Creek and Big Creek. (E) Potential debris flood terraces in Lower Big Creek.

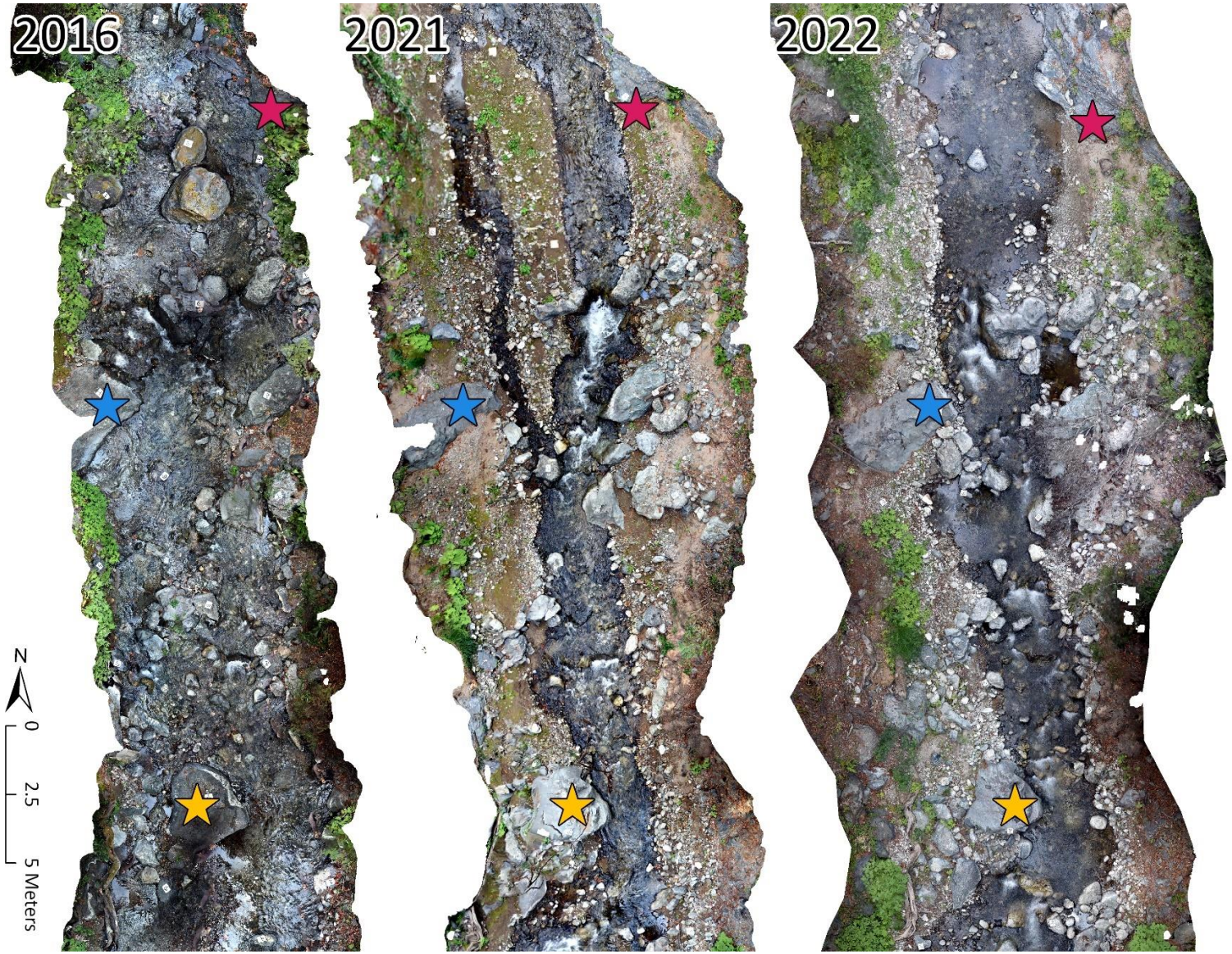

Figure 7. 2016, 2021, and 2022 orthoimages for one example reach in Upper Big Creek; stars represent landmarks visible in each timestep.

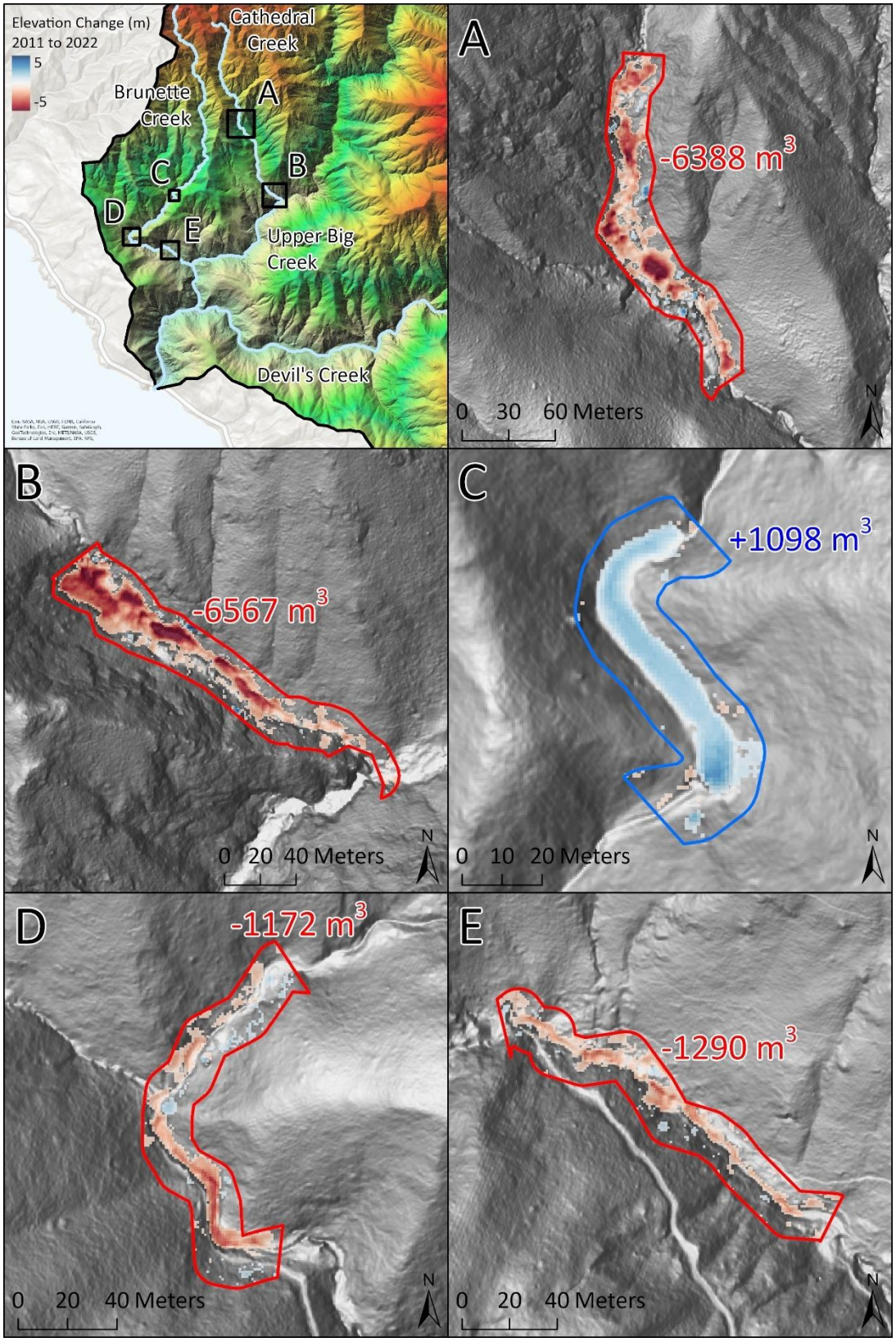

Figure 8. DEMs of difference and volumetric change from 2011 to 2022 for selected sections of Cathedral Creek and Brunette Creek which experienced substantial geomorphic change.

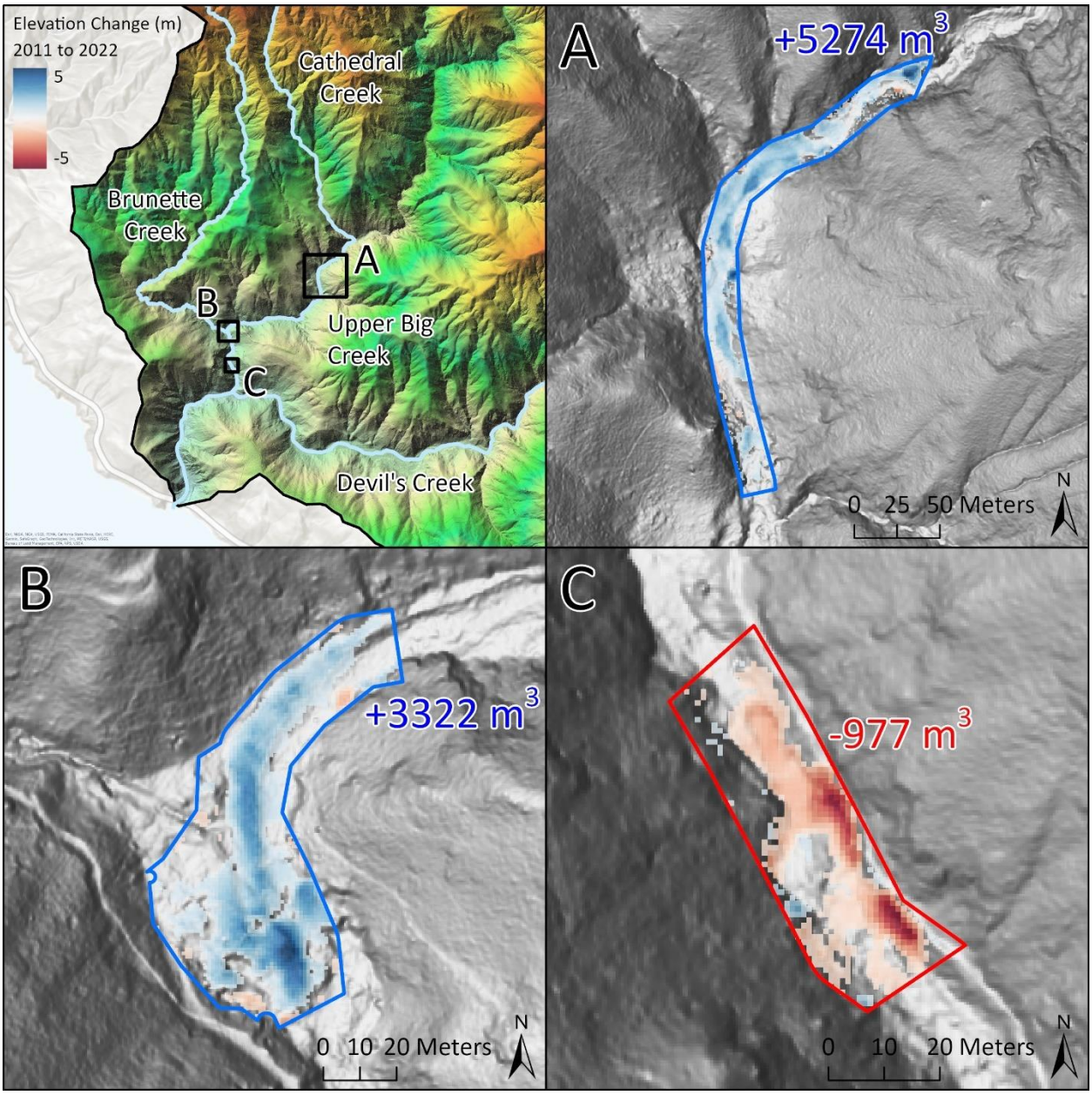

Figure 9. DEMs of difference and volumetric change from 2011 to 2022 for selected sections of Upper Big Creek which experienced substantial geomorphic change.

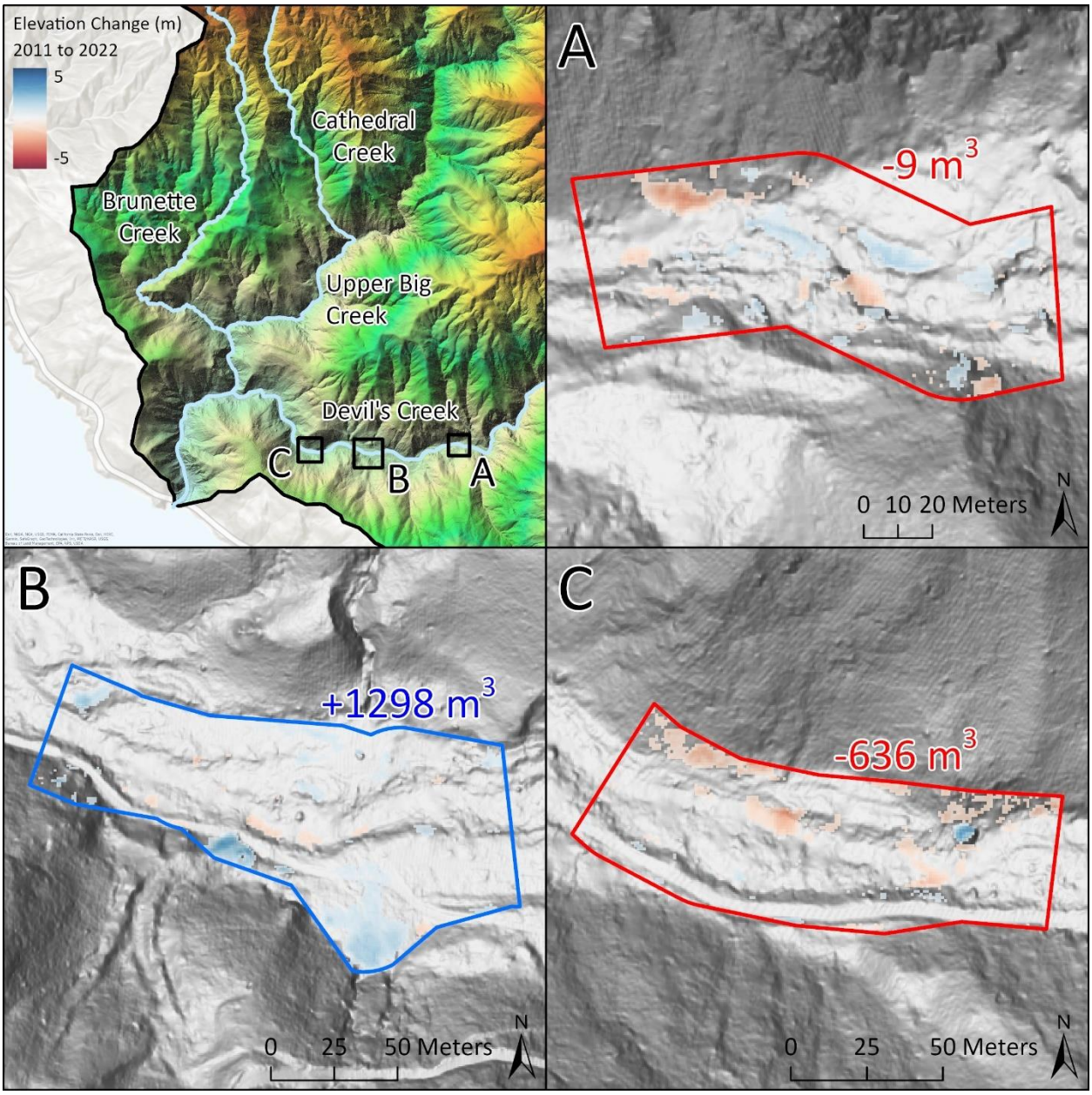

Figure 10. DEMs of difference and volumetric change from 2011 to 2022 for selected sections of Devil's Creek which experienced moderate geomorphic change.

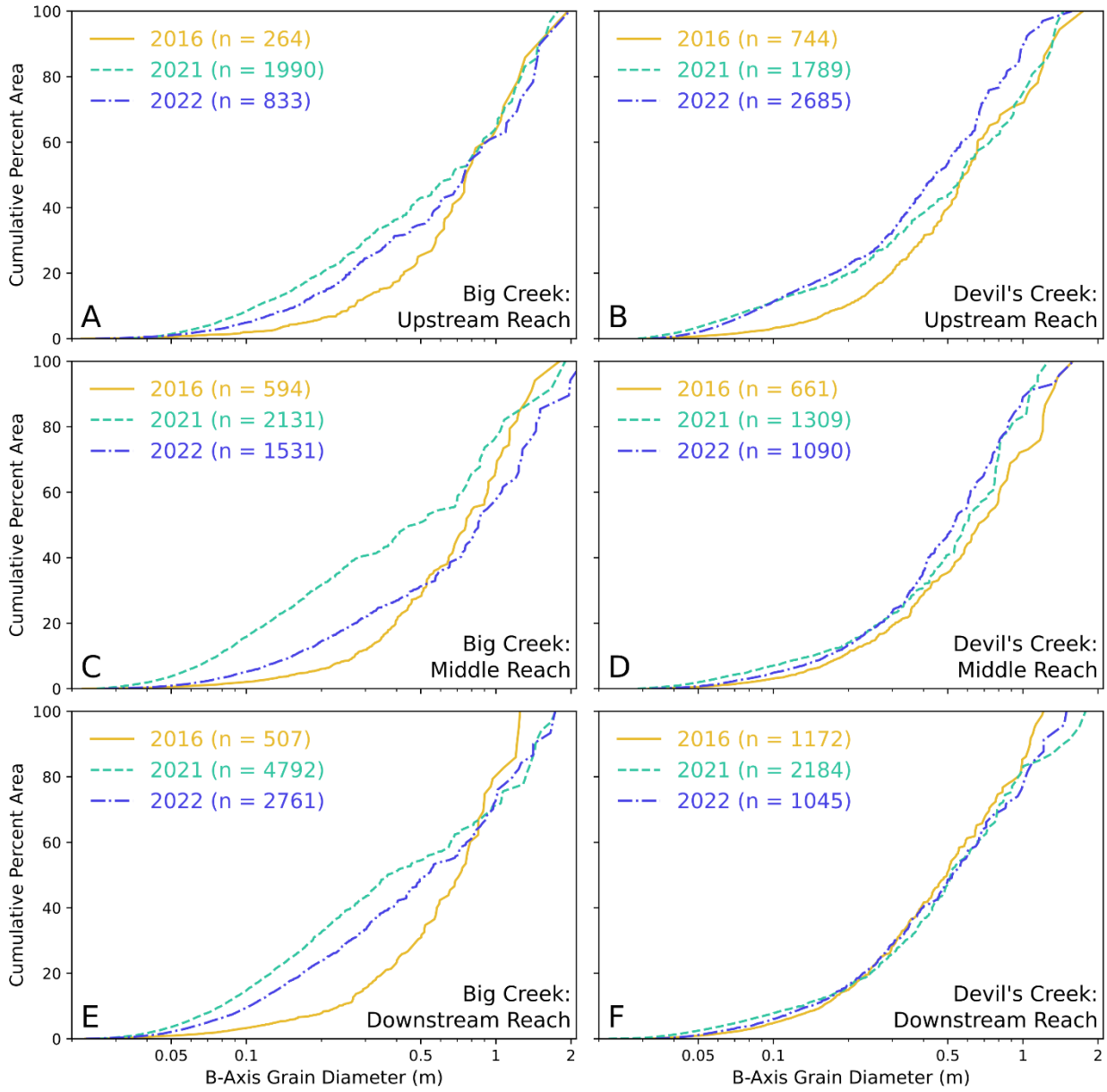

Figure 11. PebbleCounts-generated bed surface grain size distributions for each study reach in Upper Big Creek and Devil's Creek.

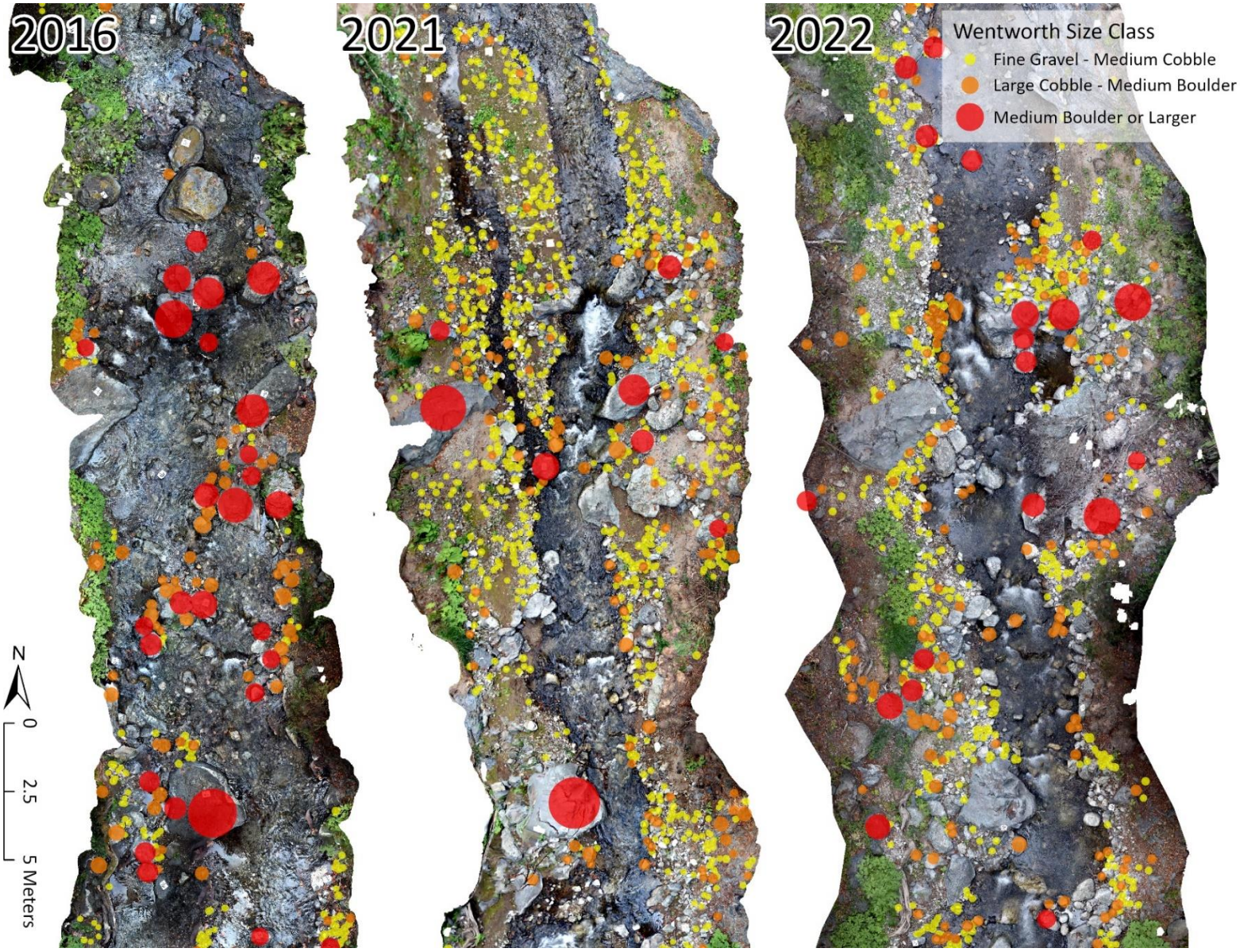

Figure 12. Grain locations, symbolized by PebbleCounts-measured b-axis diameter for one example reach in Upper Big Creek.

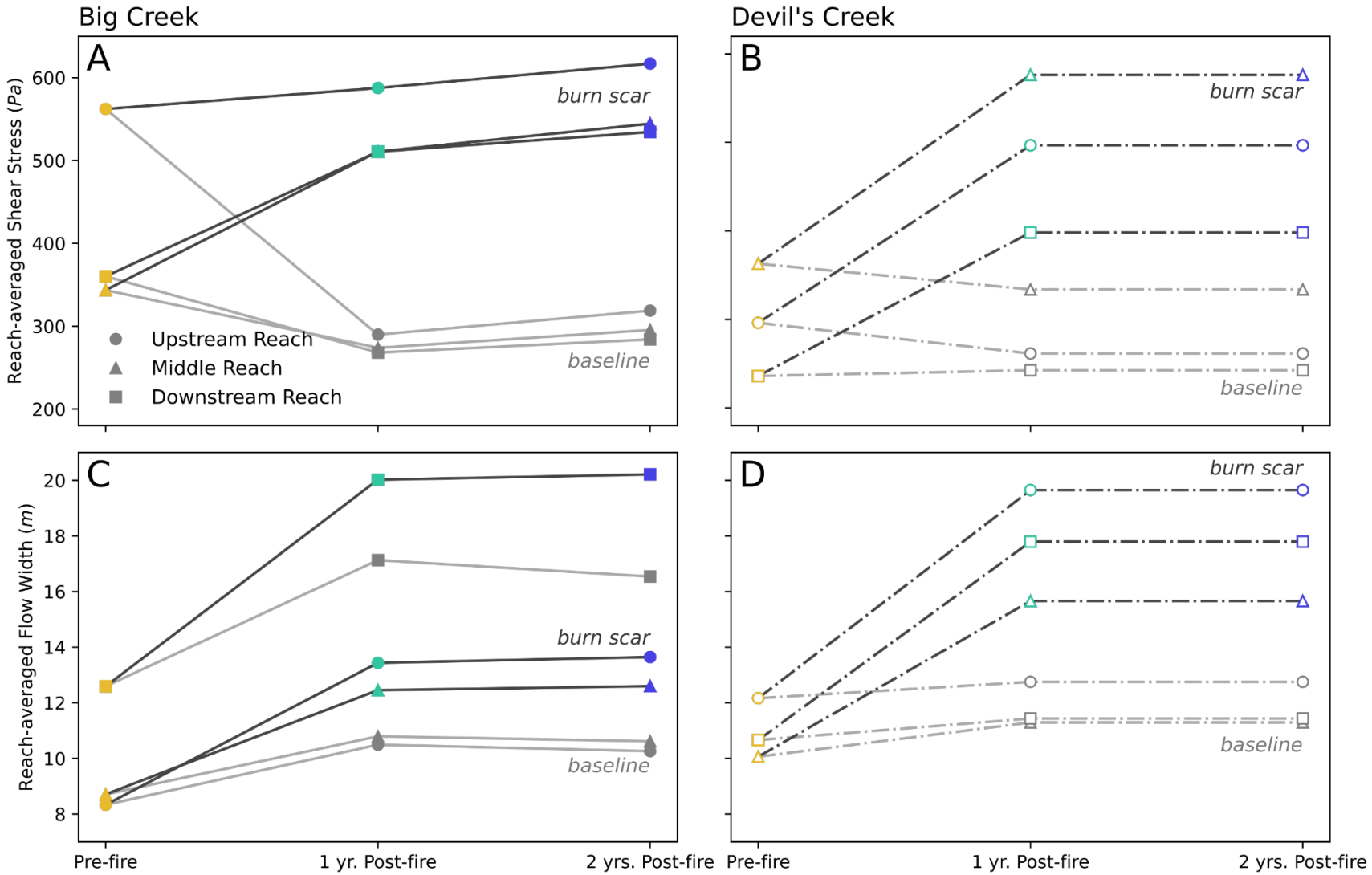

Figure 13. Reach-averaged shear stress and flow width through time in Big Creek and Devil's Creek.

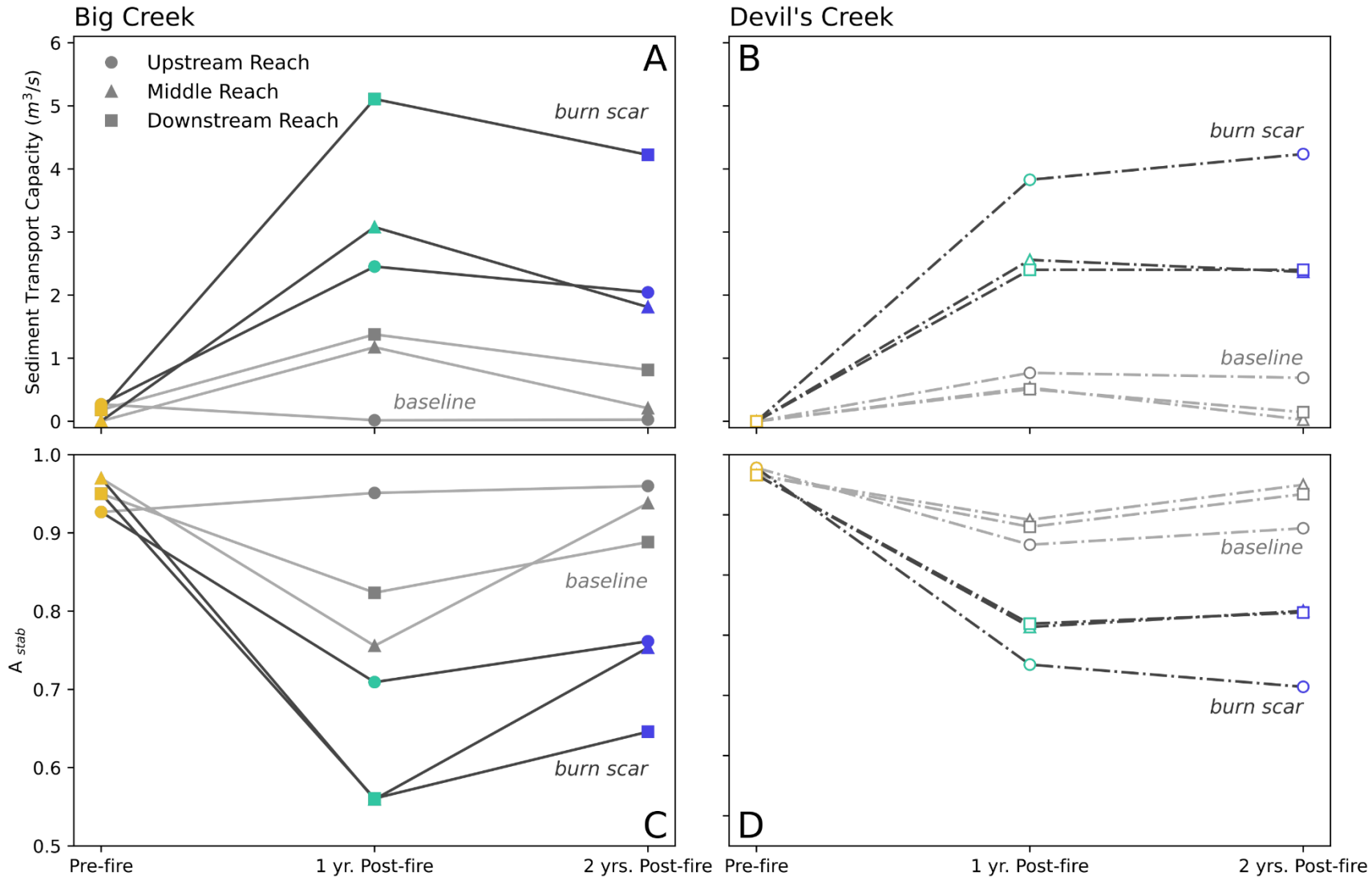

Figure 14. Sediment transport capacity and A_{stab} through time in Big Creek and Devil's Creek.

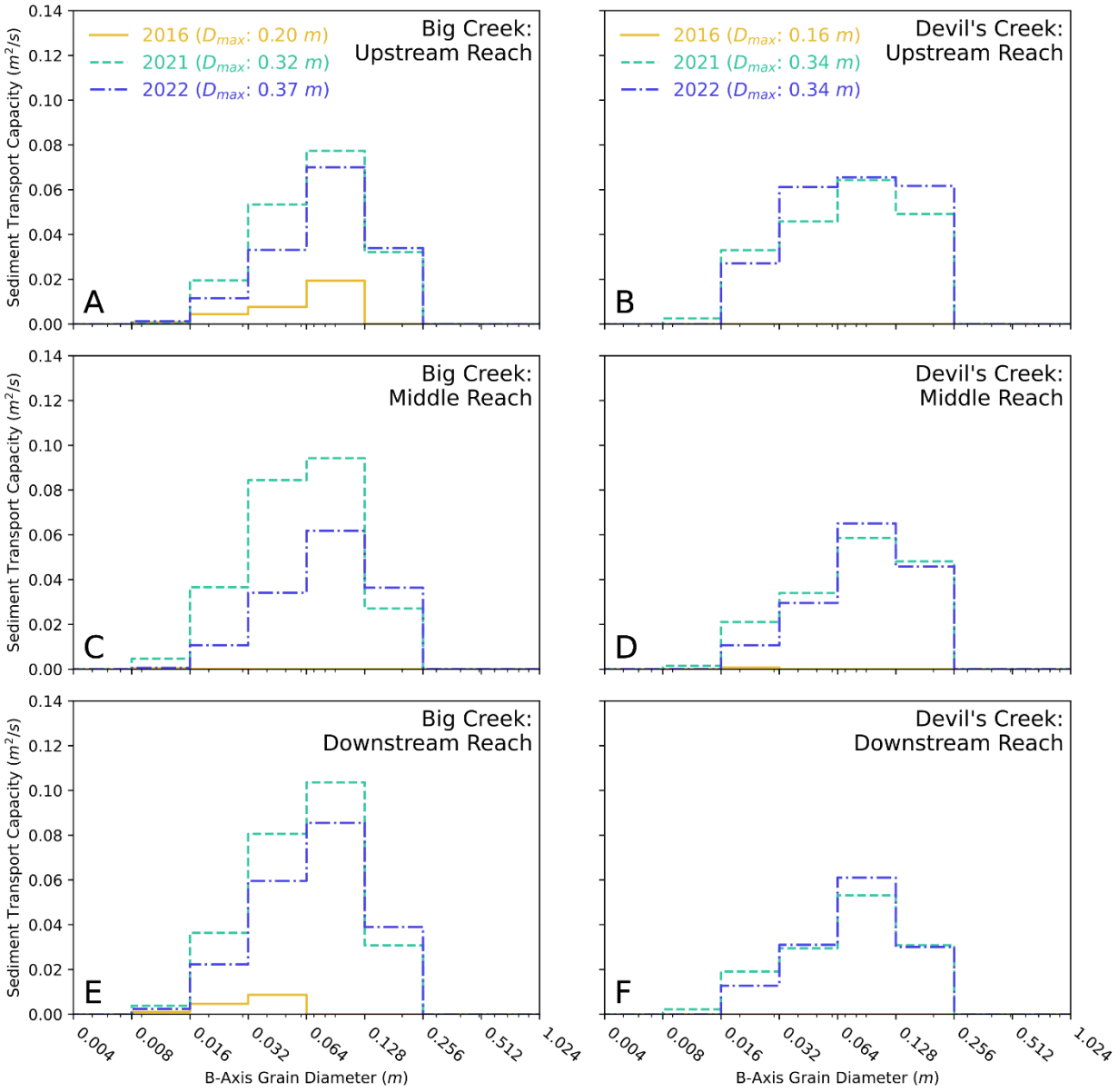

Figure 15. Area-normalized sediment transport capacity for grain size bins across all reaches in Upper Big Creek and Devil's Creek. D_{max} represents the b-axis diameter of the largest mobile grain by area (across all study reaches) during each model timestep.

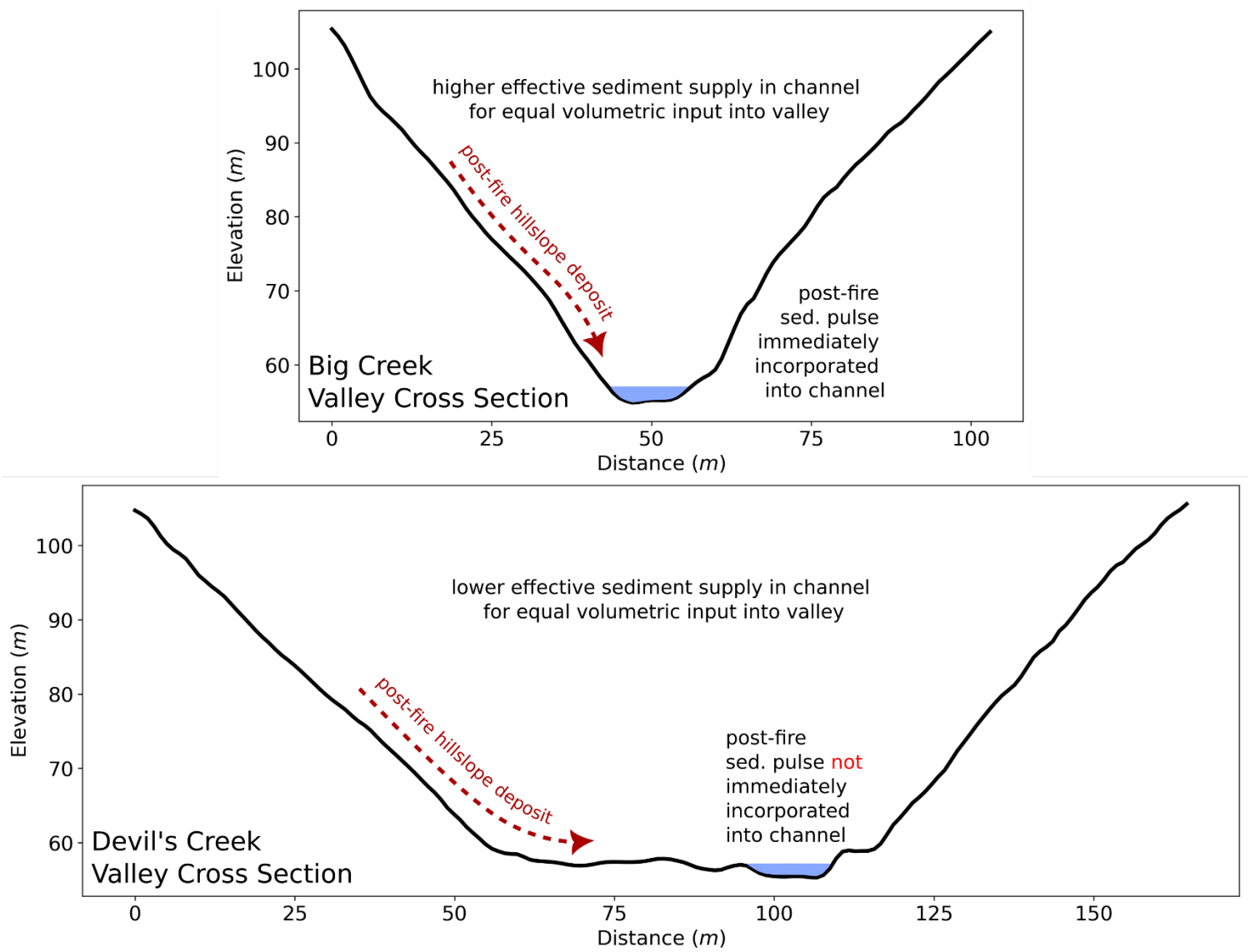

Figure 16. Valley cross sections for Upper Big Creek and Devil's Creek, with schematic illustrations of hypothetical post-fire hillslope sediment contributions.

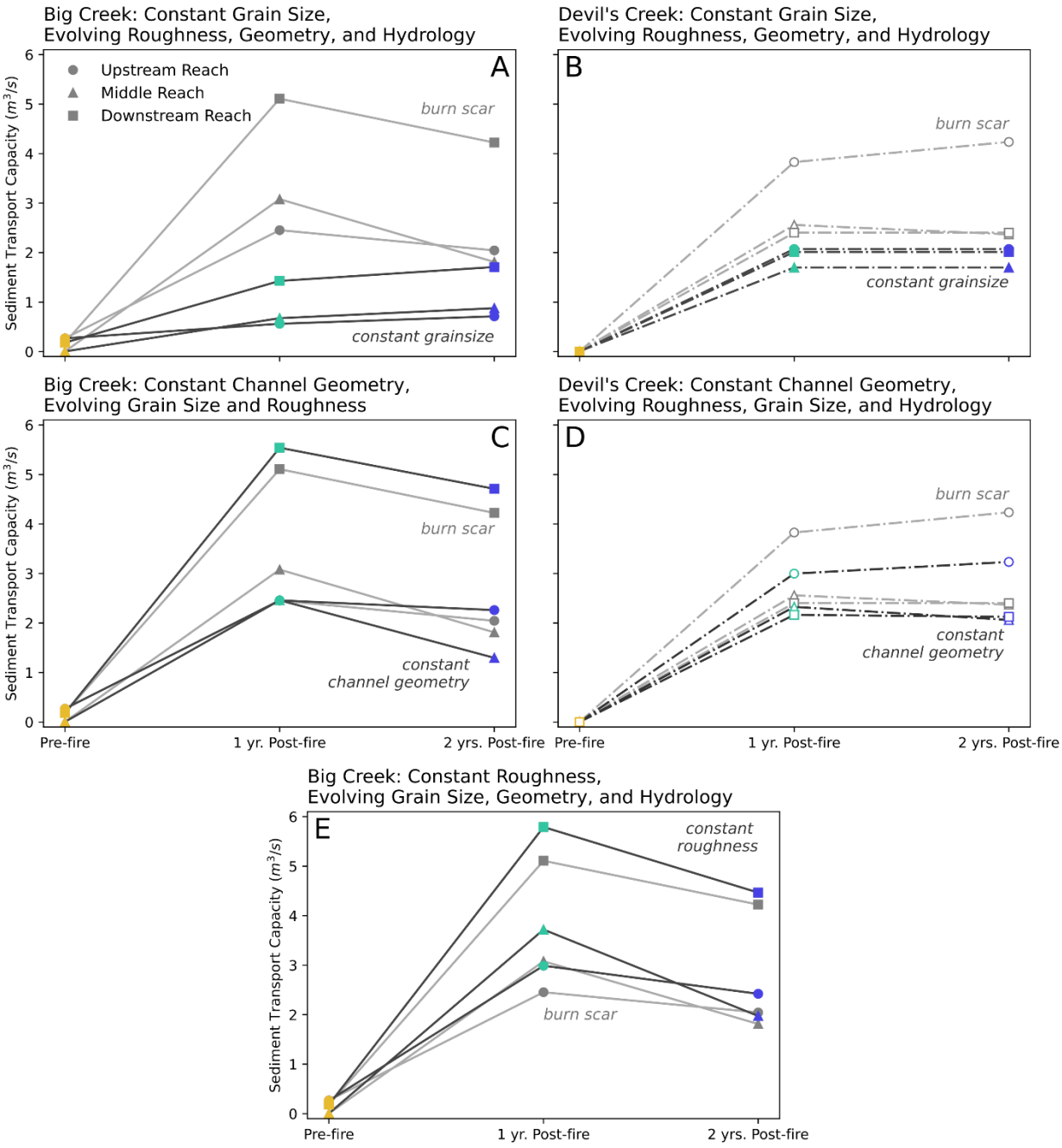

Figure 17. Sediment transport capacity through time for study reaches in Upper Big Creek with constant bed surface grain size, channel geometry, and roughness.

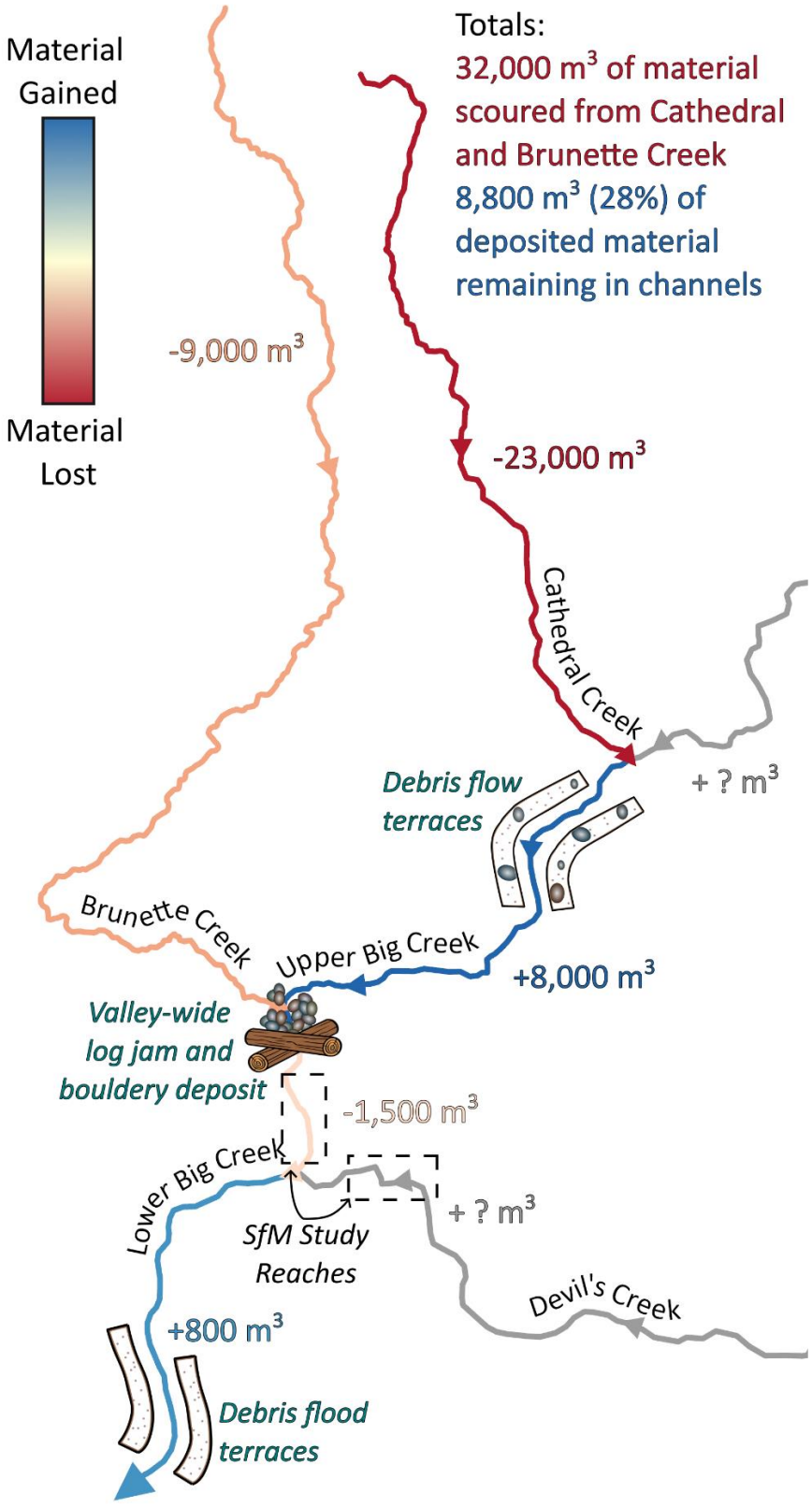

Figure 18. Schematic of post-fire sediment contributions and storage for streams in the Big Creek watershed.

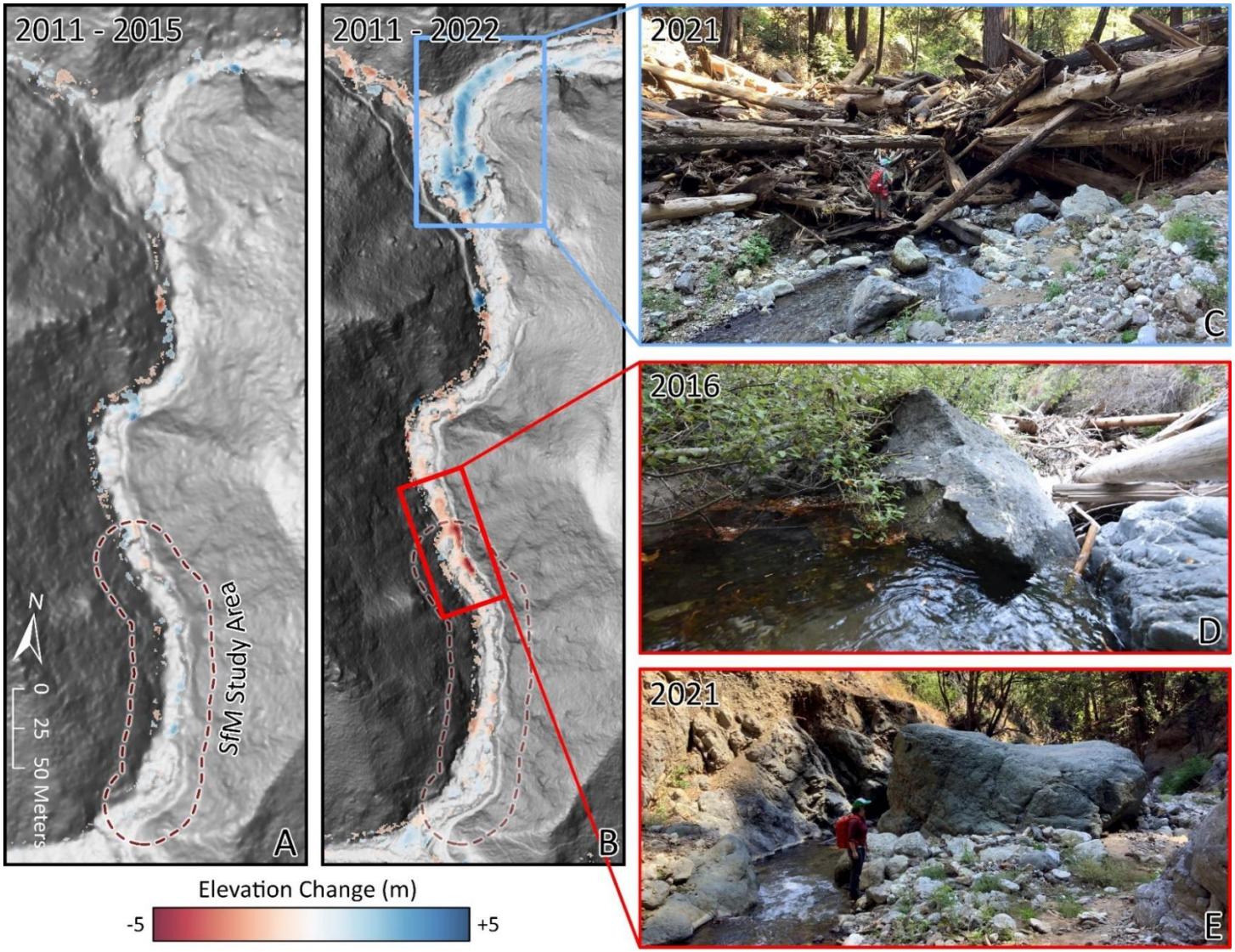

Figure 19. DEMs of difference and field photos at the confluence of Upper Big Creek and Brunette Creek and reaches downstream, which include SfM study reaches and the geomorphic features in Figures 9B, and 9C. Vertical structure in this section of the channel was reconfigured during post-fire debris flows.

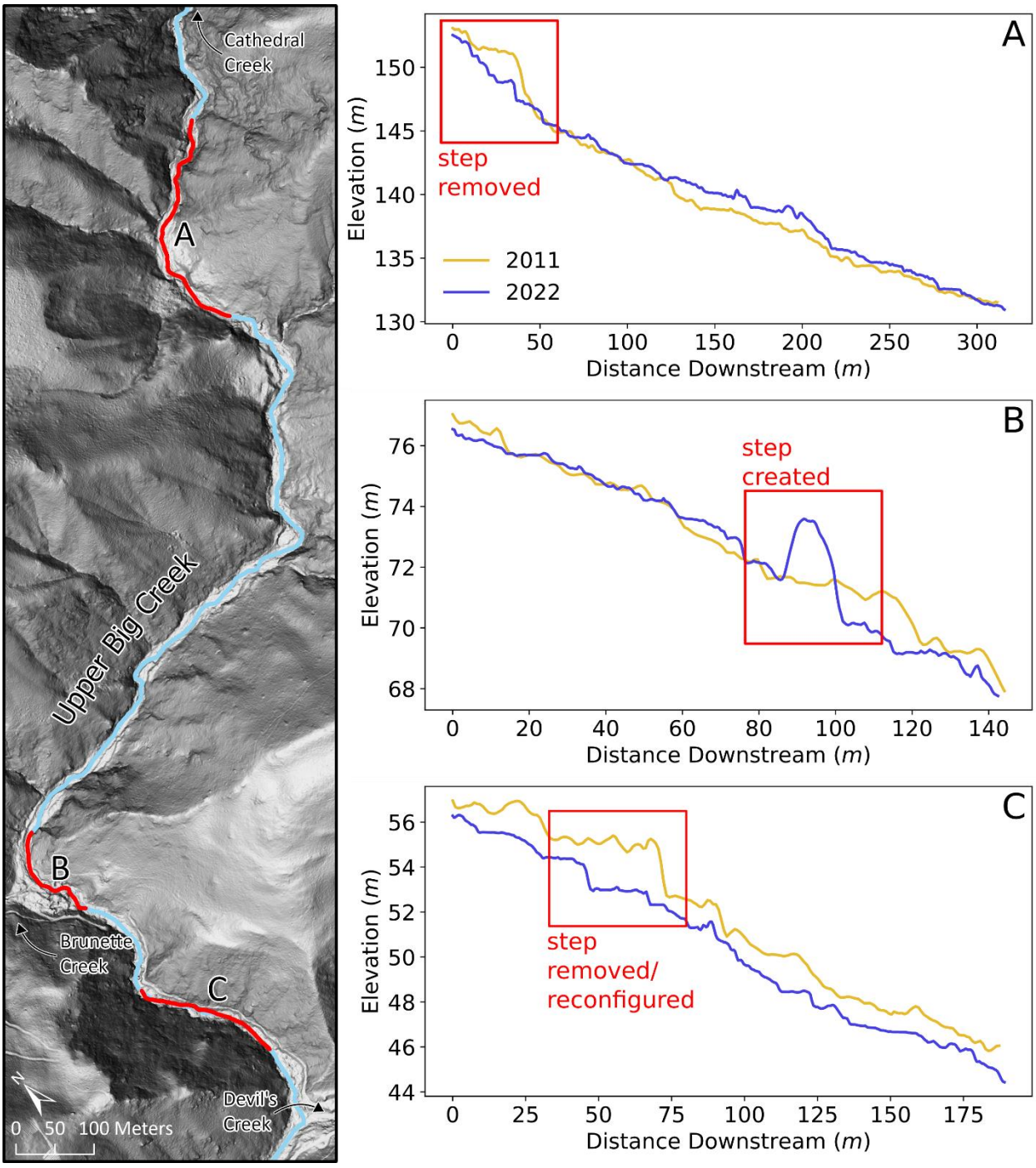

Figure 20. Longitudinal profiles from 2011 and 2022 lidar datasets for sections of Upper Big Creek in which vertical structure was reconfigured during post-fire debris flows.

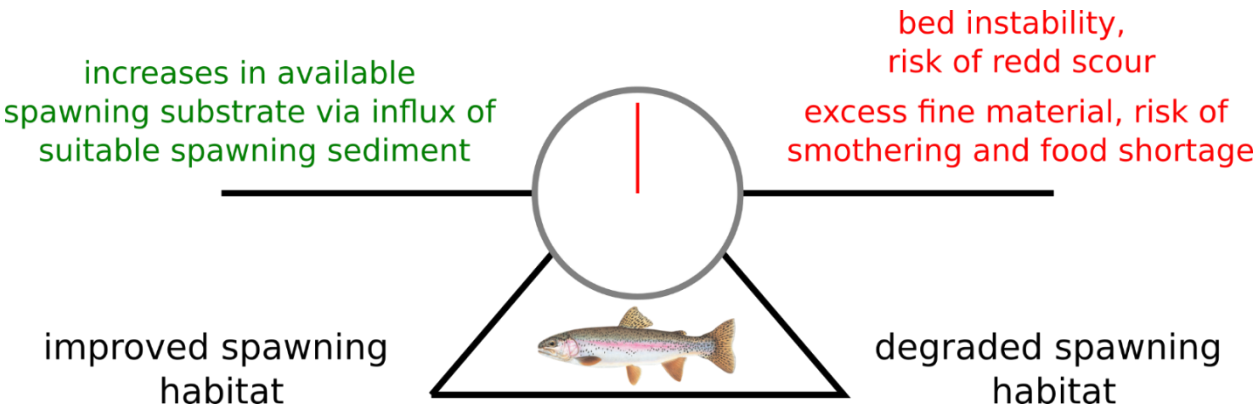

Figure 21. Schematic diagram of potential salmonid spawning habitat impacts of post-fire debris flows in Big Creek.

9.0 Supplemental Figures

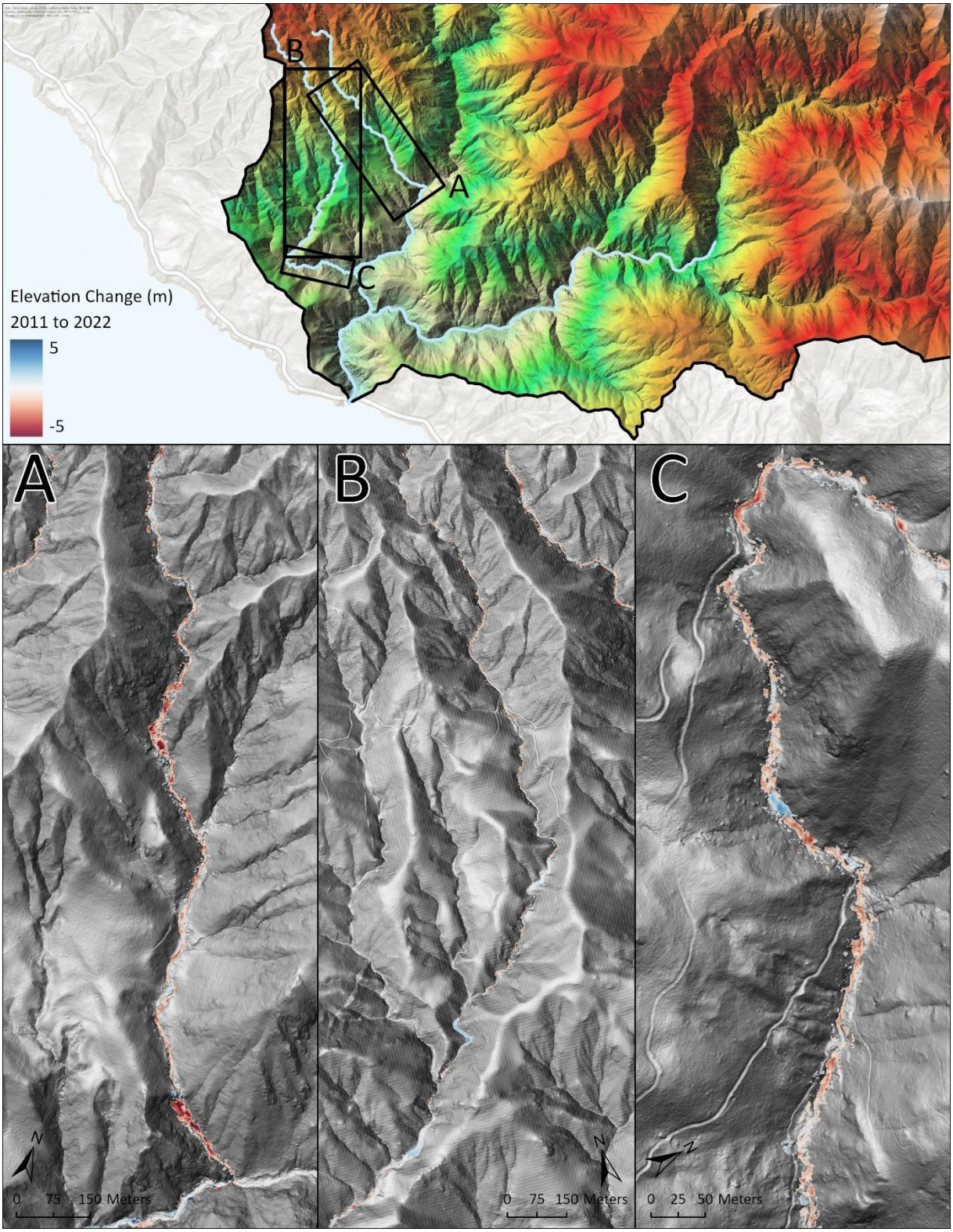

Supplementary Figure 1. Full DEM of difference from 2011 to 2022 for (A) Cathedral Creek and (B, C) Brunette Creek.

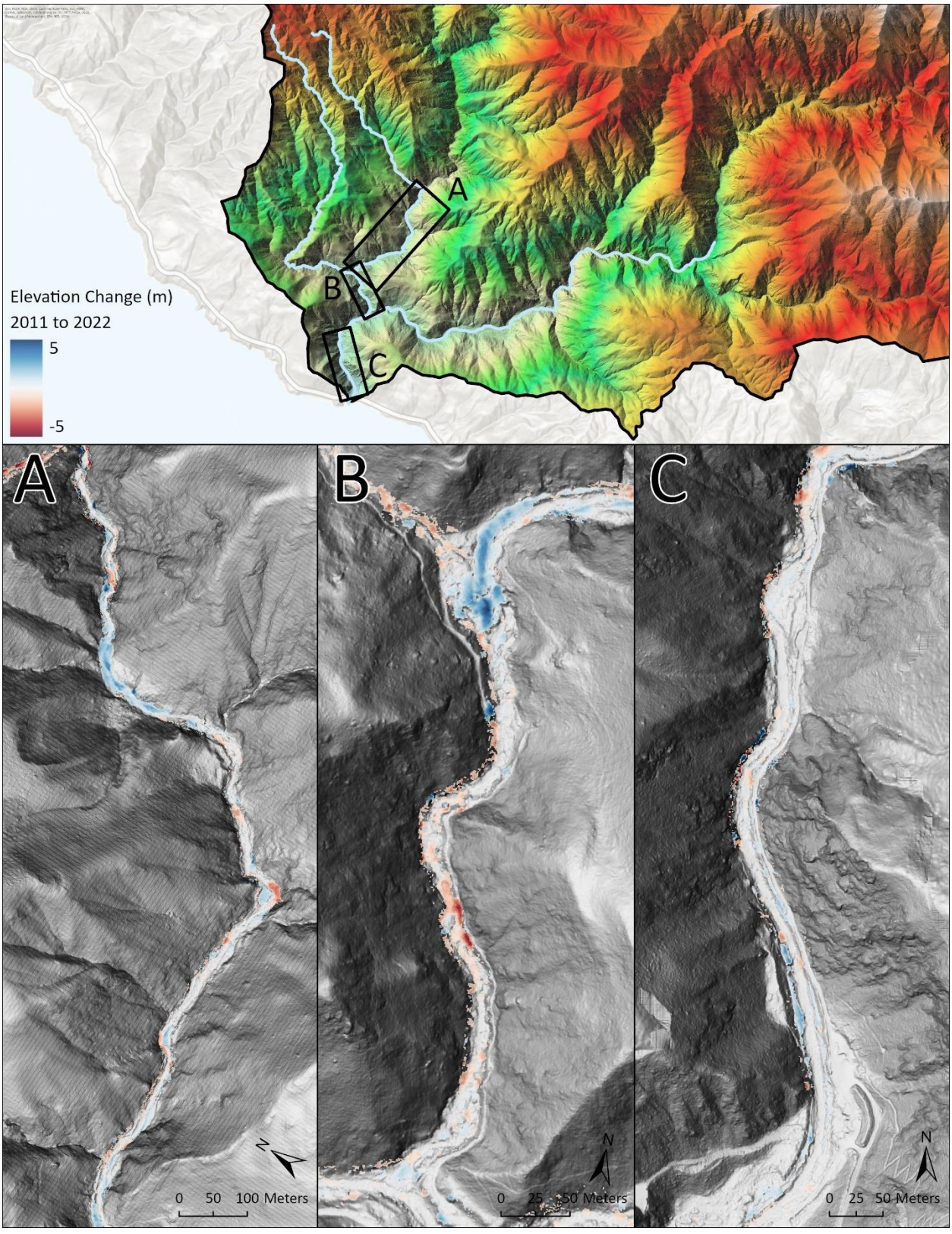

Supplementary Figure 2. Full DEM of difference from 2011 to 2022 for (A, B) Upper Big Creek and (C) Lower Big Creek.

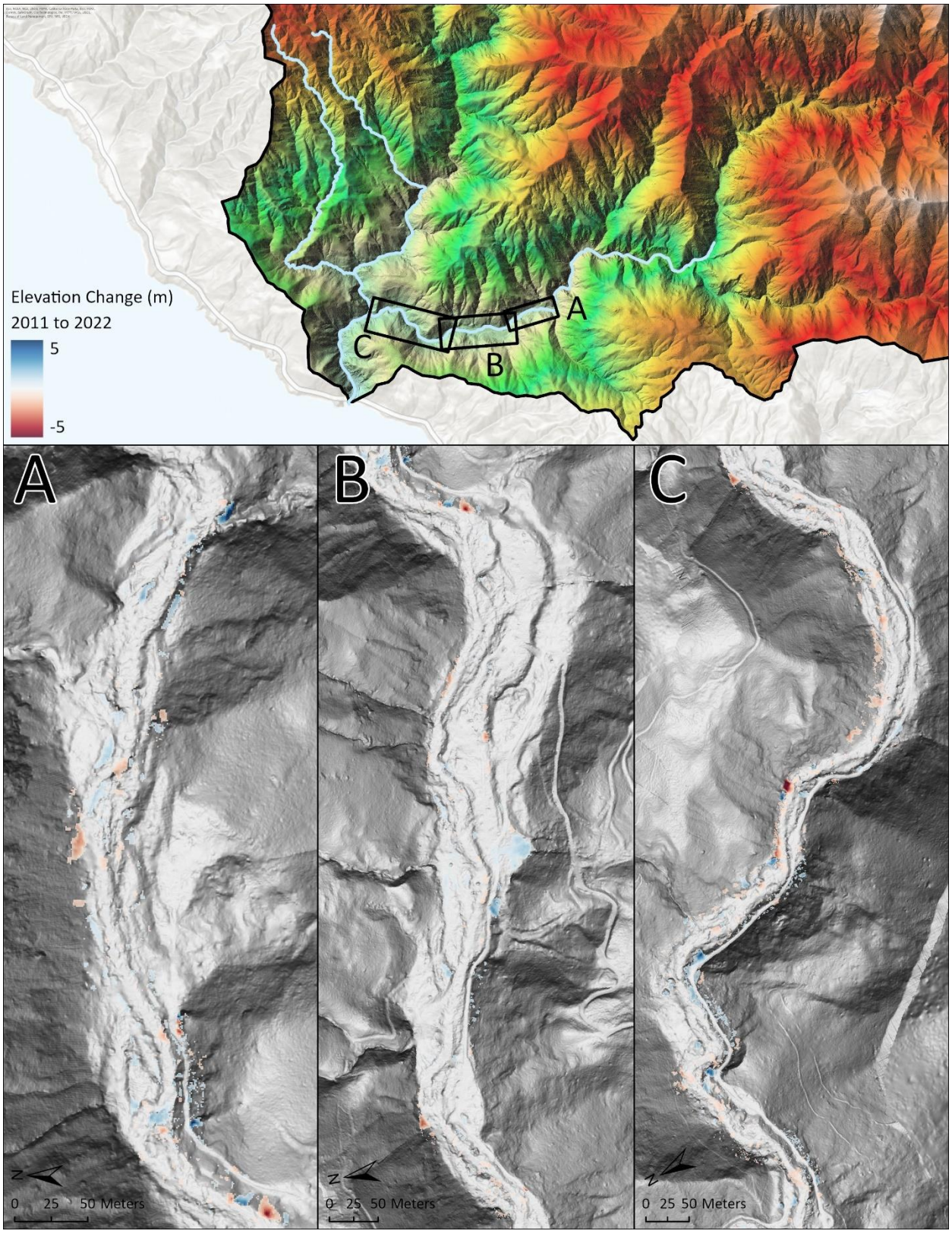

Supplementary Figure 3. Full DEM of difference from 2011 to 2022 for Devil's Creek.

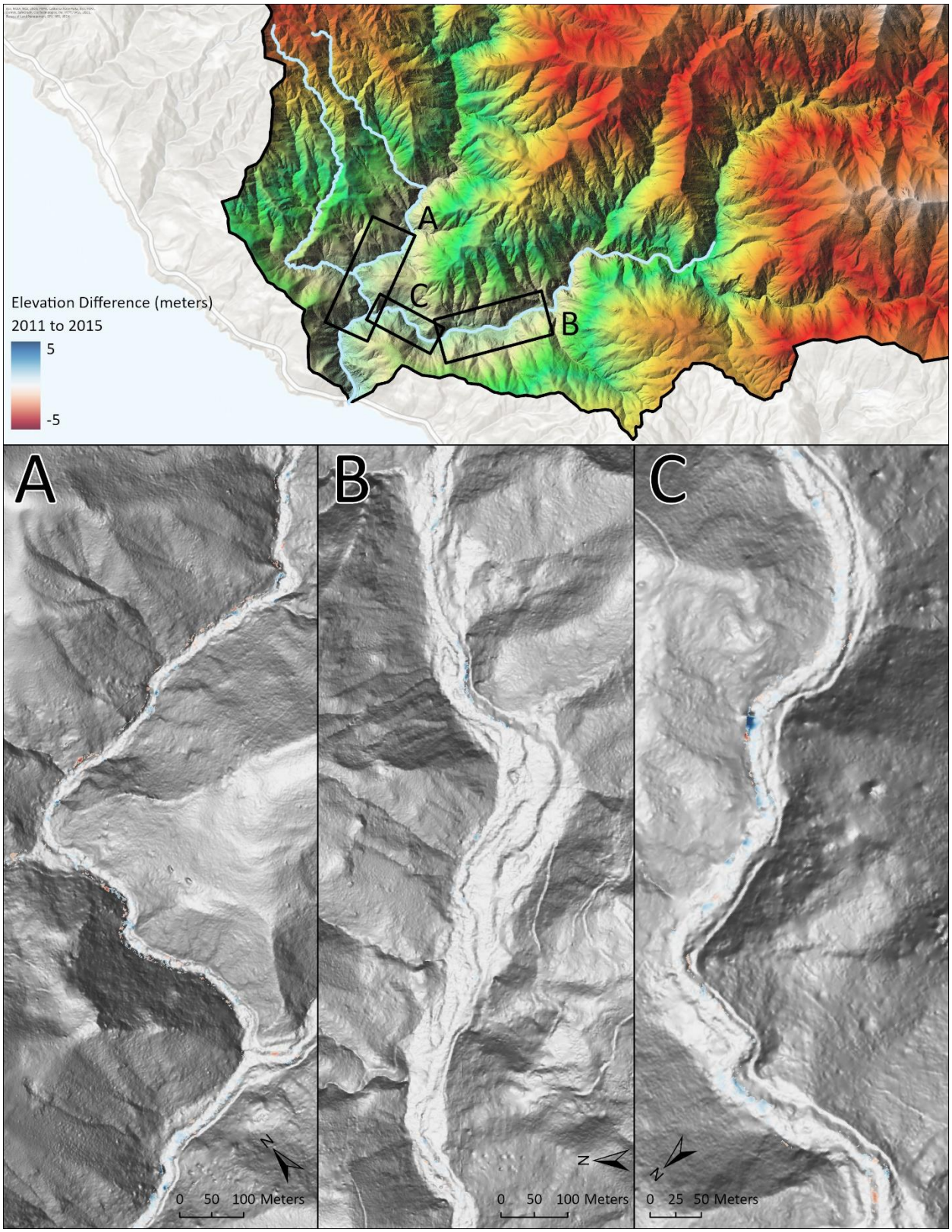

Supplementary Figure 4. Full DEM of difference from 2011 to 2015 for (A) Big Creek and (B, C) Devil's Creek.

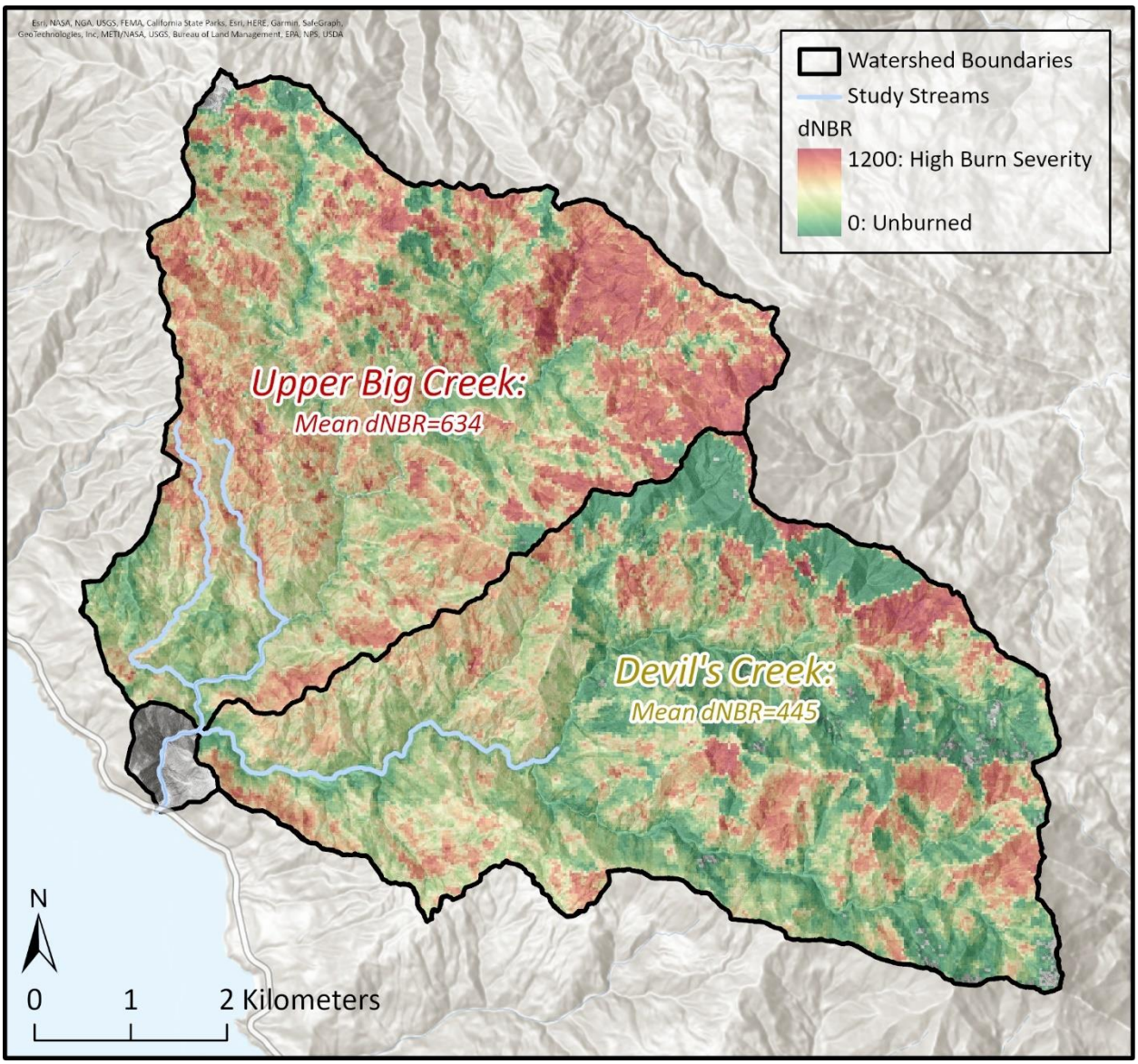

Supplementary Figure 5. Differenced normalized burn severity index in the Upper Big Creek and Devil's Creek watersheds.